inserted in the backbone using *BamHI* and *SpeI* restriction sites (see **Tables 17** and **18** for PCR reaction and cycles program).

Cloned vectors were isolated by Promega mini-prep kit and then methylated using M.SssI CpG methyltrasferase (New England Biolabs) accordingly to the manufacturer's instruction. Briefly, 5 µg of plasmid DNA was added to the reaction containing CpG methyltransferase (M.SssI) in the presence of 160 µM S-adenosylmethionine (New England Biolabs) and incubated for 4 hours at 37°C (S-adenosylmethionine was replenished after every 2 hours). Unmethylated control reaction containing the construct and methyltransferase but not SAM was used. Plasmid DNA was then purified by using Promega miniprep kit and quantified using Nanodrop. Methylation was confirmed by digestion with the methylation-sensitive restriction enzymes *HpaII*. NSC34 cells grown to $1.7x10^4$ on 6-well plates were co-transfected with each of the vectors described above and β-galactosidase mammalian expression vector using Lipofectamine 2000 (Invitrogen). A CpG Lucia vector with *EEF1A1* promoter, and CpG-free basic-Lucia empty vector were used as positive and negative control for the methylation experiment, respectively. Following 24 hours after transfection, cells were harvested and total RNA extracted using Trifast reagent as described above (session 3.5 of materials and methods). Promoter activity was evaluated through quantitative RT-PCR on Luciferase gene normalized using galactosidase as in the session 3.7 of the materials and methods.

4.4 Cloning of CpG4 island mutagenized fragments in *TARDBP* wild type mouse promoter vector

For *TARDBP* promoter functionality studies, constructs were done using the construct called "*TARDBP* extended promoter" as a backbone. The cloning of this construct has been explained in session 4.4 of materials and methods. We then generated five constructs containing different groups of mutagenized CpG sites within the fourth island. The vectors harbored CpG sites converted into CpA sites as follows: *construct 1)* CpG sites #92-95; *construct 2*) CpG sites #96-99; *construct 3*) CpG sites #100-103; *construct 4*) CpG sites #104-108; and *construct 5*) CpG sites #99, 101, 103, 105, and 108. To create these vectors we substituted the fourth island in the backbone vector with fragments of synthetic DNA containing the mutagenized sites (produced by Genescript). To substitute the fourth island in the backbone with the synthetic fragments of DNA, we inserted two enzymatic restriction sites upstream and downstream of the island (*PmeI* and *XbaI,* respectively). The high content in CpG sites in the region in which we had to insert these sites had made

impossible to design proper primers for a working quick-change strategy, so we used another system for each restriction enzyme to be inserted, which consists in multiple steps of PCR and it is illustrated in **Figure 14**. First, two adjacent PCR-fragments are generated using four oligonucleotides (Fw1 and Rv1, Fw2 and Rv2 as referred in **Figure 14**), two of which (the reverse of the Fragment 1 and the forward of the Fragment 2) contains the sites that has to be inserted and are partially overlapping between themselves. The other two primers (the forward of the Fragment 1 and the reverse of the Fragment 2) are non-mutagenic oligonucleotides that cover two convenient restriction sites already present in the backbone. Then, a third round of PCR is done. Both the two fragments produced in the first round of PCRs are used as a template for the third round of amplification using the primer forward of the Fragment 1 and the reverse of the Fragment 2. The product is a fragment containing in the middle the restriction site of interest and at the ends two restriction sites already present in the vector that allow the digestion of the total fragment and its ligation into the plasmid of interest. Fragments of interest have been amplified using PCR primer indicated in **Table 21**:

Primer	Sequence (5'-3')
PmeI ins Fw1	TGTGGCCGCCCCGGGTTTCCAGG
PmeI ins Rv1	ACCTGAATCGGGTTTAAACACGTGCTTTAAC
PmeI ins Fw2	ACGTGTTTAAACCCGATTCAGGTCCA
PmeI ins Rv2	GCGCACACTATAAGCTTCCGGTG
XbaI ins Fw1	CCCAAGCTTATAGTGTGCGCTGAG
XbaI ins Rv1	GAGATGGCTCAGTGGGTCTAGAGCACCCGACTGCTCTTC
XbaI ins Fw2	GCAGTCGGGTGCTCTAGACCCACTGAGCCA
XbaI ins Rv2	CGGGGTACCCTTTGCTTAAATCTCTTAAAGG

Table 21. List of primers for mutagenesis

Taq DNA Polymerase (BioLabs) was used for the amplification reaction. The PCR reaction and the cycling protocol are illustrated in **Tables 22** and **23**.

PCR component	Final concentration
10X Taq reaction buffer	1X
dNTPs	200 µM

Forward Primer	0,2 µM
Reverse Primer	0,2 µM
DNA	50-100 ng
Taq DNA Polymerase	1,25 units
Nuclease free water	Up to 25 µl

Table 22. Mutagenesis PCR reaction

Cycle step	Temperature (°C)	Time
Initial Denaturation	94	2’
40 cycles	94	30’’
	Tm specific for primer used	30’’
	68	1min/ kb
Final extension	68	5min

Table 23. Mutagenesis PCR cycles program

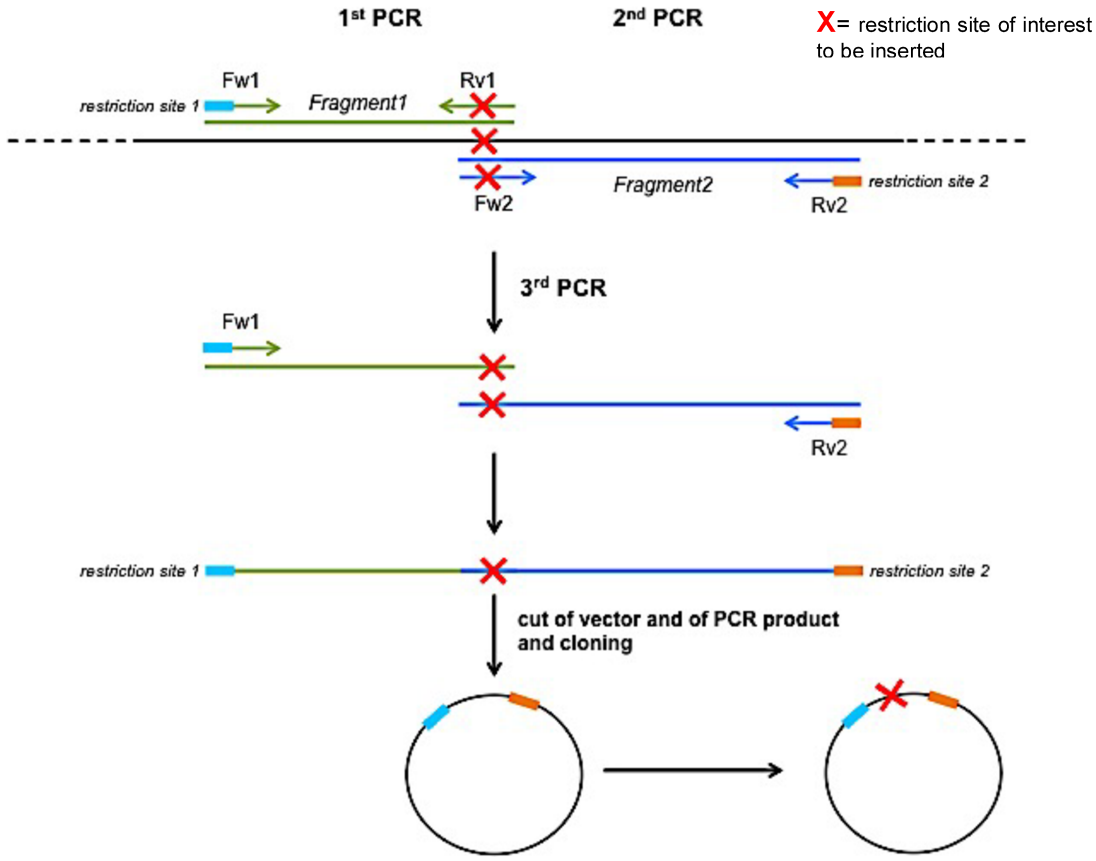

Figure 14. System of multiple PCR rounds for restriction site insertion

Once inserted the two restriction sites upstream and downstream of the fourth island we substituted it with mutagenized fragments of synthetic DNA described below. To shorten their length we took the advantage of a naturally present HindIII restriction site in the middle of the fourth island.

- *Fragment 1 CpG sites #92-95 mutagenized to CpA sites* (A of mutagenesis are indicated in capital letters in bold type) (PmeI/HindIII ends for cloning are indicated in bold)

gtttaaacccgattcaggtccaggctatagaagaaacttaattcagaatggttac**A**aaatac**A**gtagcctgtaatctgtgc**A**ctcc aggtaagaaatgac**A**agtgcaagaaaaaaaatcggggcagatacttagttctttaacaccttgtttttgtctggctttgtagccaacg ggccacatggtaacactgttgccattttagcaccgg**aagctt**

- *Fragment 2 CpG sites #96-98 mutagenized to CpA sites* (A of mutagenesis are indicated in capital letters in bold type) (PmeI/HindIII ends for cloning are indicated in bold)

gtttaaacccgattcaggtccaggctatagaagaaacttaattcagaatggttacgaaatacggtagcctgtaatctgtgcgctcca ggtaagaaatgacgagtgcaagaaaaaaaatc**A**gggcagatacttagttctttaacaccttgtttttgtctggctttgtagccaac**A** ggccacatggtaacactgttgccattttagcacc**Ag****aagctt**

- *Fragment 3 CpG sites #99-103 mutagenized to CpA sites* (A of mutagenesis are indicated in capital letters in bold type) (HindIII/XbaI ends for cloning are indicated in bold)

aagcttatagtgtgc**A**ctgagaaaatagaactggc**A**ggcagagc**A**ccacatgaacacc**A**gttttccctgtggctgccccc**A**ga actcagtagactaggccagcctcgaactcaaaaagatctgcctgcctcaagagtgctgagattaaaggcgtgggttatcgtgctcg acaaaaatcacatttttttttaaagatttattttattaatatatgtaagtacactgtagctgtcttcagacactccagaagagggagtcagat cttgttgcggatggttgtgagccaccatgtggttgctgggatttgaactctggaccttctgaagagcagtcgggtgc**tctaga**

- *Fragment 4 CpG sites #104-108 mutagenized to CpA sites* (A of mutagenesis are indicated in capital letters in bold type) (HindIII/XbaI ends for cloning are indicated in bold)

aagcttatagtgtgcgctgagaaaatagaactggcgggcagagcgccacatgaacaccggttttccctgtggctgccccggaact
cagtagactaggccagcctc**A**aactcaaaaagatctgcctgcctcaagagtgctgagattaaaggc**A**tgggttatc**A**tgctc**A**a
caaaaatcacatttttttttaaagatttattttattaatatatgtaagtacactgtagctgtcttcagacactccagaagagggagtcagatc
ttgttgc**A**gatggttgtgagccaccatgtggttgctgggatttgaactctggaccttctgaagagcagtcgggtgc**tctaga**

- *Fragment 5 CpG sites #99,101,103,105,108 mutagenized to CpA sites* (A of mutagenesis are indicated in capital letters in bold type) (HindIII/XbaI ends for cloning are indicated in bold)

aagcttatagtgtgc**A**ctgagaaaatagaactggcgggcagagc**A**ccacatgaacaccggttttccctgtggctgcccc**A**gaa
ctcagtagactaggccagcctcgaactcaaaaagatctgcctgcctcaagagtgctgagattaaaggc**A**tgggttatcgtgctcga
caaaaatcacatttttttttaaagatttattttattaatatatgtaagtacactgtagctgtcttcagacactccagaagagggagtcagatc
ttgttgc**A**gatggttgtgagccaccatgtggttgctgggatttgaactctggaccttctgaagagcagtcgggtgc**tctaga**

NSC34 cells grown to $1.7x10^4$ on 6-well plates were co-transfected with each of the vectors described above and β-galactosidase mammalian expression vector using Lipofectamine 2000 (Invitrogen). A CpG-free basic-Lucia empty vector were used as negative control for the experiment. Following 24 hours after transfection, cells were harvested and total RNA extracted using Trifast reagent as described above (session 3.5 from materials and methods). Promoter activity was evaluated through quantitative RT-PCR on Luciferase gene normalized using galactosidase as in the session 3.7 from materials and methods.

RESULTS

1. Tissue specific age related decay of mouse TDP-43 protein levels

It has been previously reported that TDP-43 levels both in fly and mouse brain decay during development and aging of the organisms[259]. The previous observations in fly and mice make us think that the reduction of TDP-43 levels was an evolutionary conserved physiological process. Starting our study on the mechanisms involved in this reduction, we have carried out first a detailed investigation of the TDP-43 expression levels at different age points and in different tissues in mice. For this study, we have used the FVB/N mouse strain because of its wide use in laboratories including the development of ALS-animal models[260]. For our purpose we extracted the proteins from brain and peripheral organs including heart, liver, lung, and skeletal muscle of mice aged 10, 20, 30, 40, 60, and 80 days and resolved the extract on SDS-PAGE. After this, TDP-43 level was assessed for each sample by western blot using a specific polyclonal antibody anti-TDP-43. As shown in **Figure 15**, in postnatal mice aged 10 days, TDP-43 was robustly and ubiquitously expressed in all the tissues analysed (**Figures 15A** to **15E**, lanes 1). On the other hand, as the mice grew, TDP-43 was undergoing different kinds of regulations that can be grouped into three trends of protein expression. In fact, by comparing lane 1 to 6 of each western blot in **Figure 15**, all the tissues undergo three different trends of regulation that can be listed into: a) a drastic drop of TDP-43 during time in skeletal muscle and heart (**Figures 15B** and **15D**); b) a mild but significant drop in brain and lung (**Figures 15A** and **15E**); c) a sustained expression in liver (**Figure 15C**). Since we examined the longitudinal expression of TDP-43 from 10 to 80 days, considering the intermediate time-points of 20, 30, 40, and 60 days we were also able to detect the exact time frame in which the main changes occur. In particular, in brain and lung the decrease is marked after 20 days as it can be observed from the comparison of the lanes 2 and 3 in **Figures 15A** and **15E**. On the other hand in the skeletal muscle and heart the big change occurs earlier between 10 and 20 days (**Figures 15B** and **15D** respectively, lanes 1 and 2). Lastly, no significant variations through ages have been shown in particular in liver, in fact looking through the lanes 1 to 6 relative to this tissue (**Figure 15C**), a constant and sustained expression of TDP-43 over time can be appreciated. For the analysis described above we tested tissues coming from three independent animals in triplicates for each time point. Here is recorded one representative blot. The ImageJ graph in **Figure 15F** shows the TDP-43 quantification

on the triplicates with error bars, normalized using the house keeping enzyme GAPDH (band detected at 37 kDa) as reference. Because sequential job has been focused on a larger screening of several proteins as described in the next sessions, we have compared the results obtained with western blot with a quicker technology: slot blot quantification of protein expression. As can be seen in **Figure 16**, both techniques yield identical results so we have adopted slot blot for the next analysis as a much more easier and faster methodology to evaluate protein expression.

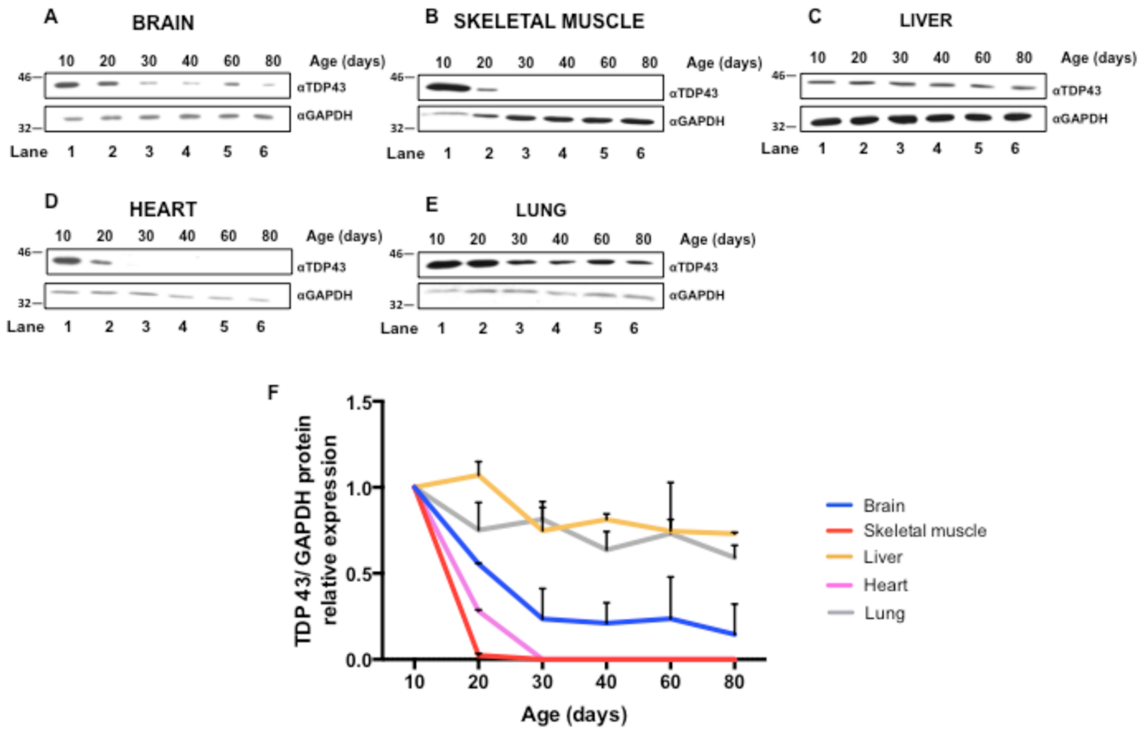

Figure 15. Tissue specific age related decay of mouse TDP-43 protein levels. A) Western blot analysis showing TDP-43 levels (upper panel) from mouse brain at 10, 20, 30, 40, 60, and 80 days. GAPDH detection (lower panel) is used as loading control. B) Western blot analysis showing TDP-43 levels (upper panel) from mouse skeletal muscle at 10, 20, 30, 40, 60, and 80 days. Antibody anti GAPDH (lower panel) is used as loading control. C) Western blot analysis showing TDP-43 levels (upper panel) from mouse liver at 10, 20, 30, 40, 60, and 80 days. GAPDH hybridization (lower panel) is used as loading control. D) Western blot analysis showing TDP-43 levels (upper panel) from mouse heart at 10, 20, 30, 40, 60, and 80 days. GAPDH detection (lower panel) is used as loading control. E) Western blot analysis showing TDP-43 levels from mouse lung at 10, 20, 30, 40, 60, and 80 days. Antibody anti GAPDH (lower panel) is used as loading control. F) ImageJ quantification of the relative expression of TDP-43 in brain (blue), skeletal muscle (red), liver (yellow), heart (pink), and lung (grey) normalized with GAPDH. Error bars indicate SD calculated on three independent experiments.

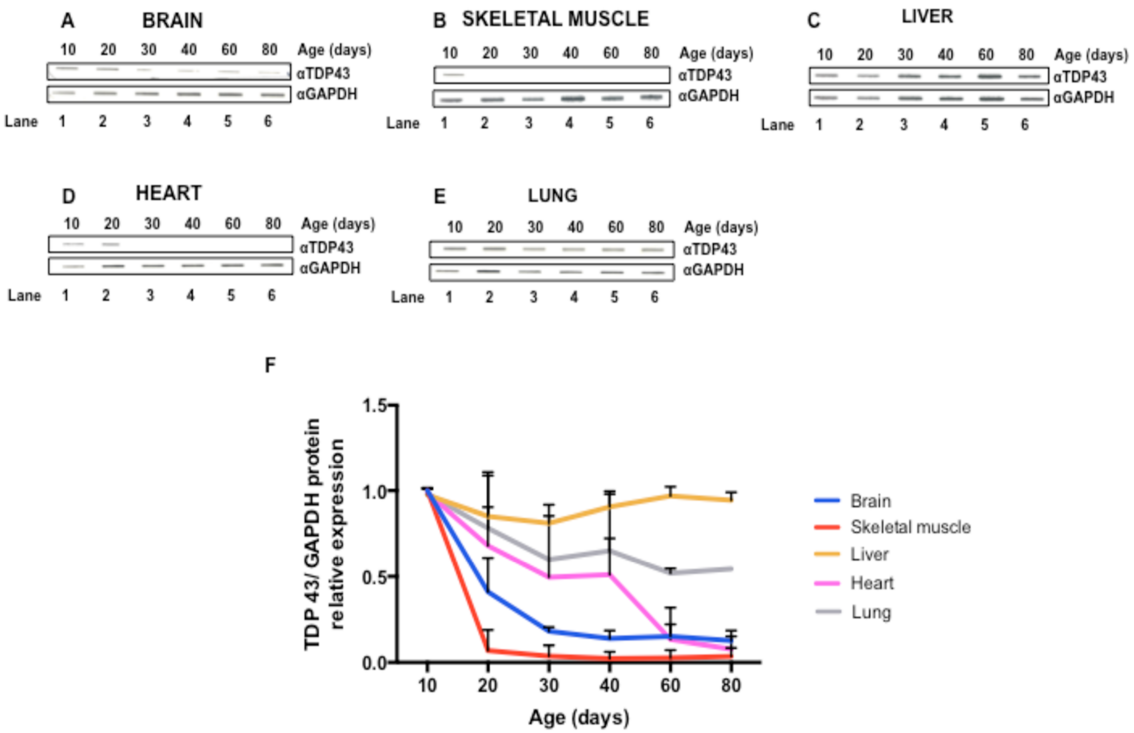

Figure 16. Tissue specific age related decay of mouse TDP-43 protein levels. A) Slot blot analysis showing TDP-43 levels (upper panel) from mouse brain at 10, 20, 30, 40, 60, and 80 days. GAPDH hybridization (lower panel) is used as loading control. B) Slot blot analysis showing TDP-43 levels (upper panel) from mouse skeletal muscle at 10, 20, 30, 40, 60, and 80 days. The lower panel shows GAPDH detection as loading control. C) Slot blot analysis showing TDP-43 levels (upper panel) from mouse liver at 10, 20, 30, 40, 60, and 80 days. Anti GAPDH antibody is used as loading control (lower panel). D) Slot blot analysis showing TDP-43 levels (upper panel) from mouse heart at 10, 20, 30, 40, 60, and 80 days. GAPDH hybridization (lower panel) is used as loading control. E) Slot blot analysis showing TDP-43 levels (upper panel) from mouse lung at 10, 20, 30, 40, 60, and 80 days. Anti GAPDH antibody is used as loading control (lower panel). F) ImageJ quantification of the relative expression of TDP-43 in brain (blue), skeletal muscle (red), liver (yellow), heart (pink), and lung (grey) normalized with GAPDH. Error bars indicate SD calculated in three independent experiments.

2. TDP-43 levels are regulated at the transcription level

For further studies of the TDP-43 expression regulation we have focused on three tissues representative of the typical trends of age related expression. In particular, we chose the skeletal muscle as a tissue in which there is a strong reduction of the expression occurring between 10 and 20 days after birth. By contrast, the liver was taken as representative of a constant TDP-43 expression during the age period considered and brain as representative of the intermediate trend. The latter was also important because the potential relationship with the age of onset of the ALS-like locomotion phenotype in the fly model at the time of the drop of TDP-43 levels in brain[259] that might be related to the pathogenesis of ALS. In mouse brain the protein undergoes a mild drop starting between 20 and 30 days after birth

and a sharper one later in life (**Figure 17A**). We decided to focus our next analyses on two time points considering 10 days as early stage of post natal development and 90 days as time in which the animal is a fully mature adult. In order to confirm previous data also for 90 days of age, we extracted total protein from mouse brain, liver, and skeletal muscle aged 10 and 90 days and after protein separation by SDS-PAGE and western blot with anti-TDP-43 antibody, we were able to confirm a tissue- and age- specific pattern of expression similar to those observed to occur between 10 and 80 days (**Figures 15A, 15B** and **15C**, compare lanes from 1 to 6). In fact, TDP-43 was highly expressed in brain (**Figure 17A**, lane 1), skeletal muscle (**Figure 17B**, lane 1), and liver (**Figure 17C**, lane 1) of young animals aged 10 days. At 90 days the situation differs in all three tissues with a drop in brain (**Figure 17A**, compare lane 1 with lane 2), a strong decrease in the skeletal muscle (**Figure 17B**, compare lane 1 with lane 2) and no differences at 90 days in liver (**Figure 17C**, compare lane 1 with lane 2). Each analysis has been done in triplicate by extracting tissues from three different animals. Below each representative blot, we showed the ImageJ quantification (normalized on GAPDH) with standard deviations relative to three experiments for each tissue (**Figures 17A**, **3B** and **3C**, panels below the blot). Every western blot has been confirmed in slot blot (**Figures 17D**, **3E** and **3F**).

To study if the variations of expression levels were also present in the mRNA we have analysed TDP-43 mRNA levels in the same tissue samples. For this purpose we extracted total RNA from wild type mouse brain, liver and skeletal muscle at 10 and 90 days after birth and performed reverse transcription (RT) and real time qPCR. TDP-43 mRNA levels were quantified and normalized with the housekeeping gene GAPDH. We could observe that in the brain the decrease of TDP-43 mRNA is mild (**Figure 17H**). To validate what observed by the real time PCR technique, the drop of TDP-43 in mouse brain was further confirmed by Northern Blot analysis (**Figure 17G**). In the liver, the level of TDP-43 mRNA remained unchanged from 10 to 90 days (**Figure 17L**). By contrast, in the skeletal muscle there is a clear drastic drop in the TDP-43 mRNA expression level as shown in **Figure 17I**. Our data showed that in each tissue mentioned above, the protein and mRNA levels are consistent with each other suggesting that the regulation of TDP-43 expression might occur at transcriptional level or at the mRNA degradation level.

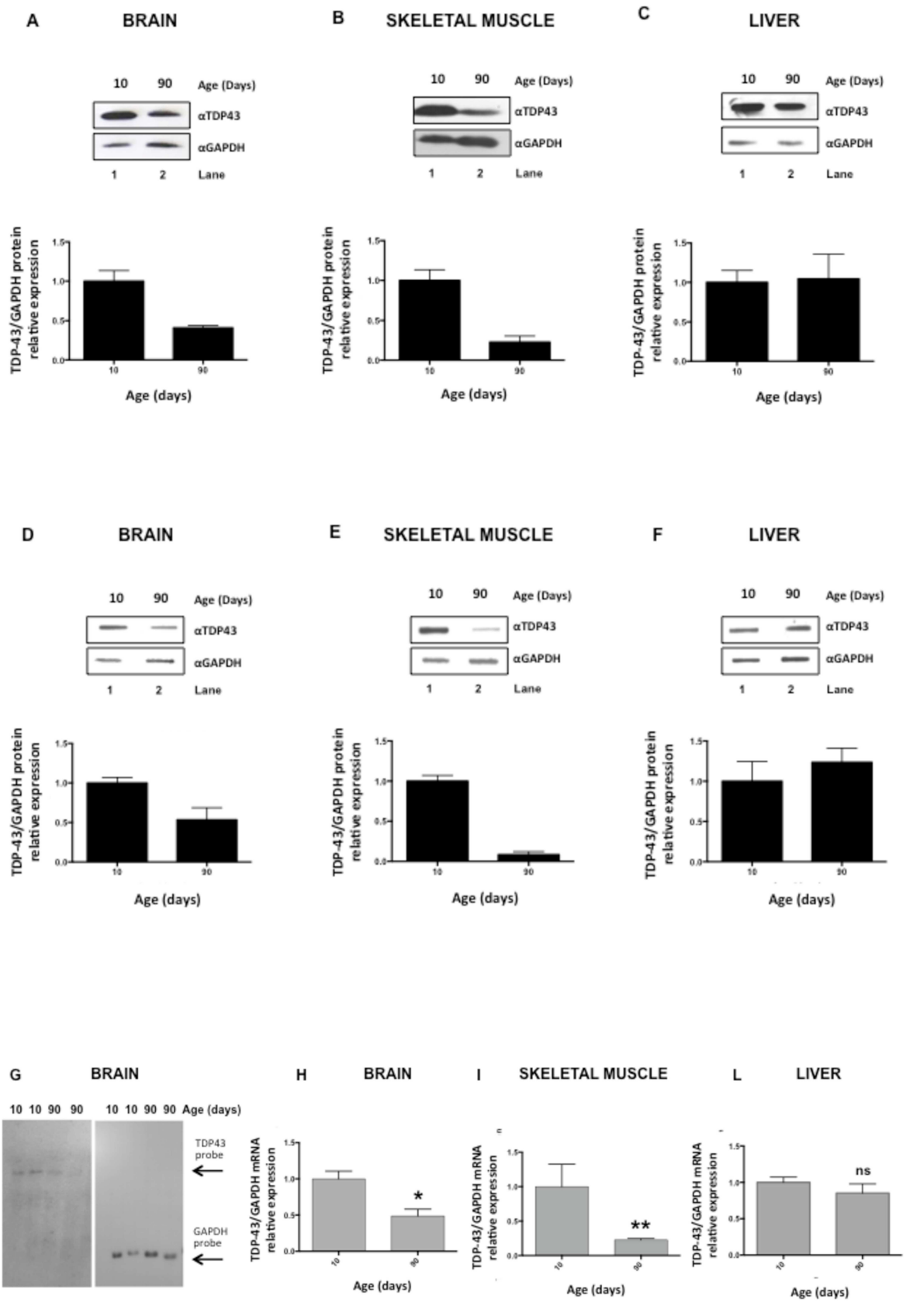
A
BRAIN
B
SKELETAL MUSCLE
C
LIVER
10
90
Age (Days)
αTDP43
αGAPDH
1
2
Lane
TDP-43/GAPDH protein relative expression
Age (days)
D
BRAIN
E
SKELETAL MUSCLE
F
LIVER
G
BRAIN
10 10 90 90
10 10 90 90 Age (days)
TDP43 probe
GAPDH probe
H
BRAIN
I
SKELETAL MUSCLE
L
LIVER
TDP-43/GAPDH mRNA relative expression
*
**
ns

Figure 17. TDP-43 levels are regulated at the transcription level. A) The upper panel on the left is a western blot analysis showing TDP-43 levels from mouse brain aged 10 and 90 days. The lower panel shows GAPDH detection as loading control. The histogram on the right shows the ImageJ quantification of TDP-43 expression levels normalized with GAPDH. Error bars indicate SD calculated on three independent experiments. B) The upper panel on the left is a western blot analysis showing TDP-43 levels from mouse skeletal muscle aged 10 and 90 days. The lower panel shows GAPDH detection as loading control. The histogram on the right shows the ImageJ quantification of TDP-43 expression levels normalized with GAPDH. Error bars indicate SD calculated on three independent experiments. C) The upper panel on the left is a western blot analysis showing TDP-43 levels from mouse liver aged 10 and 90 days. The histogram on the right shows the ImageJ quantification of TDP-43 expression levels normalized with GAPDH. Error bars indicate SD calculated on three independent experiments. D) The upper panel on the left is a slot blot analysis showing TDP-43 levels from mouse brain aged 10 and 90 days. The histogram on the right shows the ImageJ quantification of TDP-43 expression levels normalized with GAPDH. Error bars indicate SD calculated on three independent experiments. E) The upper panel on the left is a slot blot analysis showing TDP-43 levels from mouse skeletal muscle aged 10 and 90 days. The histogram on the right shows the ImageJ quantification of TDP-43 expression levels normalized with GAPDH. Error bars indicate SD calculated on three independent experiments. F) The upper panel on the left is a slot blot analysis showing TDP-43 levels from mouse liver aged 10 and 90 days. The histogram on the right shows the ImageJ quantification of TDP-43 expression levels normalized with GAPDH. Error bars indicate SD calculated on three independent experiments. G) Northern blot analysis of mouse brain TDP-43 at different time points in duplicate (left panel). GAPDH was used as loading control (left panel). H) Real-time PCR quantification of mouse brain TDP-43 mRNA at 10 and 90 days. ns indicates $p>0.05$ (not significant), * indicates $0,01<p< 0,05$, ** indicates $0,001<p<0,01$. Error bars indicate SD calculated on three independent experiments. I) Real-time PCR quantification of mouse skeletal muscle TDP-43 mRNA at 10 and 90 days. ns indicates $p>0.05$ (not significant), * indicates $0,01<p< 0,05$, ** indicates $0,001<p<0,01$. Error bars indicate SD calculated on three independent experiments. L) Real-time PCR quantification of mouse liver TDP-43 mRNA at 10 and 90 days. ns indicates $p>0.05$ (not significant), * indicates $0,01<p< 0,05$, ** indicates $0,001<p<0,01$. Error bars indicate SD calculated on three independent experiments.

3. TDP-43 time- and tissue-specific regulation mechanism is maintained during aging

Previous data have shown that TDP-43 protein levels of expression are linked to the tissue typology and to the time point considered. Furthermore, there is a correspondence between protein and mRNA levels suggesting that the underlying regulation mechanism might be at transcriptional level. Because this has been observed in mice aged from 10 to 90 days, we wondered about the conservation of this phenomenon during aging. For this, we have then extended the study to 1-year-old animals. Because of the previous validation of the slot blot technique to study the TDP-43 protein levels of expression and due to the large number of samples analysed, we decided to go further in the study by using only the slot blot methodology instead of western blot. For the protein analysis we extracted total protein from brain, liver, and skeletal muscle of wild-type mice aged 10, 90, and 365 days. The obtained protein extracts were transferred on a nitrocellulose membrane using a slot

blot acrylic device, and subsequently an anti-TDP-43 antibody was used to detect the level of expression of our protein of interest. Normalization has been performed as before using anti-GAPDH antibody. As can be seen in **Figure 18**, we confirmed the tissue specific trend observed for 10 and 90 days (compare lanes 1 with lanes 2 of **Figures 18A, 18B** and **18C**). Moreover, there was not significant variation between the 90 days and 365 days points. Indeed, the liver levels keep constant (**Figure 18C**, lane 3), the brain decreases slightly (**Figure 18A**, lane 3) and the muscle does not recover and stays to the expression level detected at day 90 (**Figure 18B**, lane 3). The ImageJ quantification on triplicates with correspondent standard deviations is shown in **Figure 18D**.

The TDP-43 mRNA expression levels in mouse brain, liver and skeletal muscle at 10, 90, and 365 days were analysed by real time RT-PCR as previously described (see methods and Section 2 of the Results). Again a decrease of TDP-43 mRNA that parallels the protein results was observed in brain (**Figure 18E**) and skeletal muscle (**Figure 18F**), while liver remains fairly constant (**Figure 18G**).

These results suggest that the age- and tissue- specific expression of TDP-43 observed during the early post-natal developmental stage (from 10 to 90 days), maintain the same trend also during aging (1 year). As earlier observed, also in the case of 1 year aged mice, the mRNA trend is similar to the protein, again suggesting a regulation occurring at transcriptional level.

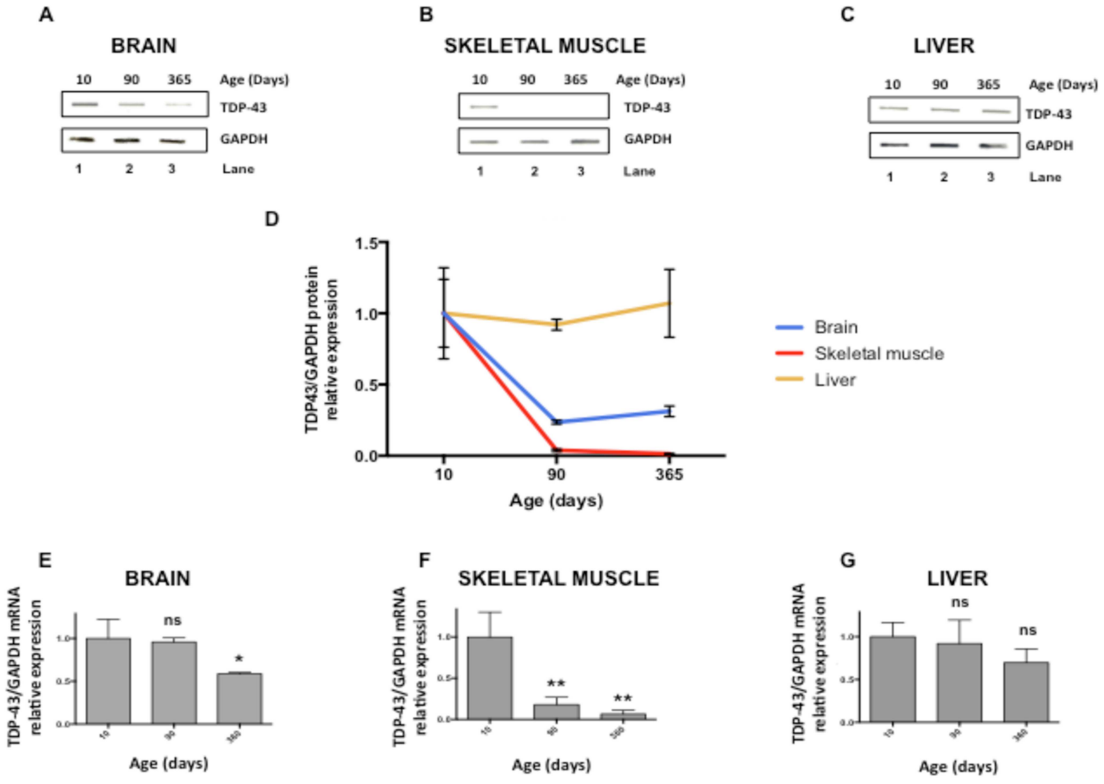

Figure 18. TDP-43 time- and tissue- specific regulation mechanism is maintained during aging. A) The upper panel is a slot blot analysis showing TDP-43 protein levels in brain from mice at 10, 90, 365 days. Lower panel shows GAPDH hybridization as loading control. B) The upper panel is a slot blot analysis showing TDP-43 protein levels in skeletal muscle from mice at 10, 90, 365 days. Lower panel shows GAPDH hybridization as loading control. C) The upper panel is a slot blot analysis showing TDP-43 protein levels in liver from mice at 10, 90, 365 days. Lower panel shows GAPDH hybridization as loading control. D) ImageJ quantification of the relative expression levels of TDP-43 normalized with GAPDH in brain (blue line), skeletal muscle (red line) and liver (yellow line). Error bars indicate SD calculated on three independent experiments. E) Real-time PCR quantification of mouse brain TDP-43 mRNA at 10, 90, and 365 days. The RNA levels are normalized with GAPDH. ns indicates $p>0.05$ (not significant), * indicates $0.01<p<0.05$, ** indicates $0.001<p<0.01$. Error bars indicate SD calculated on three independent experiments. F) Real-time PCR quantification of mouse skeletal muscle TDP-43 mRNA at 10, 90, and 365 days. The RNA levels are normalized with GAPDH. ns indicates $p>0.05$ (not significant), * indicates $0.01<p<0.05$, ** indicates $0.001<p<0.01$. Error bars indicate SD calculated on three independent experiments. G)) Real-time PCR quantification of mouse liver TDP-43 mRNA at 10, 90, and 365 days. The RNA levels are normalized with GAPDH. ns indicates $p>0.05$ (not significant), * indicates $0.01<p<0.05$, ** indicates $0.001<p<0.01$. Error bars indicate SD calculated on three independent experiments.

4. *TARDBP* promoter methylation rates show tissue- and developmental- stage specificity

We then started to investigate which mechanism could be responsible for the age related TDP-43 expression regulation. Since preliminary data previously obtained in our laboratory discarded a role for mRNA degradation induced by the self-control loop we decided to look at epigenetic modifications. DNA methylation in the promoter region of genes usually suppresses their expression and it is one of the best known and better characterized modification of the DNA, hence we decided to evaluate the methylation profiles of the 5' upstream regulatory region of the mouse *TARDBP* gene in brain, skeletal muscle and liver in young (10 days), adult (90 days), and older (365 days) animals. In order to do that we performed an *in silico* analysis of *TARDBP* 5' upstream regulatory region by using several promoter prediction tools including Promoter 2.0 prediction server (http://www.cbs.dtu.dk/services/Promoter/), Neural network promoter prediction (http://www.fruitfly.org/seq_tools/promoter.html), and Promoter scan (https://www-bimas.cit.nih.gov/molbio/proscan/), which provided information on the identity of the promoter regulatory region of our gene of interest. Because of the different algorithms used by each software, we obtained different predicted regions partially overlapping. We decided to go further by taking into account the largest regulatory sequence predicted by all the software. It resulted in a genomic area of around 1500 bp distributed 500 bp upstream and 1000 bp downstream of the Transcription Starting Site (TSS) (**Figure 19**). Following the identification of the region, we used Methprimer prediction tool (http://www.urogene.org/cgi-bin/methprimer/methprimer.cgi) to track the CpG sites within

the promoter and their density. The software revealed the presence of 108 CpG sites as a potential target for methylation within the promoter predicted sequence organised into four CpG islands containing 28, 49, 14, and 17 CpG sites, respectively (**Figure 19**). We decided to focus on this region for bisulfite conversion analysis. Specific PCR primers for the methylation analysis were designed on converted DNA to separately amplify each of the four CpG islands. Amplicons have been named as follows: CpG1 (spanning -561 to -181), CpG2A (from -191 to +102), CpG2B (from +102 to +360), CpG3 (extending from +336 to +535), and CpG4 (from +660 to +1172) (**Figure 19**). The division of the CpG2 island in two fragments (named CpG2A and CpG2B in the **Figure 19**) was due to its large length that made difficult the analysis through a single PCR fragment amplification.

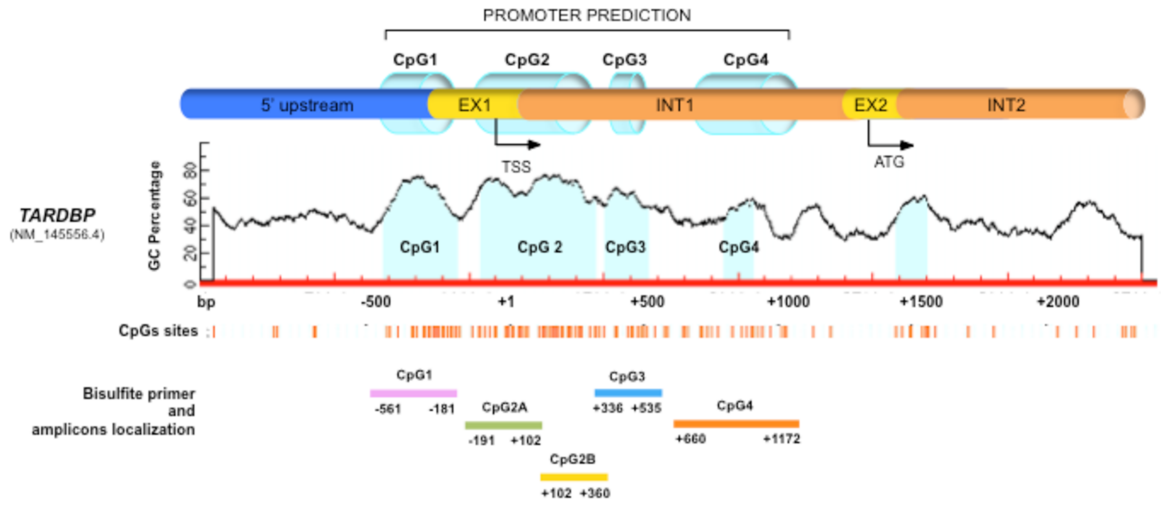

Figure 19. *TARDBP* promoter architecture and design of the bisulfite methylation analysis. Schematic representation of the *TARDBP* mouse promoter predicted fragment. +1 represents the Translation Start Site (TSS). Methprimer analysis indicates CpG islands (in light blue) distributed within the promoter as four distinct regions (CpG1, CpG2, CpG3, and CpG4). The CpG dinucleotides are indicated as orange lines under the representation of the islands. In the lower part of the image are depicted the five amplicons (pink, green, yellow, blue, and orange lines) analysed in the bisulfite experiment, with the numbers referring to the start and end point of the primer designed on the converted DNA and used for the amplification.

Interestingly, the overall DNA methylation level in all the four islands is low or not present in the promoter of every tissue analysed in the young animals aged 10 days (**Figure 20D**). In fact, any CpG sites considered do not exceed 10% of methylation rate in skeletal muscle (**Table 24A**), in brain (**Table 24B**) and in liver (**Table 24C**). In the adult mice aged 90 days the methylation rate of the CpG islands number 1, 2, and 3 is negligible in any tissue analysed (**Figure 20E**, red, blue, and yellow lines) but, on the other hand, the methylation status of the CpG island number 4 changes dependently on the considered tissue (Figures 19E, red, blue, and yellow lines). As aforementioned, the CpG4 island consists of 17 CpG sites (from #92 to #108, **Table 24**) spread in 550 bp in the last part of the promoter

predicted region. In the skeletal muscle of 90 days mouse, bisulfite analysis revealed that 3 out of 17 CpG sites are mildly methylated (**Table 24A**, orange squares) while 2 sites are highly methylated (**Table 24A**, red squares) with a methylation rate of up to 50%. We found a similar but milder scenario in 90 days aged mice brain in which the methylation content is modest in one CpG site (**Table 24B**, orange square) and high in a second site (**Table 24B**, red square). By contrast, in the liver of adult mice aged 90 days we could not detected any CpG sites showing significant change in the methylation state a part from one, which shows a methylation rate of around 11% (**Table 24C**, orange square).

In 1 year aged mice, the methylation status is similar to the 90 days one in each tissue considered, with some cases of increased methylation of CpG sites (**Table 24**). In particular, in the skeletal muscle, 2 CpG sites out of 17 are methylated at low rate (**Table 24A**, light orange squares), 2 CpG sites at modest rate (**Table 24**, orange squares) and 1 at very high rate (**Table 24A**, red square). In the brain, one CpG site is very highly methylated up to 66% (**Table 24B**, red square). On the other hand, no considerable methylation could be seen in mouse liver aged 1 year with only 2 CpG sites slightly methylated (10% or lower) (**Table 24C**, light orange squares).

METHYLATION PERCENTAGE DEGREE

0% 20% 40% 80% 100%

A

SKELETAL MUSCLE CpG4 island

	Cpg # site	#92	#93	#94	#95	#96	#97	#98	#99	#100	#101	#102	#103	#104	#105	#106	#107	#108
% METHYLATION	10 days	0	0	0	0	0	0	0	0	0	0	0	0	0	0	0	0	5,7± 9,8
	90 days	0	0	0	0	0	0	0	11± 9,8	0	15± 19	0	11± 9,8	0	25± 24	0	0	50 ± 0
	365 days	0	0	0	0	0	0	0	0	0	15± 6	0	5± 2,2	0	15± 6	10± 9,8	0	55± 15

B

BRAIN CpG4 island

	Cpg # site	#92	#93	#94	#95	#96	#97	#98	#99	#100	#101	#102	#103	#104	#105	#106	#107	#108
% METHYLATION	10 days	0	0	0	0	0	0	0	0	0	0	5,7± 9,8	0	0	0	0	0	0
	90 days	0	0	0	0	0	0	0	0	0	0	0	0	0	0	17± 10	0	45 ± 20
	365 days	0	0	0	0	0	0	0	0	0	0	0	0	0	0	0	0	66± 15

C

LIVER CpG4 island

	Cpg # site	#92	#93	#94	#95	#96	#97	#98	#99	#100	#101	#102	#103	#104	#105	#106	#107	#108
% METHYLATION	10 days	0	0	0	0	0	0	0	0	0	0	0	0	0	0	0	0	5,7± 9,8
	90 days	0	0	0	0	0	0	0	0	0	0	0	0	0	0	0	0	11± 9,8
	365 days	0	0	0	0	0	0	0	0	10± 9,8	0	0	0	0	0	0	0	5,7± 9,8

Table 24. *TARDBP* promoter methylation levels of the CpG4 island. A) Methylation percentages of the mouse skeletal muscle *TARDBP* fourth island CpG sites (from 92 to 108) at 10, 90, and 365 days. B) Methylation percentages of

the mouse brain *TARDBP* fourth island CpG sites (from 92 to 108) at 10, 90, and 365 days. C) Methylation percentages of the mouse liver *TARDBP* fourth island CpG sites (from 92 to 108) at 10, 90, and 365 days. Light orange squares indicates 0%<methylation<20%, orange squares indicates 20%<methylation<40%, red squares indicates 40%<methylation<80%.

In summary, the overall DNA methylation level in all the four islands is low or not-present in the promoter of every tissue analysed in the young animals aged 10 days (**Figure 20D**, red, blue, and yellow lines), in which the protein expression is high (**Figure 20A** lane 1, **Figure 20B** lane 1, **Figure 20C** lane 1). At 90 days, even though in the islands number 1, 2, and 3 the percentage of methylation still remains low or absent, the methylation status of the fourth island changes accordingly to the tissue considered (**Figure 20E**, red, blue, and yellow lines). In particular, the methylation index of the fourth island CpG site #108, which is not methylated in the 10 days brain, increased from 0% to 65% in 90 days mice brain (**Figures 20D** and **20E**, compare the blue lines). It is interesting to note that in this tissue we found a mild drop of protein expression from 10 to 90 days aged mice (**Figure 20B**, compare lane 1 with lane 2). The total methylation rate of the skeletal muscle promoter of adult mice (90 days) dramatically increased from almost 0% of 10 days aged mice to up to 50% in 90 days aged mice (**Figures 20D** and **20E**, compare red lines). Intriguingly in skeletal muscle, where the protein expression drastically decreases from 10 to 90 days (**Figure 20B**, compare lane 1 with lane 2), the methylation rate at 90 days is higher than the one found in some aged brain where the protein mildly decreases (**Figure 20A,** compare lanes 1 and 2). On the other hand, no changes in the methylation rate have been detected in *TARDBP* promoter of 90 days aged livers (**Figure 20E**, yellow line), in which the protein analysis showed a sustained and constant expression (**Figure 20C**, compare lane 1 with lane 2). In older mice aged 1 year, where the protein levels continue to decrease over time in brain and skeletal muscle (**Figures 20A and 20B**, compare from lane 1 to 3), the methylation rate in the CpG4 island remains at high levels, and, in some cases, it is even increased (**Figure 20F**, blue and red lines, respectively). In liver from 1 year old animals, no significant methylation changes has been found in the four CpG islands of the *TARDBP* promoter (**Figure 20F**, yellow line). In contrast to the brain and skeletal muscle, in liver the protein expression is sustained during time (**Figure 20C**, compare lanes 1, 2 and 3).

These results suggest that the *TARDBP* promoter methylation profile is time and tissue dependent, and that there is an inverse correlation between the promoter methylation rate and the protein expression.

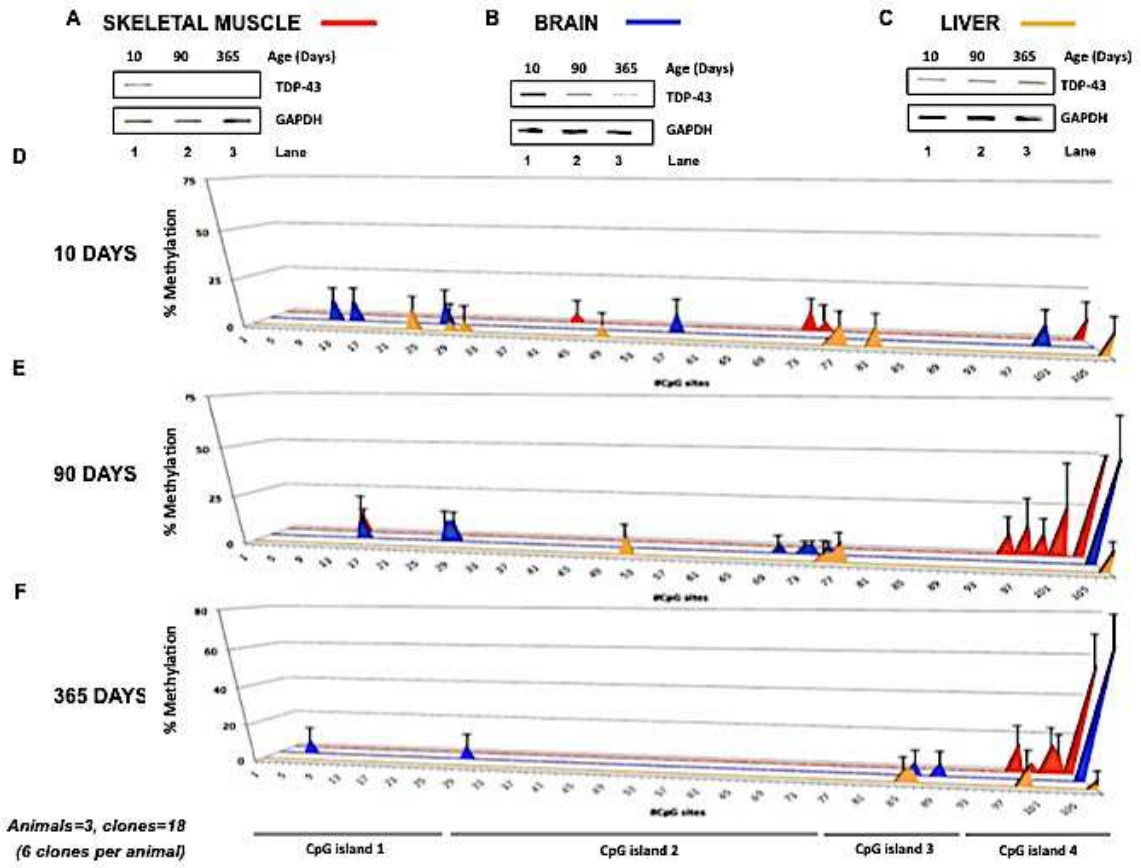

Figure 20. *TARDBP* promoter methylation levels show tissue- and developmental- stage specificity. A) Slot blot analysis showing TDP-43 protein levels (upper panel) in skeletal muscle from mice at 10, 90, 365 days. The bottom panel shows GAPDH signal as loading control. B) Slot blot analysis showing TDP-43 protein levels (upper panel) in brain from mice at 10, 90, 365 days. GAPDH is used as loading control (bottom panel). C) Slot blot analysis showing TDP-43 protein levels (upper panel) in liver from mice at 10, 90, 365 days. GAPDH is used as loading control D-F) Bisulfite sequencing analysis of the *TARDBP* promoter harbouring 108 CpG sites (represented in number on the x axis) in skeletal muscle (red line), brain (blue line), and liver (yellow line) at 10 days (D), 90 days (E), and 365 days (F). The % of methylation of each of the 108 CpG sites is shown with picks. Data are represented as mean ± S.D. from three animals (6 clones sequenced per each animal).

5. DNA demethylation increases TDP-43 expression in mouse motor neurons

In order to further explore the relationship between *TARDBP* promoter methylation and TDP-43 protein expression, we examined the effects of DNA demethylation on the expression of TDP-43 in mouse motor neurons by using 5-azacytidine. This compound is an azanucleoside that acts by inducing DNA demethylation. In fact, azacytidine can substitute for cytosine in the replication of the DNA and it is recognized by the DNA methyltransferases. After the initiation of the methylation reaction, the enzyme remains

covalently bound to the DNA and its DNA methyltransferase function is blocked. Prior to use this hypomethylating agent, we established the methylation status of the *TARDBP* promoter of the NSC-34 cell line. To do that, we extracted and converted genomic DNA form cells through bisulfite incubation. We then amplified the converted *TARDPB* promoter region with the primers described in the session 4 of the results, used for bisulfite analysis of mouse tissues. Interestingly, the methylation profile of the cells is consistent with that of the animals in which we found CpG dinucleotides significantly methylated in the case of brain and skeletal muscle of mice aged 90 and 365 days. In particular, in the mouse motor neurons, there is widespread and more pronounced methylation of almost all the CpG sites belonging to the fourth island. In fact, with the exception of not methylated dinucleotides in the sites #96, #97, #103, and #107, all the others are methylated in different degrees as follows: sites #93, #94, #95, #98, #99, #100, #102, #104, and #106 are methylated up to 10%, while the site #92 shows a percentage of methylation of around 17%. Increased methylation rate is detected in sites #101 and #105 exceeding the 25%. The CpG dinucleotide mostly targeted by this modification is the #108 with a methylation of up to 90% (**Figure 21A**).

Once established that the *TARDBP* promoter is methylated as described above, we next evaluated the effects on TDP-43 expression upon 5-azacitydine administration at both mRNA and protein levels. To do that, 5-azacytidine was added to the culture media at increasing concentration of 1 μM, 5 μM, and 10 μM. As already stated, this chemical analogue of the cytidine is able to inhibit the DNA methyltransferases enzymes, causing hypomethylation of DNA. After 48 and 72 hours of treatment, cells were harvested and total RNA and proteins were extracted. For the evaluation of the TDP-43 mRNA levels, real time RT-PCR has been performed. As shown in **Figure 21B**, the demethylating treatment significantly increased the TDP-43 mRNA in a dose- and time- dependent manner. In fact, the stronger effect is observed with higher concentration of drug and it is more evident at 72 hours (**Figure 21B**, black bars) compared to 48 hours (**Figure 21B**, grey bars) at any concentration used. For proteins analysis, the lysates were separated by SDS-PAGE and subsequently analysed by western blot using anti-TDP-43 antibody. Normalization has been performed using anti-GAPDH antibody. **Figures 21C** and **21D** show that also at protein level TDP-43 expression is increased upon 5-azacytidine treatment in a dose- and time- dependent manner. Indeed, there is an increasing gradient of protein expression from the not-treated cells to the highest drug dose-treated cells (**Figures 21C** and **21D**, from lane 1 to 4) and furthermore the effect on the expression is much more evident at 72 hours (**Figure 21D**, from lane 1 to 4). The bottom panels of **Figures 21C** and

20D are duplicates of protein expression analysis performed in biologically different 5-aza treated samples. These data suggest that DNA methylation might indeed play a role in controlling mRNA and protein expression of mouse TDP-43 in mouse motor neurons cells.

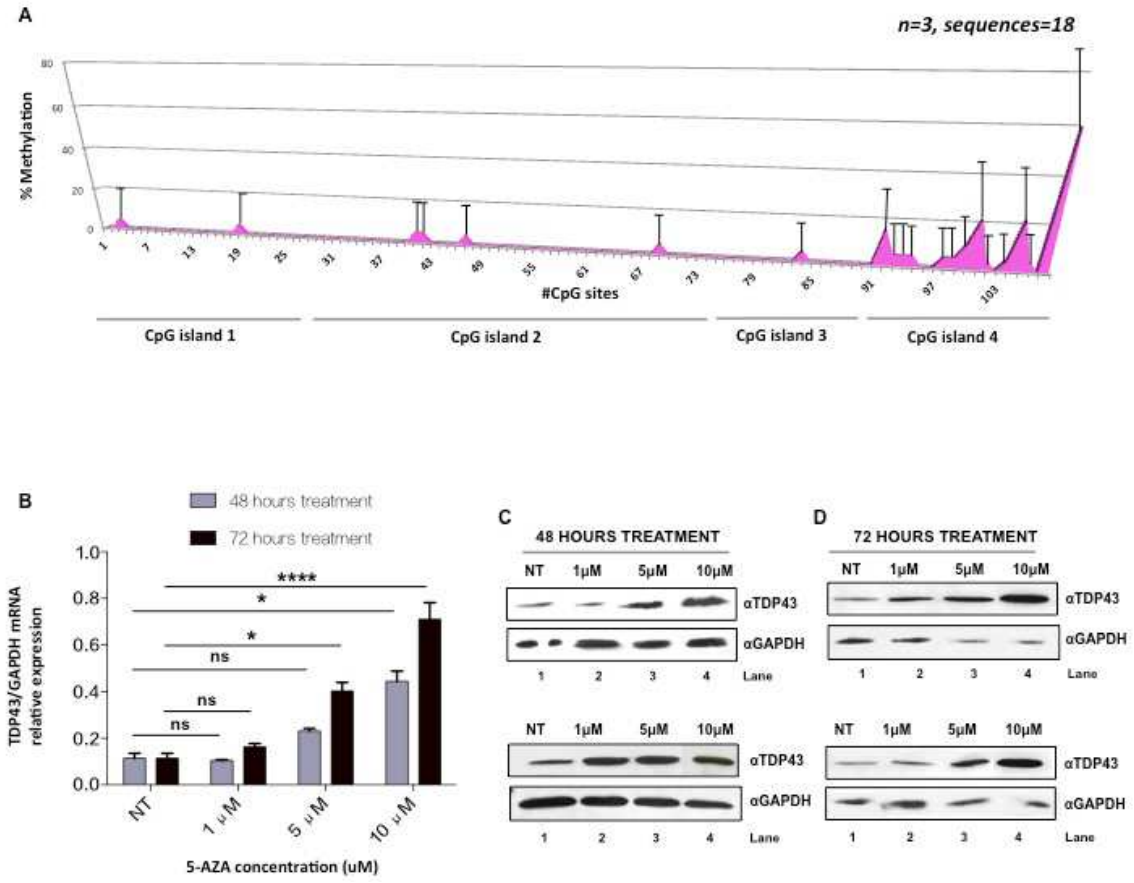

Figure 21. DNA demethylation increases TDP-43 expression in mouse motorneurons NSC34. A) Bisulfite sequencing analysis of the *TARDBP* promoter harbouring 108 CpG sites (represented in number on the x axis) in mouse motor neurons NSC34 cell line. B) Real-time PCR quantification of TDP-43 mRNA in NSC34 treated with 1 µM, 5 µM, and 10 µM of 5-azacitydine at 48 hours (grey bars) and 72 hours (black bars) . ns indicates p>0.05 (not significant), * indicates 0,01<p< 0,05, ** indicates 0,001<p<0,01. Error bars indicate SD calculated on three independent experiments. C) Western blot analysis showing TDP-43 levels (upper panels) in NSC34 cell line treated with 1 µM, 5 µM, and 10 µM of 5-azacitydine at 48 hours (left panels) and 72 hours (right panels). GAPDH (lower panels) is used as loading control.

6. *In vitro* DNA methylation decreases *TARDBP* mouse promoter activity in mouse motor neuron cells

Because it has been shown in the previous section that there is an increase in the TDP-43 expression at mRNA and protein level in condition of 5-azacytidine induced hypomethylation, we decided to go further in the investigation by studying whether the opposite condition of DNA hypermethylation was important for modulating the transcriptional activity of the core promoter of the mouse *TARDBP*. To do this, we either

in vitro methylated or not methylated a Luciferase reporter-containing plasmids fused with the promoter regions of interest and then 24 hours upon transfection we measured the promoter activity via Luciferase transcript quantification. Since previous *in silico* analysis revealed a prediction of the region critical for the transcriptional activity of *TARDBP* promoter, as first we cloned this region (the same analysed by the bisulfite technique) included between nucleotide positions -562 and +1172 (relative to the Transcription Start Site) upstream of the Luciferase synthetic reporter gene (Lucia) of the CpG-free-basic Lucia vector generating the construct named "*TARDBP* minimal promoter" (**Figure 22A**). To examine the effects of DNA methylation, the construct has been subjected to *in vitro* DNA methylation by the methyltransferase SssI and then co-transfected with the expression vector β-galactosidase (which will be used as transfection normalizer) into mouse motor neuron NSC34 cells. After 24 hours of transfection, cells were harvested and total RNA was extracted. To evaluate the influence of the methylation on the promoter activity, the Luciferase mRNA levels of expression have been evaluated by quantitative real time RT-PCR in both samples transfected with methylated or not-methylated constructs. As shown in **Figure 22B**, the *in vitro* DNA methylation before transfection reduced 5 fold *TARDBP* minimal promoter (bisulfite analysed sequence) activity in respect to the not methylated promoter. Since it has been demonstrated that the alternative splicing of around 22% of exons is regulated by DNA methylation, we included in the analysis an additional construct carrying the *TARDBP* promoter sequence with the following closest canonical splice site included (**Figure 22A**) in order to consider any alteration of the system induced by methylation and splicing. To do that, we generated a construct called "*TARDBP* extended promoter" harbouring the same promoter sequence correspondent to the region analysed by bisulfite and previously described above in this section, with the addiction of the downstream region including the 3' splice site of the intron 1 of the *TARDBP* gene and 14 nucleotides of exon 2 ending before the ATG (**Figure 22A**). The total fragment spanned the region from nucleotide -562 to +1403 (+1 is the TSS). As described above, *in vitro* methylation followed by transfection in mouse motor neuron cells has been performed as well with the construct "*TARDBP* extended promoter" and also in this case the promoter activity has been evaluated through quantitative real time RT-PCR on the Luciferase transcript normalized against β-galactosidase. Similarly to the previous construct, also in this case the activity of the methylated promoter is drastically reduced if compared with the demethylated one (**Figure 22B**).

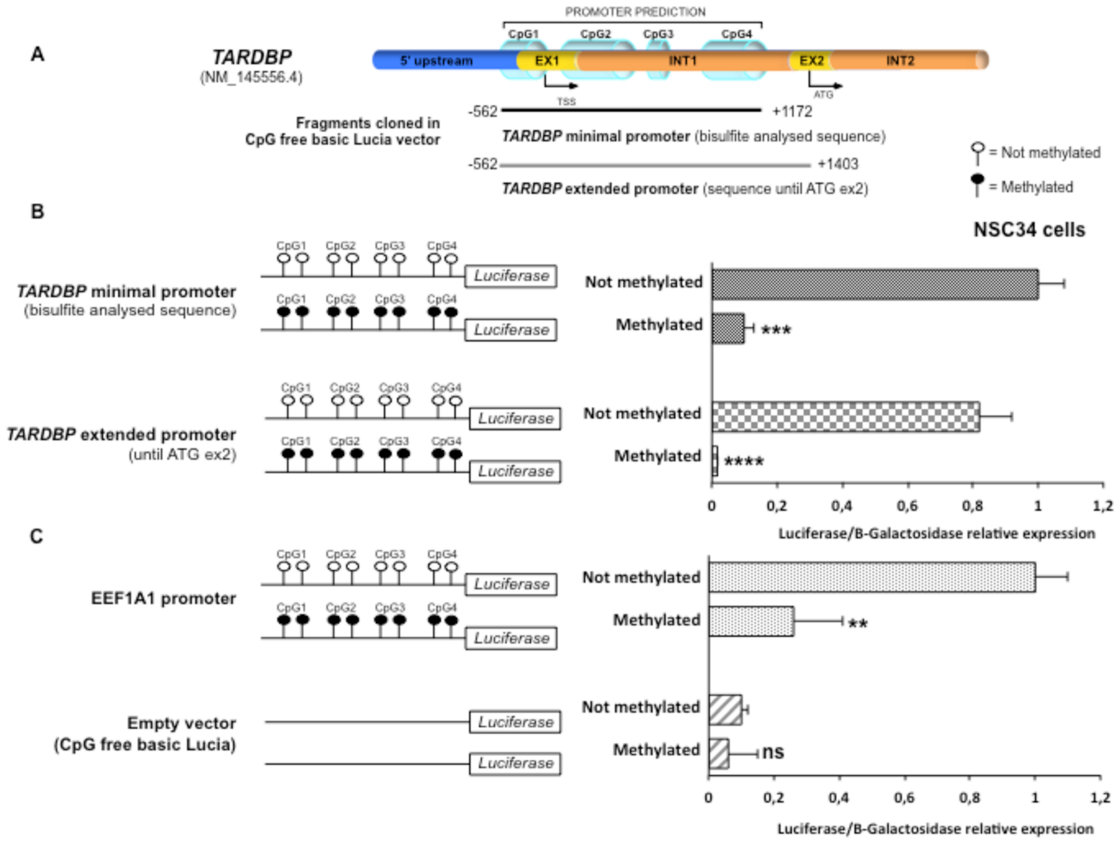

Figure 22. DNA methylation in vitro of the *TARDBP* mouse promoter decreases its activity. A) Representation of the CpG free- *TARDBP* minimal promoter construct (*TRADBP* promoter fragment from -562bp to +1172bp cloned upstream the Lucia reporter gene in the CpG free-basic lucia vector) and of the CpG free- *TARDBP* extended promoter construct (*TRADBP* promoter fragment from -562bp to +1403bp cloned upstream the Lucia reporter gene in the CpG free-basic lucia vector) B) Real-time PCR quantification of Lucia mRNA upon either methylation *in vitro* or not methylation in the two constructs named "*TARDBP* minimal promoter" and "*TARDBP* extended promoter". ns indicates p>0.05 (not significant), * indicates 0,01<p< 0,05, ** indicates 0,001<p<0,01. Error bars indicate SD calculated on three independent experiments. C) Real-time PCR quantification of Lucia mRNA upon either methylation *in vitro* or not methylation in the positive control construct construct named "*EEF1A1* promoter" and of the empty vector CpG free basic Lucia. ns indicates p>0.05 (not significant), * indicates 0,01<p< 0,05, ** indicates 0,001<p<0,01. Error bars indicate SD calculated on three independent experiments.

As positive control for the *in vitro* methylation reaction the promoter sequence of the Elongation Factor A1 (*EEF1A1*), that is known to be an imprinting-gene regulated through methylation, was cloned upstream of the Luciferase reporter gene of the CpG-free-basic Lucia vector. As expected, the activity of the positive control vector was markedly affected by *in vitro* DNA methylation, indicating that the *in vitro* reaction was correctly performed (**Figure 22C**). Furthermore, for all the constructs analysed, the promoter activity was significantly higher than the activity of the empty vector alone, which did not show significant variations when methylated **(Figure 22C)**, indicating that the backbone of the constructs studied was not altering anyhow the activity of the promoter of interest. Thus,

the changes observed between the methylated or not-methylated constructs are exclusively attributable to the promoter cloned sequence. As a consequence our data confirms that the differential status of methylation of the *TARDBP* promoter is particularly important for the regulation of the *TARDBP* gene transcription in mouse motor neuron cells.

7. Mutagenesis of specific CpG sites in the *TARDBP* fourth island induces changes in the promoter activity

Previous results from bisulfite analysis in both animal tissues and mouse motor neuron cells revealed that there are single and specific CpG units of the fourth island of the *TARDBP* promoter preferentially affected by DNA methylation. To characterize in more detail whether methylation events targeting specific CpG sites could modulate the promoter activity, we mutagenized groups of specific CpG sites of the fourth island (CpG dinucleotide was mutated into CpA) in order to prevent methylation and then we looked at the promoter activity. To do that, we used as a backbone the construct named *"TARDBP* extended promoter*"* containing the wild type mouse *TARDBP* promoter cloned upstream of the Luciferase in the CpG-free basic-Lucia vector and described before (Session 6 of the Results) (**Figure 23A**). Taking advantage of this backbone construct, we substituted the fourth island of the wild type promoter with different fragments of synthetic DNA in which specific groups of CpG sites were mutated in CpA sites and as follows: 1) Fragment 1 contains CpG mutated sites #92, 93, 94 and 95; 2) Fragment 2 with CpG mutated sites #96, 97, and 98; 3) Fragment 3 harbouring the CpG mutated sites #99, 100, 101, 102, and 103; 4) Fragment 4 with CpG mutated sites #104, 105, 106, 107, and 108 (**Figure 23B**). Lastly, we made another construct in which we substituted the fourth island with the Fragment 5 in which we mutated the CpG sites that we found significantly methylated in the mouse tissues, i.e. CpG #99, 101, 103, 105, and 108 (**Figure 23B**).

Then, the plasmids along with the expression vector for β -galactosidase were transfected in mouse motor neuron NSC34 cell line. After 24 hours of transfection, cells were harvested and total RNA was extracted. To evaluate the promoter activity, we assessed the relative expression of Luciferase using β-galactosidase as normaliser by quantitative real time RT-PCR using specific oligonucleotides targeting the two transcripts. **Figure 24** shows that when the CpG sites from #92 to #95 (**Figure 24B**), from #96 to #98 (**Figure 24C**), and from #99 to #103 (**Figure 24D**) are mutagenized, the promoter activity is comparable to the wild type. On the other hand, by mutating the CpG units belonging to the last part of the island from #104 to #108 (**Figure 24E**) the functionality of the promoter

is moderately increased in comparison to the wild type in a statistically significant manner. Furthermore, no changes in respect to the wild type have been observed in presence of mutated CpG sites #99, 101, 103, 105, and 108 (**Figure 24F**). Lastly, for all the constructs analysed, the promoter activity was significantly higher than the activity of the promoter-less backbone of the vector, which showed negligible activity **(Figure 24G)**.

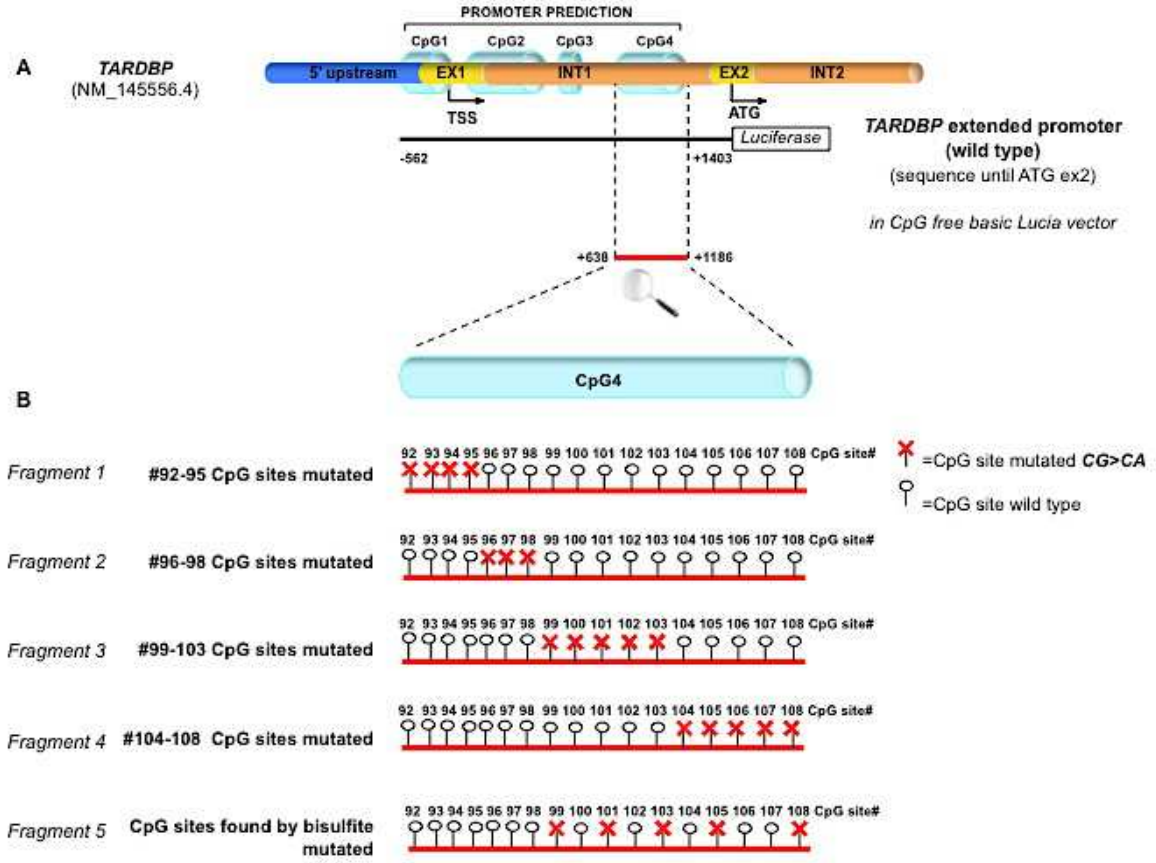

Figure 23. Mutagenesis of specific CpG sites of the fourth island. A) Representation of the CpG free- *TARDBP* extended promoter construct (*TARDBP* promoter fragment from -562bp to +1403bp cloned upstream the Lucia reporter gene in the CpG free-basic lucia vector). B) Representation of the fragments used to substitute the CpG4 island. Fragment 1 contains CpG sites mutated from #92 to #95. Fragment 2 contains CpG sites mutated from #96 to #98. Fragment 3 contains CpG sites mutated from #99 to #103. Fragment 4 contains CpG sites mutated from #104 to #108. Fragment 5 contains CpG sites mutated #99, 101, 103, 105, and 108.

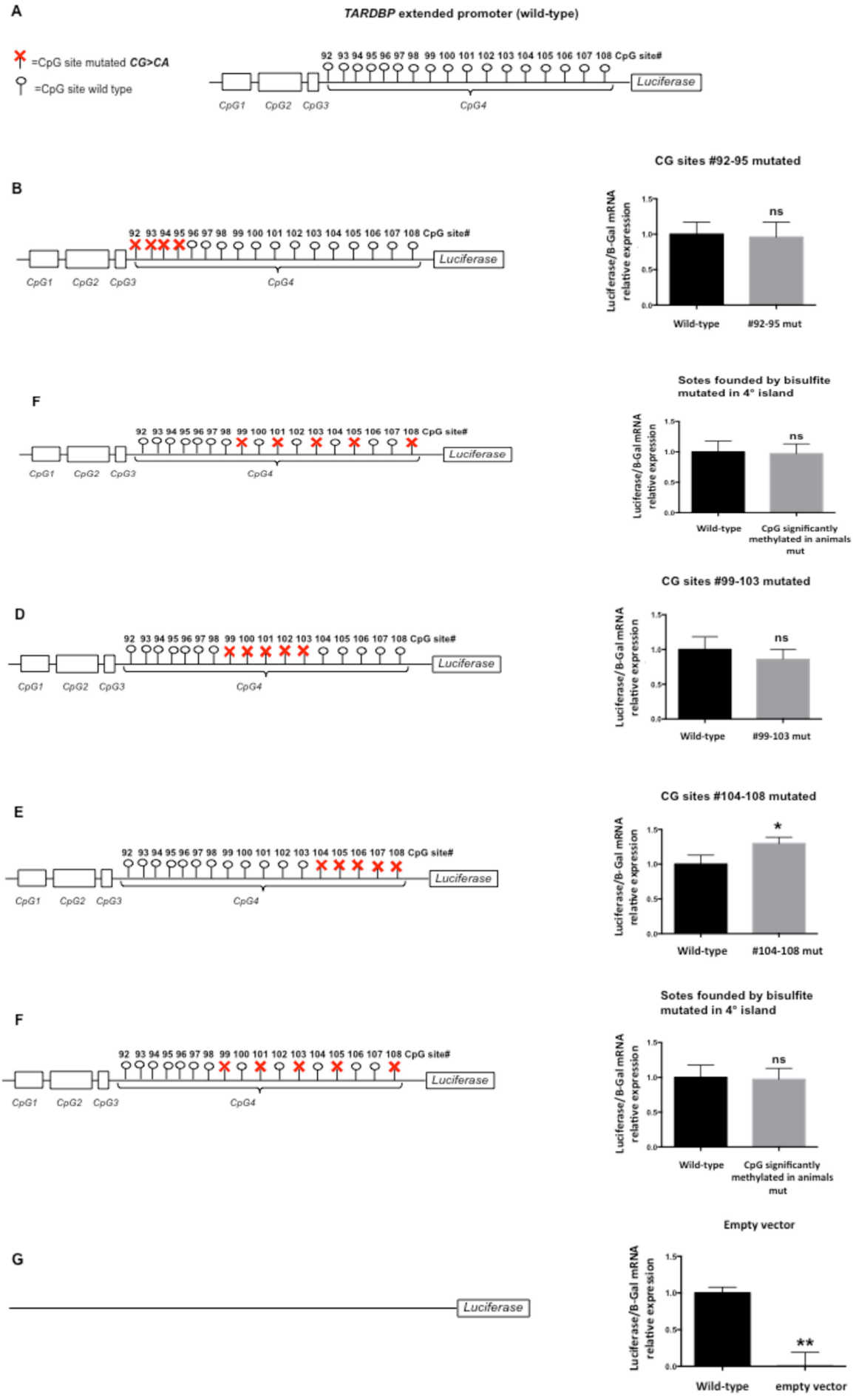
A
TARDBP extended promoter (wild-type)
=CpG site mutated CG>CA
=CpG site wild type
92 93 94 95 96 97 98 99 100 101 102 103 104 105 106 107 108 CpG site#
Luciferase
CpG1 CpG2 CpG3 CpG4
B
CG sites #92-95 mutated
Luciferase/B-Gal mRNA relative expression
ns
Wild-type
#92-95 mut
F
Sotes founded by bisulfite mutated in 4° island
ns
Wild-type
CpG significantly methylated in animals mut
D
CG sites #99-103 mutated
ns
Wild-type
#99-103 mut
E
CG sites #104-108 mutated
*
Wild-type
#104-108 mut
F
Sotes founded by bisulfite mutated in 4° island
ns
Wild-type
CpG significantly methylated in animals mut
G
Empty vector
**
Wild-type
empty vector

Figure 24. Mutagenesis of specific CG sites of the CpG4 island induces changes in the promoter activity. A) Representation of the CpG free- *TARDBP* extended promoter construct (*TARDBP* promoter fragment from -562bp to +1403bp cloned upstream the Lucia reporter gene in the CpG free-basic lucia vector). B) On the left is shown a representation of the CpG free- *TARDBP* extended promoter construct (*TARDBP* promoter fragment from -562bp to +1403bp cloned upstream the Lucia reporter gene in the CpG free-basic lucia vector) with the fourth island substituted with the fragment 1 (CpG sites mutated from #92 to #95). Panel on the right shows real-time PCR quantification of Lucia mRNA upon transfection of the wild type and mutant construct (CpG4 island substituted with the Fragment 1). ns indicates p>0.05 (not significant), * indicates 0,01<p< 0,05, ** indicates 0,001<p<0,01. Error bars indicate SD calculated on six independent experiments. C) On the left is shown a representation of the CpG free- *TARDBP* extended promoter construct (*TARDBP* promoter fragment from -562bp to +1403bp cloned upstream the Lucia reporter gene in the CpG free-basic lucia vector) with the fourth island substituted with the fragment 2 (CpG sites mutated from #96 to #98). Panel on the right shows real-time PCR quantification of Lucia mRNA upon transfection of the wild type and mutant construct (CpG4 island substituted with the Fragment 2). ns indicates p>0.05 (not significant), * indicates 0,01<p< 0,05, ** indicates 0,001<p<0,01. Error bars indicate SD calculated on six independent experiments. D) On the left is shown a representation of the CpG free- *TARDBP* extended promoter construct (*TARDBP* promoter fragment from -562bp to +1403bp cloned upstream the Lucia reporter gene in the CpG free-basic lucia vector) with the fourth island substituted with the fragment 3 (CpG sites mutated from #99 to #103). Panel on the right shows real-time PCR quantification of Lucia mRNA upon transfection of the wild type and mutant construct (CpG4 island substituted with the Fragment 3). ns indicates p>0.05 (not significant), * indicates 0,01<p< 0,05, ** indicates 0,001<p<0,01. Error bars indicate SD calculated on six independent experiments. E) On the left is shown a representation of the CpG free- *TARDBP* extended promoter construct (*TARDBP* promoter fragment from -562bp to +1403bp cloned upstream the Lucia reporter gene in the CpG free-basic lucia vector) with the fourth island substituted with the fragment 4 (CpG sites mutated from #103 to #108). Panel on the right shows real-time PCR quantification of Lucia mRNA upon transfection of the wild type and mutant construct (CpG4 island substituted with the Fragment 4). ns indicates p>0.05 (not significant), * indicates 0,01<p< 0,05, ** indicates 0,001<p<0,01. Error bars indicate SD calculated on six independent experiments. F) On the left is shown a representation of the CpG free- *TARDBP* extended promoter construct (*TARDBP* promoter fragment from -562bp to +1403bp cloned upstream the Lucia reporter gene in the CpG free-basic lucia vector) with the fourth island substituted with the fragment 5 (CpG sites mutated #99, 101, 103, 105, 108). Panel on the right shows real-time PCR quantification of Lucia mRNA upon transfection of the wild type and mutant construct (CpG4 island substituted with the Fragment 5). ns indicates p>0.05 (not significant), * indicates 0,01<p< 0,05, ** indicates 0,001<p<0,01. Error bars indicate SD calculated on six independent experiments. G) On the left is represented the empty vector structure. On the right is shown the real-time PCR quantification of Lucia mRNA upon transfection of the wild type and empty vector constructs. ns indicates p>0.05 (not significant), * indicates 0,01<p< 0,05, ** indicates 0,001<p<0,01. Error bars indicate SD calculated on six independent experiments.

In summary, by mutating the CpG sites in the first part of the fourth island (from #92 to #95; from #96 to #98; and from #99 to 103), the methylation is allowed in the second half of the island and in this condition it is observed a promoter activity similar to the wild type. The promoter activity remains unchanged also when CpG sites methylated in mouse tissues (#99, 101, 103, 105, and 108) are mutated. By contrast, once the methylation of all the CpG units belonging to the last part of the island (from #104 to #108) is prevented by the mutagenesis, the promoter function is increased. It is important to note that the CpG sites mostly subjected to methylation during aging in mouse tissues in which the TDP-43

expression decreases during time, are the #105 and #108, which indeed are localised in the fourth island region that gives rise to TDP-43 increased level when methylation is prevented via mutagenesis of the CpG sites.

The data indicates that the CpG sites located in the last part of the fourth island of the *TARDBP* mouse promoter are important in the modulation of the promoter activity through methylation.

8. TDP-43 time and tissue specific regulation is a conserved phenomenon between fly, zebrafish, and mouse

Then, we went further in the investigation of the mechanism underlying the TDP-43 tissue and time specific regulation by considering its expression during aging in *Drosophila* and zebrafish, that are two species representing farther points in the evolutionary scale in respect to mouse (**Figure 25A**). This has been done to deepen the degree of conservation of the phenomena during the evolution and hence the importance of this process. For the comparison between mouse and *Drosophila* we evaluated the trend of expression of TDP-43/TBPH (*Drosophila* orthologous of TDP-43) in brain over time, while for zebrafish we isolated the entire head because of difficulties in isolating brain due to size (in the 6 days post-fertilization case) and tissue consistency limitations. We extracted total RNA from brain of mice aged 10 and 90 days, from *Drosophila* aged 1, 7, and 14 days brains and from 6 and 60 days post-fertilization zebrafish heads. Then, reverse transcription (RT) and real time qPCR have been performed to detect TDP-43/TBPH transcript. In mouse and zebrafish, TDP-43 mRNA levels were normalized with the housekeeping gene GAPDH, while in *Drosophila* TBPH normalization has been done using Rpl-11. As it can be seen in **Figures 25B, 25C** and **25D,** TDP-43/TBPH mRNA levels decrease during aging in all the three wild type organisms tissues. Furthermore, the drop of the mRNA levels measured in aged flies in respect to the young correspond to the same trend observed to occur from 10 to 90 days in mouse and from 6 to 60 days in zebrafish.

Next we wanted to compare in the different organisms the expression of TDP-43 during aging in skeletal muscle. Due to the difficulties in the isolation of skeletal muscle in *Drosophila* , we decided to precede comparing mouse and zebrafish. For this purpose, we used mice aged 10 and 90 days as previously done, and zebrafish at 6 and 60 days post-fertilization. In the case of zebrafish, we used the entire tail for the analysis as preliminary data revealed that the contribution in terms of TDP-43 expression given by the cartilage system of the tail was negligible. After total RNA extraction from mouse and zebrafish

samples, we performed reverse transcription (RT) and quantitative real-time qPCR to detect TDP-43 transcript. Consistently, the results shown in **Figures 25E** and **25F** show that TDP-43 mRNA strongly decreases during time both in mouse skeletal muscle (as already shown) and in zebrafish tail. Regarding liver, the isolation of the tissue from the 6 days zebrafish resulted to be problematic and we are studying ways to collect isolated liver samples from this stage not contaminated by other tissues. This work will be completed soon.

So far, our data strengthen the hypothesis that the tissue- and age- specificity of TBPH/TDP-43 levels regulation is an evolutionary conserved feature.

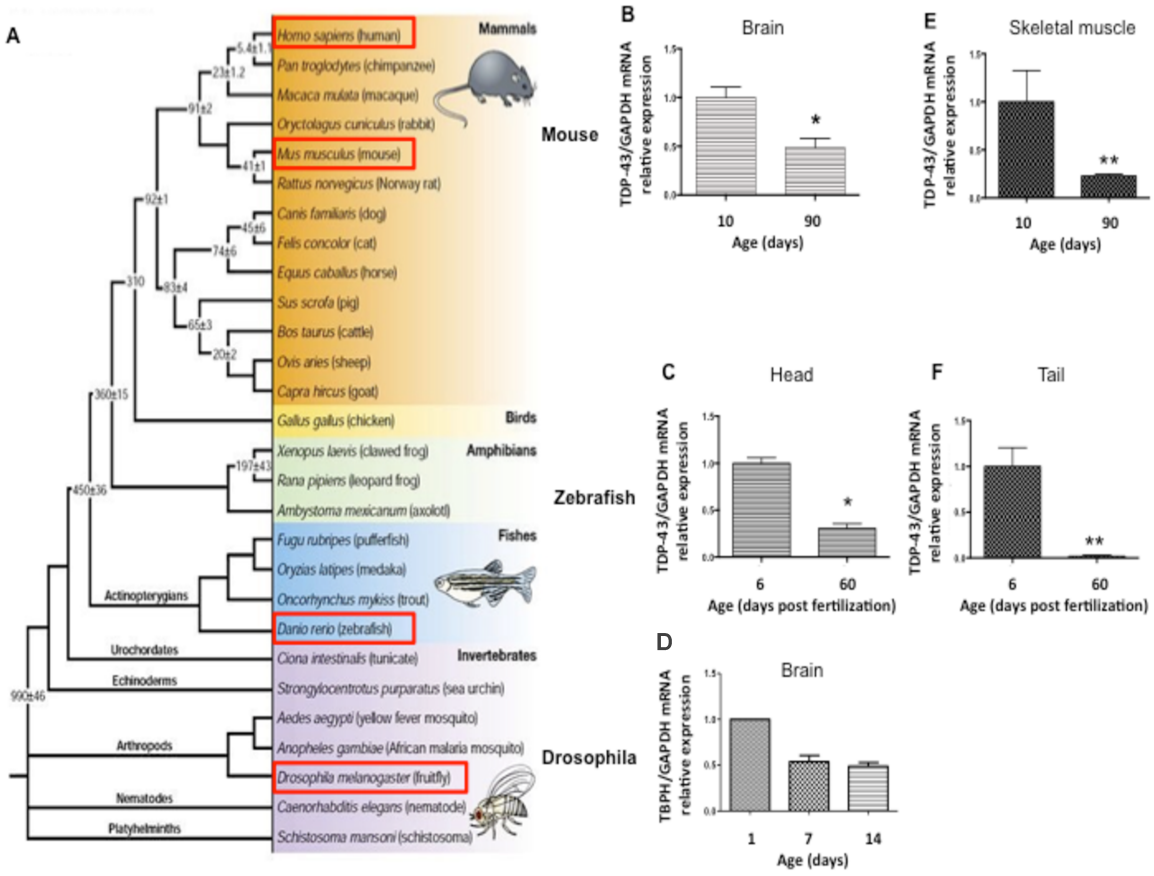

Figure 25. TDP-43 time and tissue specific regulation is a conserved phenomenon between fly, zebrafish and mouse. B) Real-time PCR quantification of mouse brain TDP-43 mRNA at 10 and 90 days. ns indicates p>0.05 (not significant), * indicates 0,01<p< 0,05, ** indicates 0,001<p<0,01. Error bars indicate SD calculated on three independent experiments. C) Real-time PCR quantification of Zebrafish head TDP-43 mRNA at 6 and 60 days post fertilization. ns indicates p>0.05 (not significant), * indicates 0,01<p< 0,05, ** indicates 0,001<p<0,01. Error bars indicate SD calculated on three independent experiments. D) Real-time PCR quantification of Drosophila brain TDP-43 mRNA at 1, 7, and 14 days. ns indicates p>0.05 (not significant), * indicates 0,01<p< 0,05, ** indicates 0,001<p<0,01. Error bars indicate SD calculated on three independent experiments. E) Real-time PCR quantification of mouse skeletal muscle TDP-43 mRNA at 10 and 90 days. ns indicates p>0.05 (not significant), * indicates 0,01<p< 0,05, ** indicates 0,001<p<0,01. Error bars indicate SD calculated on three independent experiments. F) Real-time PCR quantification of Zebrafish tail TDP-43

mRNA at 6 and 60 days post fertilization. ns indicates p>0.05 (not significant), * indicates 0,01<p< 0,05, ** indicates 0,001<p<0,01. Error bars indicate SD calculated on three independent experiments.

9. TDP-43 trends of expression during aging are similar between mouse and human in liver and stomach

Previous analysis on the conservation of the TDP-43 tissue- and time- specific mechanism of regulation suggested that it is evolutionarily conserved between mouse, zebrafish and fly. To deepen the degree of conservation of the phenomena and in order to evaluate if the same mechanism could be also ascribed to humans, we moved our analysis in human tissues to perform a comparison with mouse.

The extension of these studies to human was problematic for ethical and logistic reasons and we managed to obtain fairly good biopsy samples from bariatric surgery. Because of the difficulty to have access to skeletal muscle human biopsies, we decided to move from skeletal muscle (as done in previous analysis) to stomach muscle since, as well as liver, was an available tissue from our collaborators. This decision was conforted by the observation of a sharp decay of TDP-43 levels in mouse stomach muscle that was similar to the decay observed to occur in the skeletal muscle. In fact, in both the muscle typology analysed TDP-43 decreases from 10 days to 1 year both at protein (**Figures 26A** and **26C**) and RNA levels (**Figures 26B** and **26D**).

In order to allow an appropriate comparison of TDP-43 levels between mouse and human tissues during aging we analysed the life phase equivalencies between the two organisms and assessed that mouse aged 10 days corresponds to an individual aged around 4 years, a 90 days aged mouse corresponds to 20 years old individual and that 1 year old mouse corresponds to 43 years old individual (**Figures 27A** and **27B**). Because human samples from our medical collaborators were widely variable about time points, we grouped them into windows of aging as illustrated in the time line of the **Figure 27B**. In particular, we could not have access to samples from individuals aged less than 19 years old; hence we had not the human correspondent to 10 days aged mice. We then grouped all the samples from individuals who range in age from 19 to 30 and compare them with 90 days mice. In the case of 1 years old mice, the comparison has been performed with the group of human individuals ranging from 41 to 50 years. Moreover, we had access to other three groups of human samples pooled as follows: from 31 to 40, from 51 to 60, and more than 61 years old. Even though we did not have the availability of mice samples correspondent to these last three human time windows, we decided to include them into the analysis as well

because this is a study made to investigate TDP-43 behaviour occurring over time and the overlapping windows covered by the samples coming from the two different species were big enough to allow us a reliable comparison.

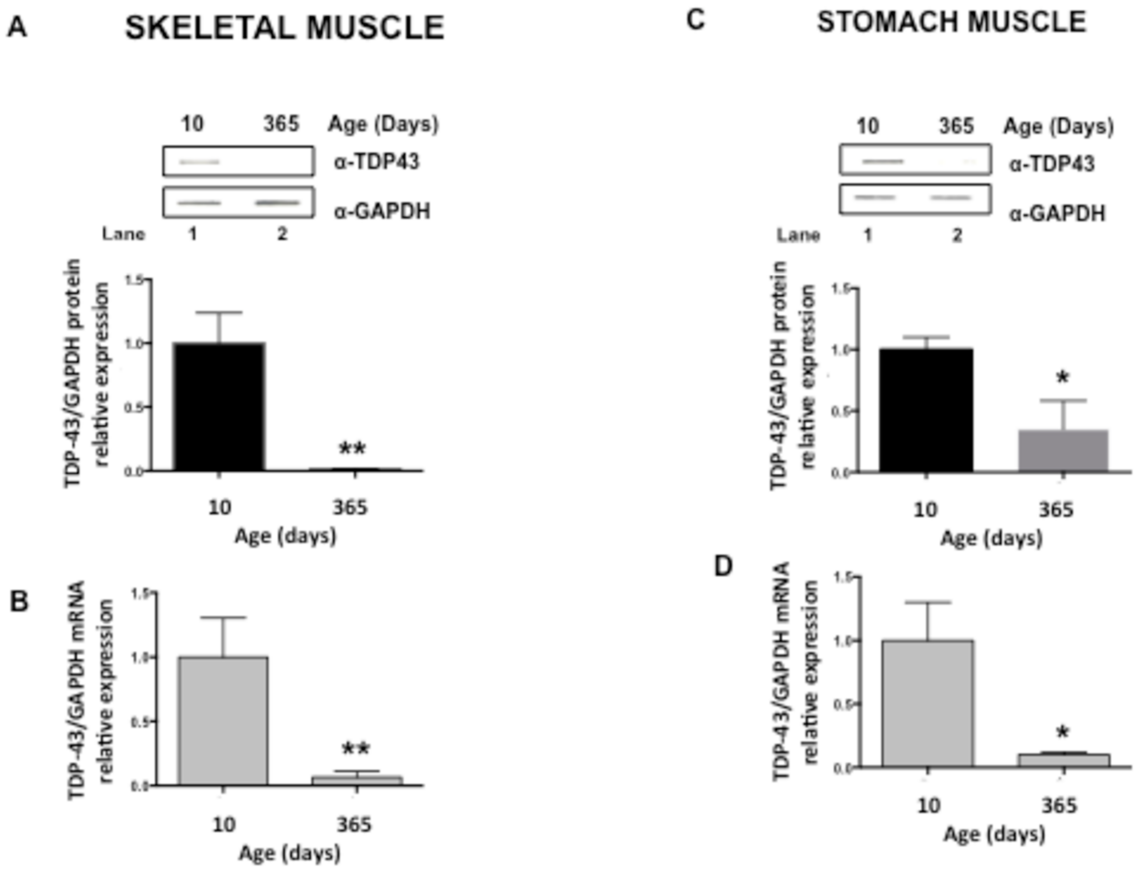

Figure 26. Comparison of mouse TDP-43 expression in different muscle typologies. A) The upper panel is a slot blot analysis showing TDP-43 levels from mouse skeletal muscle aged 10, and 365 days. The lower panel shows GAPDH detection as loading control. The histogram below shows the ImageJ quantification of TDP-43 expression levels normalized with GAPDH. Error bars indicate SD calculated on three independent experiments. B) The graph shows real-time PCR quantification of mouse skeletal muscle TDP-43 mRNA at 10, and 365 days. ns indicates $p>0.05$ (not significant), * indicates $0,01<p< 0,05$, ** indicates $0,001<p<0,01$. Error bars indicate SD calculated on three independent experiments. C) The upper panel is a slot blot analysis showing TDP-43 levels from mouse stomach muscle aged 10, and 365 days. The lower panel shows GAPDH detection as loading control. The histogram below shows the ImageJ quantification of TDP-43 expression levels normalized with GAPDH. Error bars indicate SD calculated on three independent experiments. D) The graph shows real-time PCR quantification of mouse stomach muscle TDP-43 mRNA at 10, and 365 days. ns indicates $p>0.05$ (not significant), * indicates $0,01<p< 0,05$, ** indicates $0,001<p<0,01$. Error bars indicate SD calculated on three independent experiments

We then extracted proteins from liver and stomach from human individuals aged between 19-30, 31-40, 41-50, 51-60, and >61 years old and fixed the extract on a nitrocellulose membrane by slot blot. After this, TDP-43 level was assessed for each sample by using a specific polyclonal antibody anti-TDP-43. The same has been done for liver and stomach

muscle from mice aged 10 and 365 days. As shown in **Figure 28A** in human liver in every time point considered TDP-43 expression is sustained and constant (**Figure 28A**, lanes from 1 to 5). On the other hand, in human stomach muscle the protein is subjected to a decrease from 22 to 61 years old (**Figure 28C**, compare lanes 1 and 2). Similarly to human, in the mouse liver the protein is constantly expressed at 10 and 365 days (**Figure 28B**, compare lanes from 1 to 2), while it drastically drops from 10 to 365 days in the stomach muscle (**Figure 28D,** compare lanes 1 and 2). Below each representative blot in **Figure 28**, we showed the ImageJ quantification (normalized using GAPDH) with standard deviations relative to three experiments for each tissue (**Figures 28A, 28B, 28C,** and **28D,** lower panels), with the exception of the human liver for which we had six replicates.

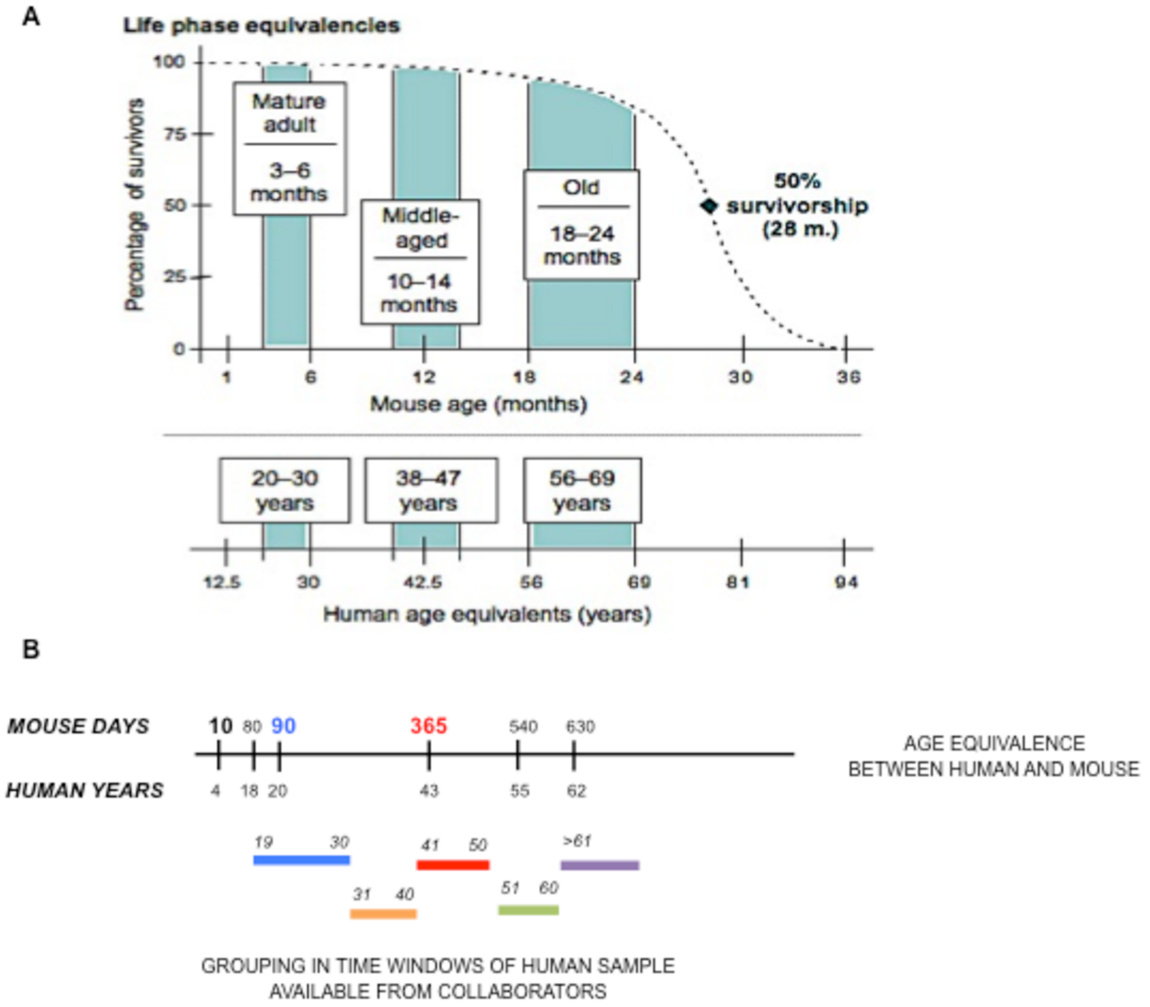

Figure 27. Age equivalence between human and mouse and human samples grouping. A) Representative age ranges for mature life history stages in mice compared with human being. The upper curve is representative of the mouse life and time points are expressed in months. In the lower part of the image are indicated the ranges of the human life span expressed in years. B) Age equivalences between human and mouse. In the upper part is represented a time line indicating the mouse time points (days) corresponding to the human years. In the lower part, coloured fragments indicate the groups of human individuals available for sampling.

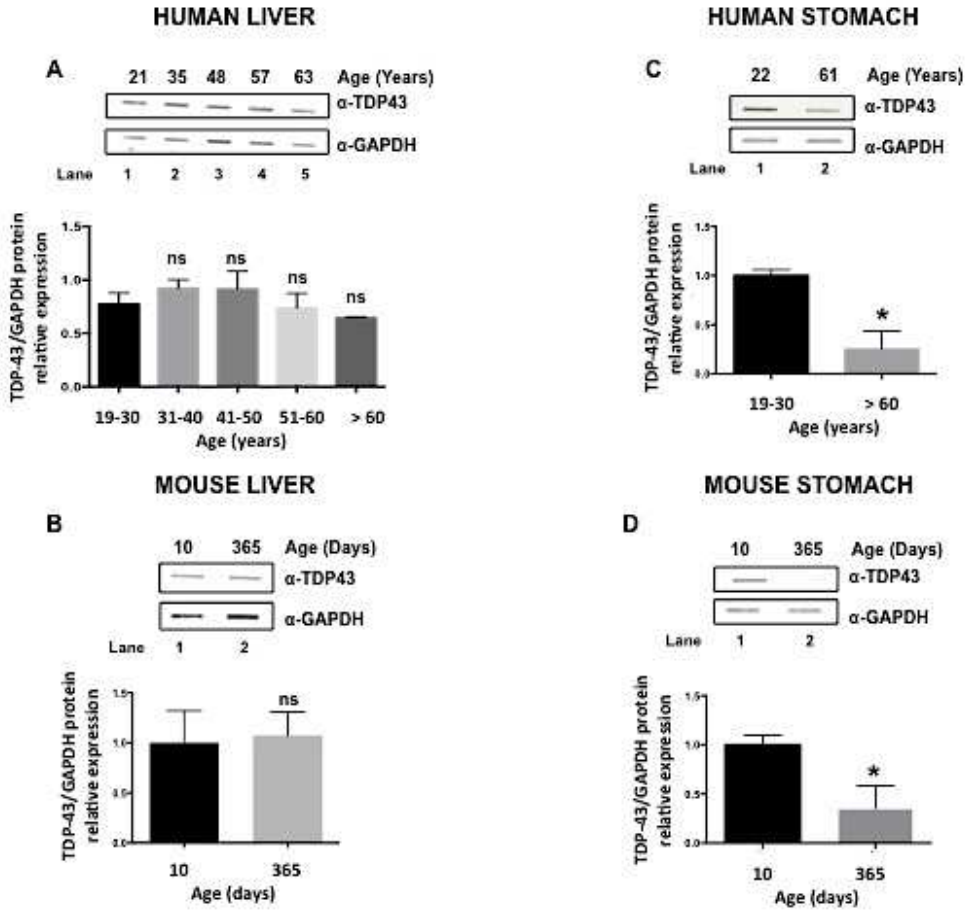

Figure 28. TDP-43 protein trends of expression during aging are similar between mouse and human in liver and stomach. A) The upper panel is a slot blot analysis showing TDP-43 levels from human liver aged 21, 35, 48, 57, and 63 years. The lower panel shows GAPDH detection as loading control. The histogram below shows the ImageJ quantification of TDP-43 expression levels normalized with GAPDH. Error bars indicate SD calculated on three independent experiments. B) The upper panel is a slot blot analysis showing TDP-43 levels from mouse liver aged 10, and 365 days. The lower panel shows GAPDH detection as loading control. The histogram below shows the ImageJ quantification of TDP-43 expression levels normalized with GAPDH. Error bars indicate SD calculated on three independent experiments. C) The upper panel is a slot blot analysis showing TDP-43 levels from human stomach aged 22 and 61 years. The lower panel shows GAPDH detection as loading control. The histogram below shows the ImageJ quantification of TDP-43 expression levels normalized with GAPDH. Error bars indicate SD calculated on three independent experiments. D) The upper panel is a slot blot analysis showing TDP-43 levels from mouse stomach aged 10, and 365 days. The lower panel shows GAPDH detection as loading control. The histogram below shows the ImageJ quantification of TDP-43 expression levels normalized with GAPDH. Error bars indicate SD calculated on three independent experiments.

We further compared human and mouse TDP-43 trends of expression in liver and stomach during aging at transcriptional level. For this purpose we extracted total RNA from human liver samples belonging to the window 19-30 years old individuals, 41-50, and <61 years

old. On the other hand we extracted RNA from human stomach muscle samples belonging to the age window of 19-30 and >61 years old. We then performed reverse transcription (RT) and Real time qPCR targeting TDP-43 transcript. TDP-43 mRNA levels were normalized with the housekeeping gene GAPDH. As shown in **Figure 29** we could observe a constant expression in liver (**Figure 29A**) and a decrease occurring over time in the stomach muscle (**Figure 29C**). In both the tissues analysed the mRNA levels measured follow the protein trends (**Figures 29A** and **29C**). In parallel we extracted total RNA from mouse liver (10, 90, and 365 days) and mouse stomach muscle (10 and 365 days) and after reverse transcription (RT), we performed a real time qPCR to detect TDP-43 transcript. TDP-43 mRNA levels were quantified and normalized with the housekeeping gene GAPDH. As shown in **Figures 29B** and **29D** the mRNA level was constant during time in the liver while it decreased from 10 to 365 days in the stomach muscle, as observed in human. Also in this case, mRNA level follows the protein trend of expression in all the tissues considered.

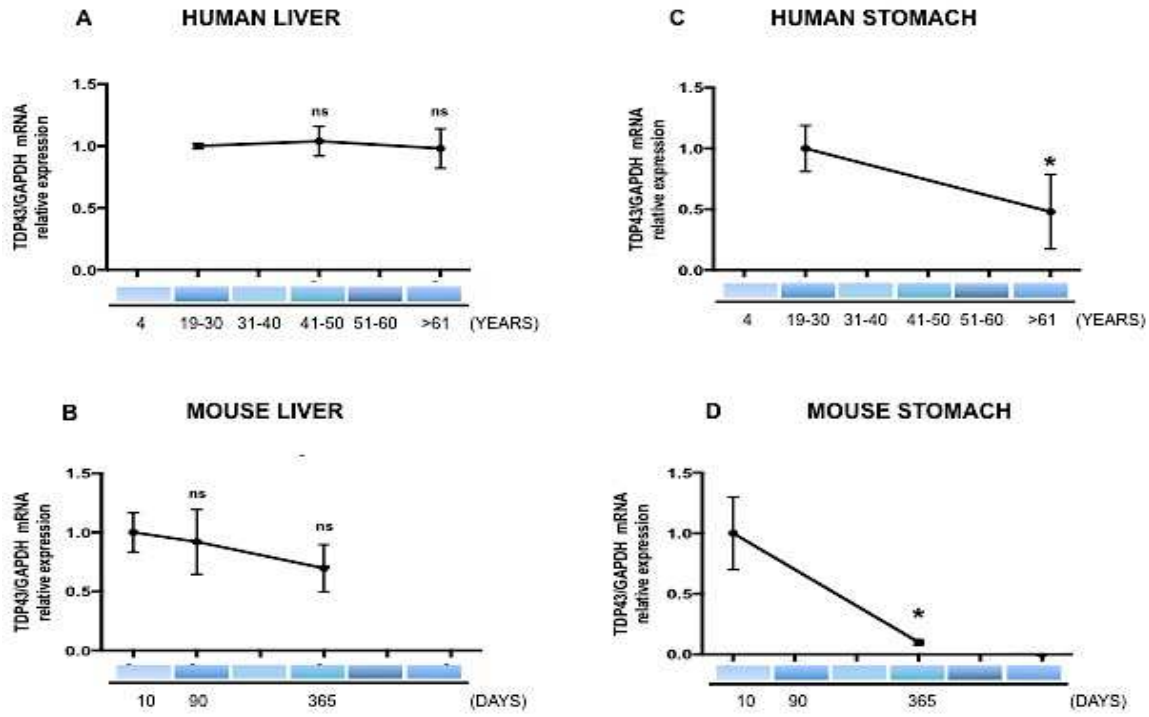

Figure 29. TDP-43 mRNA trends of expression during aging are similar between mouse and human in liver and stomach. A) Graph showing real-time PCR quantification of human liver TDP-43 mRNA at 21, 48, and 63 years. ns indicates p>0.05 (not significant), * indicates 0,01<p< 0,05, ** indicates 0,001<p<0,01. Error bars indicate SD calculated on three independent experiments. B) Graph showimg real-time PCR quantification of mouse liver TDP-43 mRNA at 10, 90, and 365 days. ns indicates p>0.05 (not significant), * indicates 0,01<p< 0,05, ** indicates 0,001<p<0,01. Error bars indicate SD calculated on three independent experiments.C) Graph shows real-time PCR quantification of human stomachTDP-43 mRNA at 22 and 61 years. ns indicates p>0.05 (not significant), * indicates 0,01<p< 0,05, ** indicates 0,001<p<0,01. Error bars indicate SD calculated on three independent experiments. D) Graph showing real-time PCR quantification of mouse stomach TDP-43 mRNA at 10, and 365 days. ns indicates p>0.05 (not significant), * indicates 0,01<p< 0,05, ** indicates 0,001<p<0,01. Error bars indicate SD calculated on three independent experiments. The lower

graph shows real-time PCR quantification of mouse stomach TDP-43 mRNA at 10, and 365 days. ns indicates p>0.05 (not significant), * indicates 0,01<p< 0,05, ** indicates 0,001<p<0,01. Error bars indicate SD calculated on three independent experiments.

Our data demonstrate the existence of a physiological pre-translational age- and tissue-specific mechanism of regulation of TDP-43 levels in the samples considered above. Furthermore these evidences suggest that it is an evolutionary conserved phenomenon between mouse and human species.

10. DNA demethylation increases TDP-43 expression in human bone marrow neuroblasts

Considering the evolutionary conservation of the TDP-43 tissue- and time- specific regulation mechanism between human and mouse, it was of interest to see if the methylation patterns in the human promoter were also at least in part responsible of the TDP-43 age related decay levels in human. As first, we performed an *in silico* analysis of the 5' upstream regulatory area of the *TARDBP* human promoter as already done in mouse (**Figure 30A**) (Session 4 of the Results). By using several promoter prediction tools including Promoter 2.0 prediction server (http://www.cbs.dtu.dk/services/Promoter/), Neural network promoter prediction (http://www.fruitfly.org/seq_tools/promoter.html), and Promoter scan (https://www-bimas.cit.nih.gov/molbio/proscan/), we accessed information on the identity of the promoter regulatory region of our gene of interest. The outcomes from different algorithms were partially overlapping, then we decided to consider the largest region predicted from all the tools used. It resulted in a genomic area of around 1500 bp distributed 1000 bp upstream and 500 bp downstream of the Transcription Starting Site (TSS) (**Figure 30B**). Next, we used Methprimer prediction tool (http://www.urogene.org/cgi-bin/methprimer/methprimer.cgi) to track the CpG sites within the promoter and their relative density. The software revealed the presence of 125 CpG sites as a potential target for methylation within the promoter predicted sequence. The area consists in three CpG islands characterized by elevated density of CpGs dinucleotides content and containing 16, 80, and 29 CpG sites respectively (**Figure 30B**). The aforementioned islands are indicated in **Figure 30B** as CpG1 (spanning -826 to -637), CpG2 (from -403 to -220), and CpG3 (from -97 to +538) (**Figure 30B**).

Even though the mouse and human *TARDBP* genes share very high similarity in the coding sequence, they have lower sequence homology of the regulatory 5'-upstream untranslated area. Despite the sequence differences between the two promoters, it can be observed a

similar architecture in the pattern of distribution of the regulatory elements. In fact, the mouse and human TSS and ATG are located in the same positions (exon 1 and 2, respectively) **(Figures 30A** and **30B)**. Furthermore, in both cases, the promoter predicted area encompasses a portion of the 5' upstream region, the exon 1 and the intron 1, with high content of CpGs sites organized in three islands in the human (**Figure 30B**) and in four islands in the mouse (**Figure 30A**) promoter. As a further note, in both cases, the high density of CpG sites are found in the region spanning from the nucleotide position -1500 to -500 upstream of the ATG (considering in this case nucleotide position +1 the A of ATG) **(Figures 30A** and **30B)**.

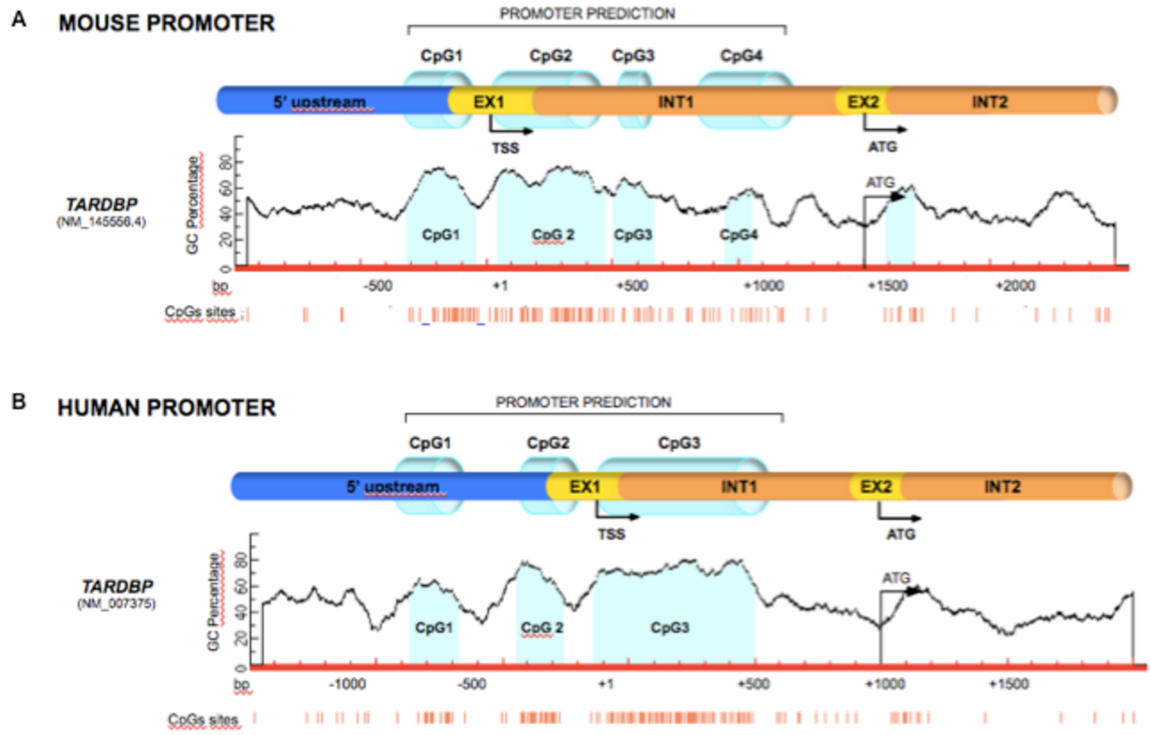

Figure 30. *In silico* comparison between *TARDBP* mouse and human promoter. A) Schematic representation of the *TARDBP* mouse promoter predicted fragment. +1 represents the Transcription Start Site (TSS). Methprimer analysis indicates CpG islands (in light blue) distributed within the promoter as four distinct regions (CpG1, CpG2, CpG3, and CpG4). The CpG dinucleotides are indicated as orange lines under the representation of the islands. B) Schematic representation of the *TARDBP* human promoter predicted fragment. +1 represents the Transcription Start Site (TSS). Methprimer analysis indicates CpG islands (in light blue) distributed within the promoter as three distinct regions (CpG1, CpG2, and CpG3). The CpG dinucleotides are indicated as orange lines under the representation of the islands.

To go further in the study of human *TARDBP* promoter methylation, our intent would have been to analyse different human tissues. However, given the difficulty in obtaining good quality human samples for analysis we decided to move to SH-SY5Y human cell line.

As first we mapped SH-SY5Y *TARDBP* promoter methylation status via bisulfite analysis. To do so, we extracted and converted genomic DNA form cells through bisulfite

incubation. Specific PCR primers for the methylation analysis were designed on converted DNA to separately amplify each of the three CpG islands identified by the software Methprimer as described above. Amplicons have been named as follows: CpG1 (spanning -875 to -561), CpG2 (from -507 to -162), CpG3A (from -144 to +399), CpG3B (extending from +377 to +992) (**Figure 31**). As it is shown in the **Figure 31**, because CpG3 island was too large to be analysed through a single PCR fragment amplification, we designed 2 primers pairs (which give rise to amplicons CpG3A and CpG3B) to have a complete coverage of that area.

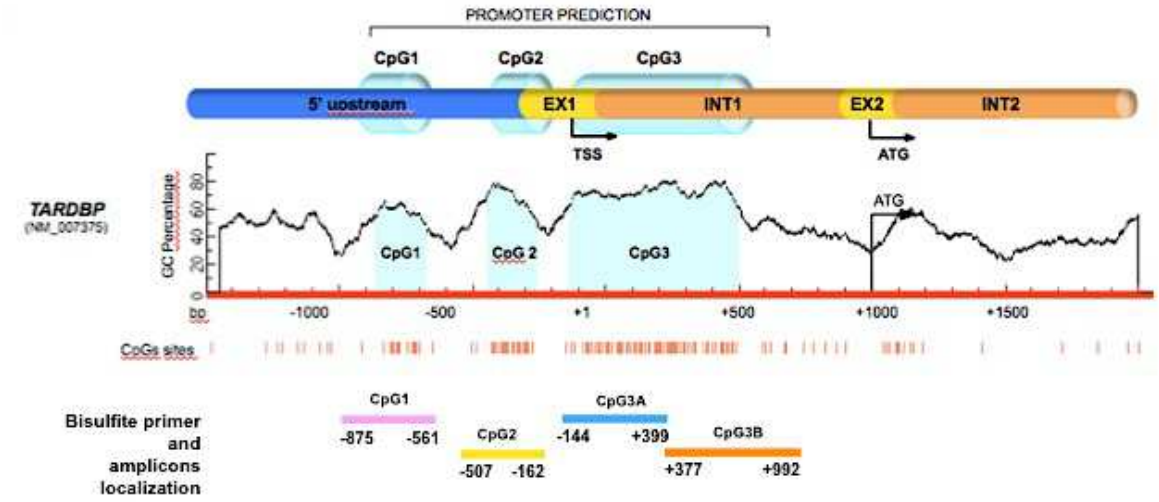

Figure 31. Human *TARDBP* promoter architecture and design of the bisulfite methylation analysis. A) Schematic representation of the human *TARDBP* promoter predicted fragment. +1 represents the Transcription Starting Site (TSS). Methprimer analysis indicates CpG islands (in light blue) distributed within the promoter as three distinct regions (CpG1, CpG2, and CpG3). The CpG dinucleotides are indicated as orange lines under the representation of the islands. In the lower part of the image are depicted the four amplicons (pink, yellow, blue, and orange lines) analysed in the bisulfite experiment, with the numbers referring to the start and end point of the primer designed on the converted DNA and used for the amplification.

As expected, the methylation profile of the human cell line is not matching with the one detected in mouse cells. In fact, as illustrated before, the sequences of the 5' upstream regulatory regions show low similarity between human and mouse. However, in human, as it happens in the mouse promoter, we found a single island (the first one instead of the fourth of the mouse) strongly and consistently methylated and this is a common feature between the two species.

In particular, in human SH-SY5Y TDP-43 promoter, there is a widespread and highly frequent methylation of almost all the CpG sites belonging to the first island. In fact, with the exception of the dinucleotides sites #13, #14, #15, and #16 which are methylated less than 50% of the cases, all the others are strongly methylated in percentage of around 100% (sites #1, #2, #3, #4, #5, #6, #7, #8, #9, #10, #11, and #12). The methylation rate in all the

other sites of the second and third island is negligible with the exception of the last site (#125) in the CpG3 island exhibiting a significant methylation percentage of around 30% (**Figure 32A**).

Once assessed that *TARDBP* promoter is subjected to methylation as described above, we next analysed eventual methylation effects on TDP-43 mRNA expression upon 5-azacitydine treatment of the cells. To do that, 5-azacytidine was added to the culture media at increasing concentration of 1 µM, 5 µM, and 10 µM. As already stated, this chemical analogue of the cytidine is able to inhibit the DNA methyltransferases enzymes, causing hypomethylation of DNA. After 48 and 72 hours of treatment, cells were harvested and total RNA was extracted. For the evaluation of the TDP-43 mRNA levels, real time RT-qPCR has been performed. As shown in **Figure 23B**, the demethylating treatment significantly increased TDP-43 mRNA in a dose- and time- dependent manner. In fact, the stronger effect is observed with higher concentration of the drug and it is more evident at 72 hours (**Figure 32B**, black bars) compared to 48 hours (**Figure 32B**, grey bars) at any concentration used.

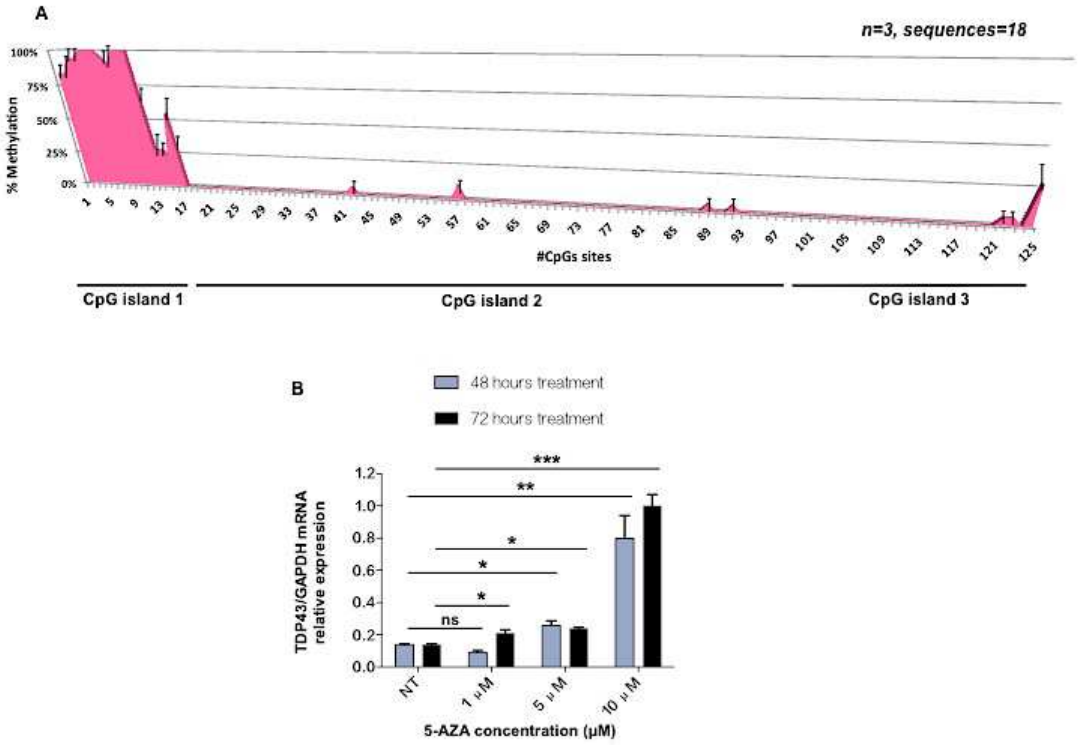

Figure 32. DNA demethylation increases TDP-43 expression in human bone marrow neuroblast SH-S5Y5. A) Bisulfite sequencing analysis of the human *TARDBP* promoter harbouring 125 CpG sites (indicated as numbers on the x axis) in SH-SY5Y cells. B) Real-time PCR quantification of TDP-43 mRNA in SH-SY5Y treated with 1 µM, 5 µM, and 10 µM of 5-azacitydine at 48 hours (grey bars) and 72 hours (black bars) . ns indicates $p>0.05$ (not significant), * indicates $0,01<p< 0,05$, ** indicates $0,001<p<0,01$. Error bars indicate SD calculated on three independent experiments.

These data shows that, as observed in mouse, *TARDBP* human promoter is highly methylated at single specific island level even though the target island for the methylation is differently positioned between the two species: the last part of the promoter for the mouse versus the first part of the promoter for the human. Moreover 5-azacytidine treatment effects suggest that methylation might play a role in controlling mRNA expression of human TDP-43 in human SH-SY5Y cells.

11. TDP-43 age- and tissue-specific regulation during development is not alone: other RNA binding proteins follow similar trend

Previous reports have shown that splicing factors expression and altered alternative splicing are deregulated in association with aging in human and other species. In particular, changes in splicing factors expression were reported in human blood, and they have also been associated with mouse strain lifespan in spleen and in muscle[3]. TDP-43 is a member of the heterogeneous ribonucleoproteins (hnRNPs) family that act as regulators of the RNA metabolism together with the "cousin" family of SR splicing factors. However, no systematic associations have been made so far regarding the tissue-specificity of the aging related changes and splicing factors levels. We wondered whether the changes observed previously in this study were a strict characteristic of TDP-43 or were also involving other SFs. We have explored this possibility by looking at the expression of different members of the major families of the RNA binding proteins (RBPs) in brain, skeletal muscle, and liver of mouse aged 10 and 90 days. Among the members of the hnRNPs we analysed hnRNP A1, hnRNP H1, hnRNP I, hnRNP L, hnRNP Q, and hnRNP R. Then we considered SRp55 and SRp75 that belong to the SR proteins family and snRNP U1A and snRNP 70 which are part of the snRNPs family. The protein extracts of 10 and 90 days mouse brain, liver and skeletal muscle were analysed by western blot as previously described and when established that there was a specific contribution of only one species (no unspecific bands detected by antibodies), the slot blot technique was used. The expression of the hnRNPs, SRs and snRNPs was then compared with the one of TDP-43.
As it is shown in **Figure 33**, all the SFs analysed including members of hnRNPs (**Figure 33A**), some representative components of the SR proteins (**Figure 33C**) and snRNP U1A and 70 as components of the spliceosome complex (Fig. 19B), followed the trend of TDP-43 in brain, corresponding to a mild decay from 10 to 90 days (**Figures 33A**, **33B**, and **33C**, compare lane 1 and 2 of each blot). Since we observed a widespread decrease of

protein expression over time involving several members of the RBPs, we sought to discard an age-related generalized loss of efficiency in protein expression evaluating the fluctuation of the levels of proteins involved in different cellular processes such as cell signalling (Akt, GSK3 β), structure organization (tubulin), cell metabolism (GAPDH), and ROS metabolism (SOD1). Interestingly, all these proteins maintained their levels of expression from 10 to 90 days in brain (**Figure 33D**, compare lane 1 and 2 of each blot). These data indicate that the reduction of TDP-43 and of other RBPs analysed is a feature of this class of proteins and it is not due to a generalized age-related loss of efficiency in the protein production as in that case a similar decrease in other proteins involved in other cellular processes would have been observed.

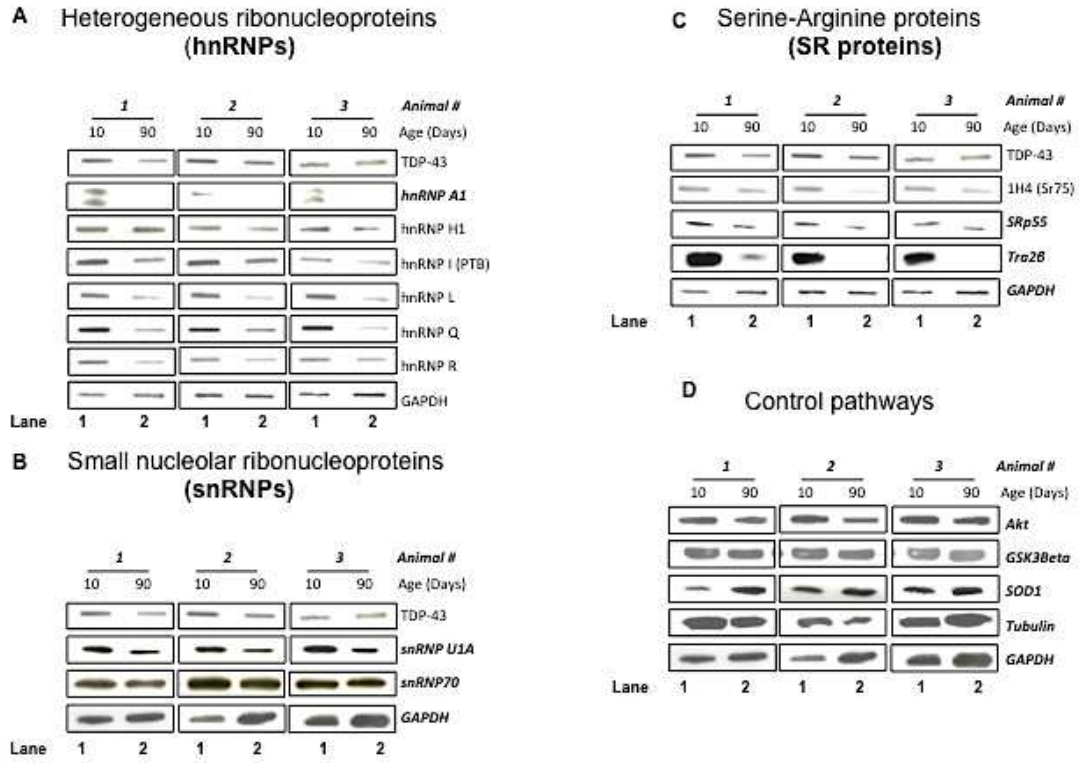

Figure 33. RNA-binding proteins expression decay is associated to development in brain. A) Blots showing TDP-43 and heterogeneous ribonucleoproteins (TDP-43, hnRNP A1, hnRNP H1, hnRNP I, hnRNP L, hnRNP Q. hnRNP R) expression in mouse brain at 10 and 90 days. Antibodies used in Western Blot are indicated in bold font, antibodies used in slot blot are indicated in regular font. Each row reports three indipendent experiments for each protein analysed. The last row of the panel shows GAPDH as loading control. B) Blots showing TDP-43 and small nuclear ribonucleoproteins (TDP-43, snRNP U1A, snRNP 70) expression in mouse brain at 10 and 90 days. Antibodies used in Western Blot are indicated in bold font, antibodies used in slot blot are indicated in regular font. Each row reports three indipendent experiments for each protein analysed. The last row of the panel shows GAPDH as loading control. C) Blots showing TDP-43 and Serine-Arginine proteins (TDP-43, SRp75, SRp55, Tra2Beta) expression in mouse brain at 10 and 90 days. Antibodies used in Western Blot are indicated in bold font, antibodies used in slot blot are indicated in regular font. Each row reports three indipendent experiments for each protein analysed. The last row of the panel shows GAPDH as loading control. D) Blots showing proteins not belonging to the RNA metabolism (Akt, GSK3Beta, SOD1, Tubulin) expression in mouse brain at 10 and 90 days. Antibodies used in Western Blot are indicated in bold font, antibodies used in slot blot are indicated in regular font. Each row reports three indipendent experiments for each protein analysed. The last row of the panel shows GAPDH as loading control.

In skeletal muscle we also detected, for all the RBPs considered, the same trend of expression observed for TDP-43 during development that is a stronger drop in levels than that observed in brain (**Figures 34A**, **34B**, **34C**). In fact, in all the hnRNPs considered (hnRNP A1, hnRNP H1, hnRNP I, hnRNP L, hnRNP Q, and hnRNP R) it could be observed a drastic drop to an extent that the protein is no longer detectable at 90 days by this methodology (below the limit of sensitivity of the western/slot) (**Figure 34A**, compare lane 1 and 2). Also in the case of the snRNPs analysed (snRNP 70 and U1A) (**Figure 34B**) and the SRp75 (**Figure 34C**) the expression decrease is strong by comparing the protein level at 10 and 90 days (**Figures 34B, 34C**, compare lane 1 and 2). Here again, the evaluation of the protein levels of members not belonging to the class of proteins involved in the regulation of the RNA metabolism revealed that the tissue- and time- specificity of the protein drop observed in the skeletal muscle is not a general cellular mechanism occurring over time and that it is specific for the RBPs studied. In fact, for the members of other cellular pathways such as actin, tubulin, SOD1, GSK3- β , and GAPDH the decay at 90 days is not occurring (**Figure 34D**).

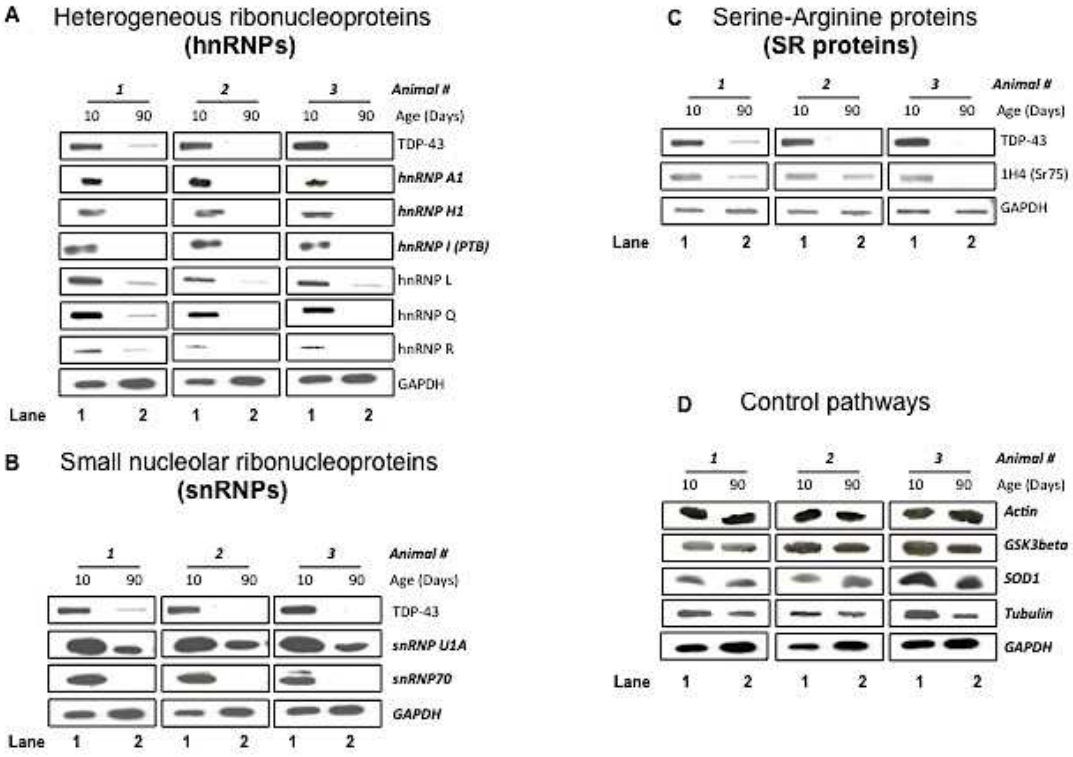

Figure 34. RNA-binding proteins expression decay during development in the skeletal muscle is stronger than in brain. A) Blots showing TDP-43 and heterogeneous ribonucleoproteins (TDP-43, hnRNP A1, hnRNP H1, hnRNP I, hnRNP L, hnRNP Q. hnRNP R) expression in mouse skeletal muscle at 10 and 90 days. Antibodies used in Western Blot are indicated in bold font, antibodies used in slot blot are indicated in regular font. Each row reports three indipendent experiments for each protein analysed. The last row of the panel shows GAPDH as loading control. B) Blots showing TDP-43 and small nuclear ribonucleoproteins (TDP-43, snRNP U1A, snRNP 70) expression in mouse skeletal muscle at 10 and 90 days. Antibodies used in Western Blot are indicated in bold font, antibodies used in slot blot are indicated in regular font. Each row reports three indipendent experiments for each protein analysed. The last row of the panel shows GAPDH as loading control. C) Blots showing TDP-43 and Serine-Arginine proteins (TDP-43, SRp75) expression in mouse skeletal muscle at 10 and 90 days. Antibodies used in Western Blot are indicated in bold font, antibodies used in slot blot are indicated in regular font. Each row reports three indipendent experiments for each protein analysed. The last row of the panel shows GAPDH as loading control. D) Blots showing proteins not belonging to the RNA metabolism (Actin, GSK3Beta, SOD1, Tubulin) expression in mouse skeletal muscle at 10 and 90 days. Antibodies used in Western Blot are indicated in bold font, antibodies used in slot blot are indicated in regular font. Each row reports three indipendent experiments for each protein analysed. The last row of the panel shows GAPDH as loading control.

In liver, TDP-43 shows a different behaviour in respect to the brain and skeletal muscle with no changes in the protein expression between 10 and 90 days (**Figure 35**). Also in the case of this tissue, the evaluation of the RBPs expression was in agreement with the TDP-43 trend, revealing a generalized unchanged expression of the proteins considered during time. In fact, as shown in **Figure 35A** almost all the hnRNPs analysed show a sustained expression from 10 to 90 days (**Figure 35A**, compare lane 1 and 2) with the exceptions of hnRNP A1 and hnRNP I which were undergoing a dramatic decrease (**Figure 35A**, compare lane 1 and 2). Overall, the SR proteins considered (SRp55, and SRp75) were constantly expressed during time (**Figure 35C**, compare lane 1 and 2), and the snRNPs exhibited slight heterogeneity with a sustained expression of snRNP U1A from 10 to 90 days and a mild decrease of snRNP 70 registered at 90 days in some cases (**Figure 35B**, compare lane 1 and 2). We also analysed SOD1, GSK3-β, and GAPDH as proteins belonging to other cellular pathways not involved in the RNA metabolism. As observed in brain and in skeletal muscle, also in liver they showed constant and sustained expression with no tissue-specific changes occurring over time (**Figure 35D**, compare lane 1 and 2 of each blot).

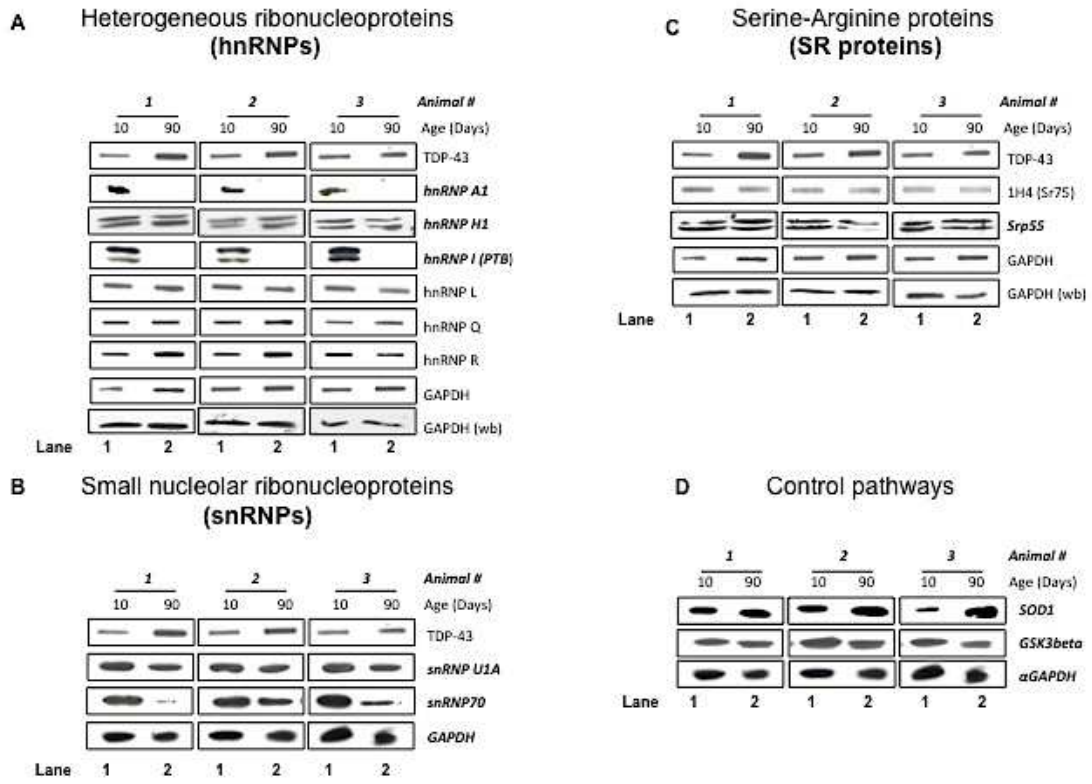

Figure 35. RNA-binding proteins expression is generally sustained in liver over time. A) Blots showing TDP-43 and heterogeneous ribonucleoproteins (TDP-43, hnRNP A1, hnRNP H1, hnRNP I, hnRNP L, hnRNP Q. hnRNP R) expression in mouse liver at 10 and 90 days. Antibodies used in Western Blot are indicated in bold font, antibodies used in slot blot are indicated in regular font. Each row reports three indipendent experiments for each protein analysed. The last row of the panel shows GAPDH as loading control. B) Blots showing TDP-43 and small nuclear ribonucleoproteins (TDP-43, snRNP U1A, snRNP 70) expression in mouse liver at 10 and 90 days. Antibodies used in Western Blot are indicated in bold font, antibodies used in slot blot are indicated in regular font. Each row reports three indipendent experiments for each protein analysed. The last row of the panel shows GAPDH as loading control. C) Blots showing TDP-43 and Serine-Arginine proteins (TDP-43, SRp75, SRp55) expression in mouse liver at 10 and 90 days. Antibodies used in Western Blot are indicated in bold font, antibodies used in slot blot are indicated in regular font. Each row reports three indipendent experiments for each protein analysed. The last row of the panel shows GAPDH as loading control. D) Blots showing proteins not belonging to the RNA metabolism (GSK3Beta, SOD1) expression in mouse liver at 10 and 90 days. Antibodies used in Western Blot are indicated in bold font, antibodies used in slot blot are indicated in regular font. Each row reports three indipendent experiments for each protein analysed. The last row of the panel shows GAPDH as loading control.

To address whether the tissue- and age- specific regulation observed to occur in several members of the RBPs was acting at transcriptional rather than translational level, we examined the transcript levels of some of the genes previously analysed by quantitative real-time qPCR. For this purpose we extracted total RNA from brain, skeletal muscle, and liver of wild-type mice aged 10 and 90 days. We first performed a reverse transcription and then a real-time qPCR. We quantified the mRNA levels of some representatives of the RBPs previously analysed at protein levels. We choose hnRNP H1 and hnRNP I among

the hnRNPs family, and the SRp55 for the serine-arginine rich proteins. As before we used as a control transcripts not related to the RBPs. In this case we selected Akt and SOD1 as a genes not involved in the RNA metabolism. Normalization has been performed with the housekeeping gene GAPDH. In the case of TDP-43 we previously showed that in every tissue considered the trend of the protein was correspondent to the levels of mRNA measured over time, suggesting the existence of a pre-translational mechanism. We could confirm that in the brain mRNA of all the RBPs members analysed (hnRNP H1, hnRNP I, and SRp55) mildly decreases (**Figures 36A, 36B, 36C**) as the protein does. Similarly, the mRNA levels were following the protein trends also in skeletal muscle where there is a drastic drop as shown in **Figures 36F, 36G, 36H**. As expected, in liver, the level of mRNA is sustained as observed in the protein expression from 10 to 90 days for hnRNP H1 (**Figure 36M**) and SRp55 (**Figure 36O**). The transcript of the hnRNP I also followed the trend of the protein showing a moderate decrease (**Figure 36N**). It should be noticed that in all the tissues we analysed, the transcripts of genes not involved in the RNA metabolism regulation such as Akt and SOD1 showed constant expression independently from age (**Figures 36D, 36E, 36I, 36L, 36P**, and **36Q**).

These results indicate that the age- and tissue- specific expression of TDP-43 observed during the early post-natal developmental stage (from 10 to 90 days) could be extended to other members of the RBPs to which it belongs. Moreover, as earlier observed for TDP-43, also in the case of the RBPs considered, the mRNA trend follows the protein one in every tissue studied, again suggesting a regulation occurring at transcriptional level.

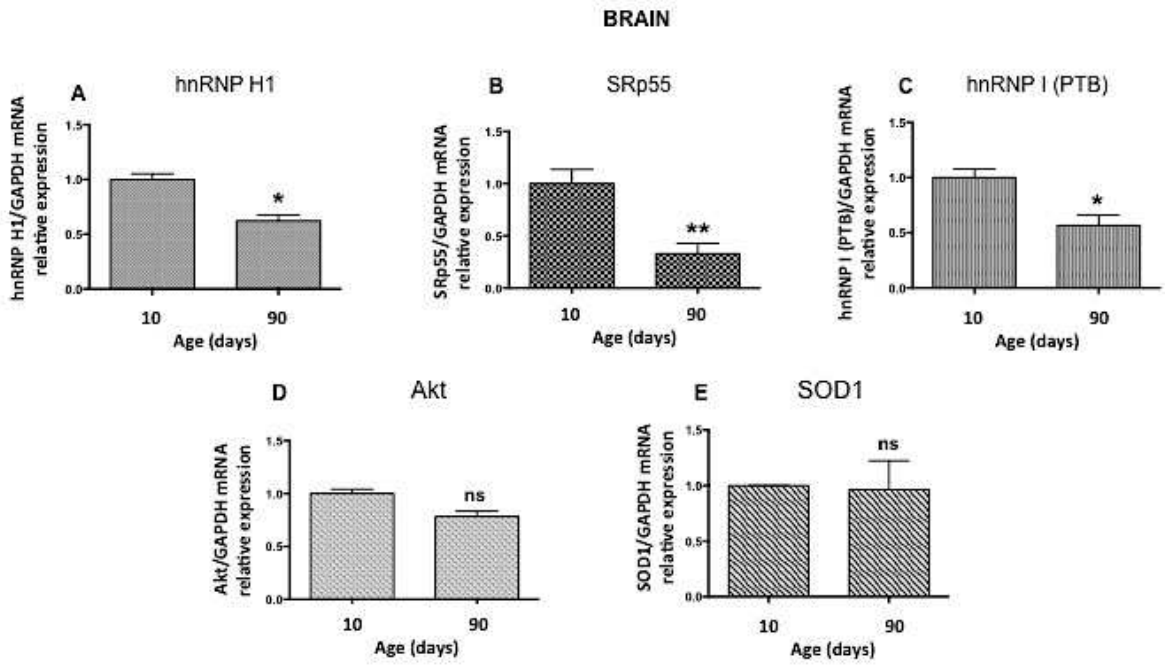

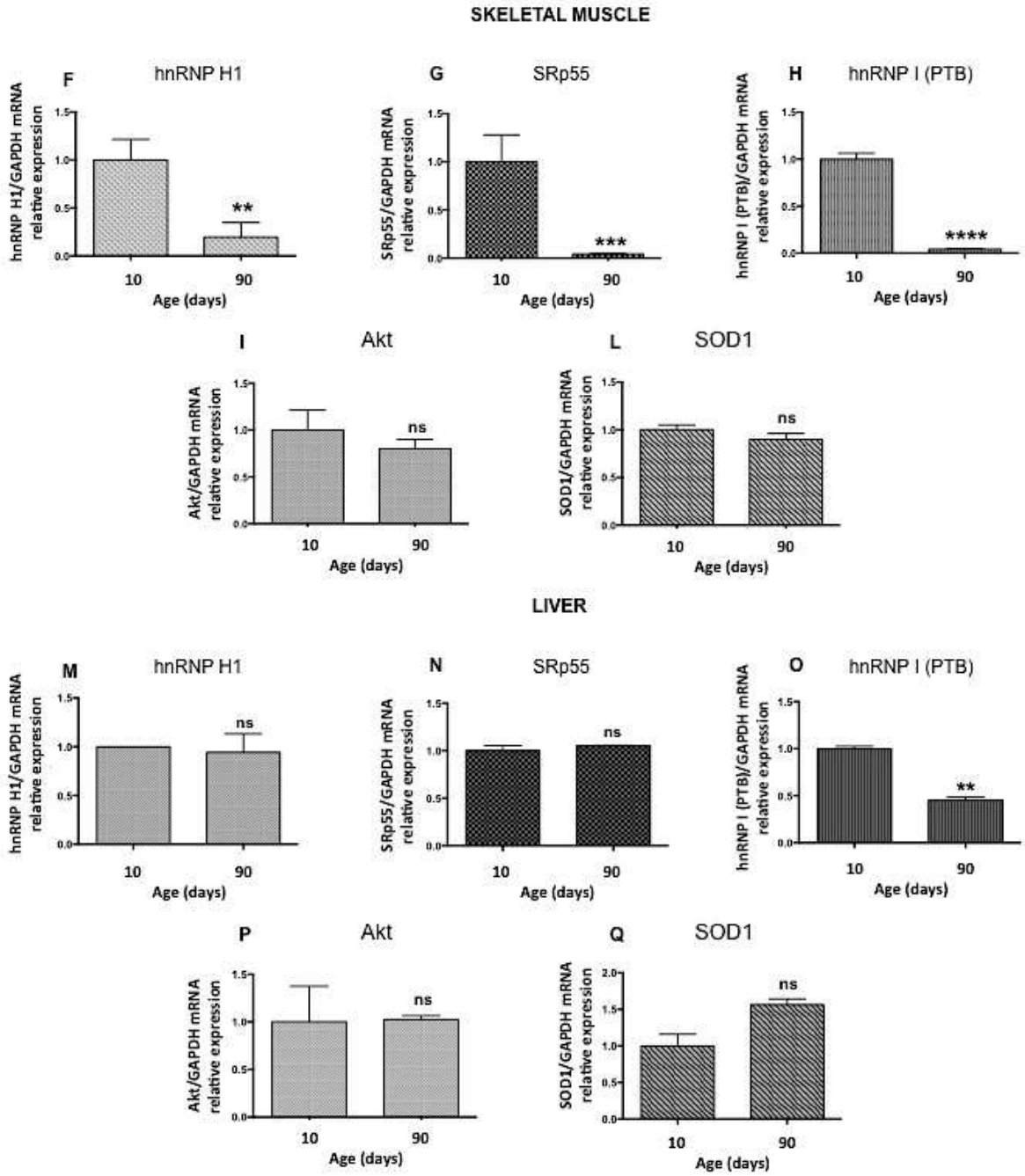

Figures 36. RNA-binding proteins tissue-specific regulation during development is transcriptionally mediated. A) Real-time PCR quantification of mouse brain hnRNP H1 mRNA at 10 and 90 days. B) Real-time PCR quantification of mouse brain SRp55 mRNA at 10 and 90 days. C) Real-time PCR quantification of mouse brain hnRNP I (PTB) mRNA at 10 and 90 days. D) Real-time PCR quantification of mouse brain AKT mRNA at 10 and 90 days. E) Real-time PCR quantification of mouse brain SOD1 mRNA at 10 and 90 days. F) Real-time PCR quantification of mouse skeletal muscle hnRNP H1 mRNA at 10 and 90 days. G) Real-time PCR quantification of mouse skeletal muscle SRp55 mRNA at 10 and 90 days. H) Real-time PCR quantification of mouse skeletal muscle hnRNP I (PTB) mRNA at 10 and 90 days. I) Real-time PCR quantification of mouse skeletal muscle AKT mRNA at 10 and 90 days. L) Real-time PCR quantification of mouse skeletal muscle SOD1 mRNA at 10 and 90 days. M) Real-time PCR quantification of mouse liver hnRNP H1 mRNA at 10 and 90 days. N) Real-time PCR quantification of mouse liver SRp55 mRNA at 10 and 90 days. O) Real-time PCR quantification of mouse liver hnRNP I (PTB) mRNA at 10 and 90 days. P) Real-time PCR quantification of mouse liver AKT mRNA at 10 and 90 days. Q) Real-time PCR quantification of mouse liver SOD1 mRNA at 10 and 90 days. ns indicates $p>0.05$ (not significant), * indicates $0,01<p< 0,05$, ** indicates $0,001<p<0,01$. Error bars indicate SD calculated on three independent experiments.

DISCUSSION AND CONCLUDING REMARKS

The majority of ALS cases (around 95%) share a common feature, which is the presence of TDP-43 cytoplasmic and/or nuclear inclusions in brain[261,262]. The role played by the aggregates has been and still is continuously debated. Different hypothesis have been made to explain the mechanism that contribute to the onset and progression of the disease. Indeed, if on one hand TDP-43 aggregates could act as a sink for the newly synthesized protein resulting in the depletion of its soluble functional fraction and consequently giving rise to a loss of function phenotype [109,160], on the other hand aggregation intermediates or aggregates themselves might display toxic gain of function properties[263]. While the debate is open it is certainly true that depletion of TDP-43 results in a severe loss of function phenotype. For example, experiments in flies with genetic suppression of TBPH (conserved TDP-43 orthologous in *Drosophila*) result in defective locomotion phenotype and atrophy of the neuromuscular junctions (NMJ) that is consistent with the loss of TDP-43 normal function model of ALS pathogenesis. Interestingly, at least in the fly, the locomotive phenotype is reversible as TBPH late induction in the null flies is able to recover normal locomotion in the adult[264], indicating that recovery of TDP-43 levels (high levels are toxic), might be beneficial in regards to disease progression.

Another issue related to the loss of function is the stoichiometry of TDP-43. In cells, we have previously shown that EGFP-fused-TDP-43 mutant form (TDP-43 F4L) along with 12 repetitions of its prion like Q/N- rich region (EGFP TDP-43 F4L 12X Q/N) sequesters either exogenous or endogenous full-length TDP-43[247] and thus mimics the TDP-43 pathologic “sinks” of ALS patients. The transgenic fly created with the same construct shows reduced lifespan, impaired neuromuscular junctions (NMJ)[264], and locomotive phenotype like the knock out fly but with the fundamental difference that the onset of the defective locomotion is a later age phenomena beyond the start of the reproductive period of the fly. This occurs notwithstanding the aggregates are already present since fertilization through the larval stage and early adult life. Further investigations highlighted the fact that the climbing deficit correlated with a physiological reduction in brain of the endogenous TBPH levels[259]. This was the first observation that the defect may be related to the amount of endogenous TDP-43. In particular, it is interesting to speculate that the effect of aggregation is counteracted, in young animals, by a sufficient amount of newly synthesised TBPH but with aging, the lower cellular capacity of TBPH production leads to its physiological reduction, then the protein amount is no longer sufficient to compensate the entrapment in the aggregates and the loss of TBPH function triggers the pathological

cascade of events eventually leading to the disease. In fact, reduction of TBPH mRNA levels was able to anticipate the locomotion defect to the larval stage, providing the first existing link between aggregation and the age-related reduction of TBPH with the onset of an ALS-like locomotion defect in *Drosophila* model[259].

We observed, in brain, a similar physiological age-related drop of TDP-43 mRNA and protein levels in three species (*Drosophila melanogaster, Danio rerio, Mus musculus*), that cover over 500 million years during the evolution (**Figure 25**). This indicates that the decrease of TBPH/TDP-43 levels represents an evolutionary conserved feature characteristic of aging of the organisms and consequently of biological relevance. Our hypothesis is that in the presence of TDP-43 aggregates, the physiological drop in TDP-43 expression level could represent a "break point" leading to loss of function of TDP-43/TBPH and hence to ALS symptoms and neurodegeneration onset. It was therefore important to elucidate the molecular mechanisms behind the expression levels of TDP-43 during aging.

Initially, we analysed the longitudinal expression of TDP-43 protein levels during aging in mice and observed that it was globally expressed during post-natal development in brain and several peripheral organs such as heart, liver, lung, and skeletal muscle (**Figures 15 and 16**) but, except for liver, where the levels were sustained, it was undergoing a decrease over time in the other tissues considered (**Figures 15 and 16**).

TDP-43 is not the only protein that decreases its levels in tissue and age specific manner. In fact, we found an age- and tissue- specific trend of expression also for several other members of the RBP family (**Figures 33, 34 and 35**), to which TDP-43 belongs. Furthermore we observed that, as for TDP-43, also for the RBPs the mRNA trend follows that of the protein (**Figure 36**), suggesting a regulation occurring at transcriptional level. Alterations in the RBP family, is increasingly emerging as a contributing factor to age-related neurodegenerative diseases with a growing number of studies focusing on the presence of several of these proteins into the pathological aggregates [45]. Even though multiple reports have already associated a deregulated expression of key splicing factors with aging [3,9,17,44], our data provide the important novelty of the tissue specificity of this mechanisms and this could be useful in trying to underlie their regulation pathways. Shading light on the players causing the altered RNA metabolism in neurodegeneration might be helpful also considering that it has been already proved that reversing some of these altered factors could be beneficial by slowing down the progression of the disease [43,265–268].

Coming back to the specific case of TDP-43, we also observed that its time- and tissue-specific expression occurs not only at protein but also at mRNA levels (**Figure 17**). The fact that this specific behaviour was different in liver than other tissues gave us a model with which try to understand the mechanism behind the TDP-43 protein regulation. Not only, this could open up the possibility that the gene may be differentially regulated in the specific tissue or cell types and thus provide an eventual therapeutic pathway aimed at increasing the levels of functional TDP-43 by increasing its synthesis once the mechanism that partially decreases it during aging is understood.

There are several possible mechanisms that may be acting in the age related reduction of TDP-43 levels. For example, one of these may be the alteration in the self-regulation mechanism that has been described for TDP-43 and discussed in section 6.1.2 of the introduction. Preliminary experiments in the laboratory before my period discarded this option (F. E. Baralle and L. De Conti personal communication). In consequence in this study, we concentrated on the modulation of the transcriptional processes. We first looked at DNA epigenetics modification. We carried out the mapping of the methylation status of *TARDBP* promoter in two of the tissues that showed a reduction during time of TDP-43 protein levels (brain and skeletal muscle) compared to liver that showed steady state levels of TDP-43 during age. This analysis showed a clear inverse correlation between methylation rate of specific CpG sites and protein expression occurring over time in wild-type animals, thus suggesting a plausible role of DNA methylation in controlling the reduction of TDP-43 expression over time. Particularly, our data showed that during mice aging, the methylation status of the fourth CpG island (NM_145556.4, region between +660bp and +1172bp, relative to the Transcription Start Site) of *TARDBP* promoter is higher in those tissues in which TDP-43 was observed to decrease with the age while in liver, where the protein expression was sustained over time, the methylation rate did not vary (**Figure 20**). Interestingly, we found that the CpG sites alternatively methylated during aging are the same in brain and skeletal muscle supporting their crucial role in down regulating TDP-43. The importance of the methylation in modulating *TARDBP* promoter activity has been further characterised by *in vitro* work. Indeed, through the *in vitro* methylation assay we showed that *TARDBP* promoter is sensitive to methylation since it undergoes a decrease in the activity once it is methylated (**Figure 22**). Furthermore, mutagenesis to prevent methylation induces an increase in promoter activity only when it affects the CpG sites belonging to the last part of the fourth island that we found significantly methylated in those mouse tissues with decreased expression of TDP-43 (**Figure 24**). The demethylating treatment with 5-aza of mouse motor neurons NSC34

cell line induces increased expression at both mRNA and protein levels of TDP-43 and not of GAPDH (**Figure 21**). All together, these data conclusively identify the methylation as a player in the regulation of TDP-43 mRNA and protein expression.

In humans an analogue scenario was also observed. In fact, DNA methyltransferase inhibitor 5-aza induces *TARDBP* mRNA expression also in human neuronal cell line (**Figure 32**). Furthermore, notwithstanding the human promoter differs from the mouse in the architecture and genomic sequence of the CpG islands, the analysis of its methylation profile lead to the identification of a unique CpG island, as for the mouse *TARDBP* promoter, highly methylated in almost all the CpG sites (reference sequence NM_007375, area included between -875bp and -561bp, relative to the TSS). The islands which seem to be the key regulators through methylation, as they have been found exclusively and highly methylated, are the fourth in mouse and the first in human (**Figures 21 and 32**).

Thus we identified, for the first time, hypermethylated specific sites in *TARDBP* promoter and demonstrated that these regulate its protein levels. Taking into consideration the age related drop and the age of disease onset, it is tempting to speculate that in an individual in the presence of TDP-43 aggregates, which is a universal landmark seen in end point patients brains, the rate of the age-related physiological drop of TDP-43 expression could tip the balance for developing ALS. In this view, individuals with low methylation rate at promoter level, (and for that reason with higher capacity of protein production) would be able to overcome the threshold limit beyond which the cell loses the normal TDP-43 function, while in individuals with a high methylation rate, TDP-43 "inactivation" is no longer compensated by the newly synthesized protein. Indeed the TDP-43 levels may also be critical per se and it would be of extreme interest to understand the degree of expression of endogenous TDP-43 in that 30-40% of normal individuals under 65 years old[235] where TDP-43 aggregation has been observed but no pathology. In fact, a possible explanation could be that in these individuals the physiological drop of TDP-43 is not dramatic enough to overstep the "break point" which would lead to loss of function consequences and neurodegeneration onset.

Further indications in regards to a potential role of epigenetic modifications in ALS pathogenesis comes from recent studies suggesting that DNA methylation, one of the main epigenetic changes, could play a pivotal role in the pathogenesis of ALS[269,270]. Additionally, recent reports indicate that DNA methylation controlled by methyltransferases (Dnmts) can mediate motor neurons death[270]. In fact, it has been described that enhanced expression of Dnmt3A induced degeneration in mouse motor neurons NSC34 cell line. The same report also showed that there is an increased amount of

Dnmt1 and Dnmt3A and accumulation of 5-methylcitosine in motor neurons coming from sporadic ALS patients' brains[270]. Even more importantly, a growing number of studies performed in blood of ALS patients attest that there is an aberrant genome wide methylation content [271–274,275]. For example, it has been shown a genome wide enrichment of 5-methylcitosine in blood samples of *C9orf72* ALS patients, and, even more importantly for us, they showed that *C9orf72* promoter was one of the hypermethylated players [276–278]. These data propose a plausible correlation between the increased global DNA methylation in ALS patient's blood samples and the contribution given by specific ALS-causing genes hypermethylated promoters. It would be then of undoubted interest to look at the methylation status of *TARDBP* promoter in ALS conditions to make a connection with the increased levels of methylation that other groups found globally in diseased samples.

Besides the importance of providing insights into basic science, several of these studies aim also to identify potential ALS epigenetic biomarkers as a minimal invasive alternative for ALS diagnostic and prognostic assessment. In fact, because of the lack of an early diagnostic method, there is the urgent need to develop a potent ALS biomarker. Even more important, there are on going and promising therapeutic approaches on animal models of ALS that are effective only when applied prior to disease onset because neurons lack of the regenerative feature[279]. Thus, we believe it would be of interest to investigate the methylation status of *TARDBP* promoter also in blood, serum, and other bodily fluids of ALS affected and healthy individuals to see whether there is a difference among the promoter methylation trends. In this case, methylated DNA would be a sure attractive choice as a biomarker substrate because of the abundance in extracellular environments, the resistance to degradation, and the not invasiveness of the technique.

In line with our hypothesis of the central role of TDP-43 levels in ALS pathology, possible therapeutic approaches could aim in either decreasing aggregates to a point that the newly synthesised protein is enough to undertake cellular functions or increasing functional TDP-43 levels to overcome aggregates sequestration. Considering the second option we propose modulation of DNA methylation as one of the potential targets for a therapeutic strategy to adjust TDP-43 expression levels in the adulthood. One evidence that supports this therapeutic option comes from recent investigations showing that SAM supplementation can be beneficial in delaying the age onset of transgenic mouse models of ALS[280]. The great potential of the pathogenic epigenetic modifications for therapeutic strategies is that they are reversible. Indeed, we showed that the DNA methyltransferase inhibitor 5-azacytidine in mouse motor neurons cell line remarkably enhances TDP-43 expression both at RNA and protein levels (**Figure 21**). Interestingly, demethylating agents have been

extensively studied to reverse aberrant epigenetic changes, in particular when associated with cancer. Particularly, subcutaneous azacitidine is approved in the treatment of myelodysplastic syndromes (MDS), chronic myelomonocytic leukemia (CMML), and acute myeloid leukemia (AML) patients who are not eligible for hematopoietic stem cell transplantation[281,282]. In these cases, azacitidine administration is the only therapy showing a significant prolonged survival compared with conventional care. Moreover, this drug is associated with lower risk of AML progression and higher rates of complete remission, partial remission, haematological improvement and red blood cell (RBC) transfusion independence[156]. Recently, azacitidine has become a valid option for the first-line treatment of patients with MDS/AML. In fact it has a tolerable profile with peripheral cytopenias occurring as a most common adverse event[155]. Because of the large use of azacitidine in approved cancer therapeutic strategies, because of its ability to cross the blood-brain barrier[283] and also considering our data showing an increased expression of TDP-43 in mouse motor neuron cell line upon 5-aza treatment, it would be of certain interest to look at the consequences of the administration of this nucleoside analogue in ALS animal models. In this regards it would be useful to consider not only our *Drosophila*-based ALS model, but also an appropriate mouse model. It is important to say that even though the presence of 5-methylcitosine in *Drosophila* has been under debate for long time, recently DNA methylation has been unequivocally confirmed even though it happens with a very low frequency[284,285].

Another intriguing path to pursue for a better understanding of the epigenetic-driven TDP-43 modulation would be to monitor potential changes in chromatin structure during mice ageing such as histones methylation or histone acetylation modifications that could accompany the already observed changes of *TARDBP* promoter methylation in mice. Also it would be interesting to see whether specific Transcription Factors (TFs) binding ability is sensitive to the methylation of the crucial CpG sites that we found located in the *TARDBP* promoter fourth island in the different mice tissues. The *in vivo* comparison of the TFs signatures on the fourth island of the different tissues *TARDBP* promoter would implement the global information concerning the influence of the *TARDBP* methylation in term of gene expression.

In conclusion this study provides new insights into the mechanism involved in the TDP-43 physiological tissue- and age- specific expression in mouse. We started showing a similar behaviour of TDP-43 expression during aging in human tissues (TDP-43 sustained expression in liver during aging and decreased expression in stomach muscle) and this part of the study will be pursued in the very next future. Our previous data in a *Drosophila*

model showed that ALS-like symptoms onset was correlating with a physiological drop of TBPH and that the rescue of protein expression resulted in improved phenotype. All together these findings have contributed to:

1. Establish that exists a physiological modulation program of TDP-43 levels through all the temporal stages of the organism life
2. Shown that at least in part, this modulation is partially regulated by epigenetic mechanisms through particular tissue specific promoter methylation
3. Open the way to further search to understand more in detail the role of epigenetics changes in TDP-43 physiological regulation and establish modulation of epigenetic changes as an attractive target for ALS treatment.

BIBLIOGRAPHY

1. United Nations. *World Population Ageing 2015*. *Department of Economic and Social Affairs, Population Division* (2015). doi:ST/ESA/SER.A/390
2. Wyss-Coray, T. Ageing, neurodegeneration and brain rejuvenation. *Nature* **539,** 180–186 (2016).
3. Lee, B. P. *et al.* Changes in the expression of splicing factor transcripts and variations in alternative splicing are associated with lifespan in mice and humans. *Aging Cell* **15,** 903–913 (2016).
4. Deschênes, M. & Chabot, B. The emerging role of alternative splicing in senescence and aging. *Aging Cell* **16,** 918–933 (2017).
5. López-Otín, C., Blasco, M. A., Partridge, L., Serrano, M. & Kroemer, G. The hallmarks of aging. *Cell* **153,** (2013).
6. Hayflick, L. & Moorhead, P. S. The serial cultivation of human diploid cell strains. *Exp. Cell Res.* (1961). doi:10.1016/0014-4827(61)90192-6
7. Nelson, G. *et al.* A senescent cell bystander effect: Senescence-induced senescence. *Aging Cell* **11,** 345–349 (2012).
8. Baker, D. J. *et al.* Opposing roles for p16Ink4a and p19Arf in senescence and ageing caused by BubR1 insufficiency. *Nat. Cell Biol.* **10,** 825–836 (2008).
9. Harries, L. W. *et al.* Human aging is characterized by focused changes in gene expression and deregulation of alternative splicing. *Aging Cell* **10,** 868–878 (2011).
10. Brunk, U. T. & Terman, A. The mitochondrial-lysosomal axis theory of aging: Accumulation of damaged mitochondria as a result of imperfect autophagocytosis. *European Journal of Biochemistry* **269,** 1996–2002 (2002).
11. Dubois, B. *et al.* Preclinical Alzheimer's disease: Definition, natural history, and diagnostic criteria. *Alzheimer's and Dementia* **12,** 292–323 (2016).
12. Shadyab, A. H. & LaCroix, A. Z. Genetic factors associated with longevity: A review of recent findings. *Ageing Research Reviews* **19,** 1–7 (2015).
13. Hjelmborg, J. B. *et al.* Genetic influence on human lifespan and longevity. *Hum. Genet.* **119,** 312–321 (2006).
14. Herskind, A. M. *et al.* The heritability of human longevity: A population-based study of 2872 Danish twin pairs born 1870-1900. *Hum. Genet.* **97,** 319–323 (1996).
15. Newman, A. B. & Murabito, J. M. The epidemiology of longevity and exceptional survival. *Epidemiol. Rev.* **35,** 181–197 (2013).

16. Johnson, A. A. *et al.* The Role of DNA Methylation in Aging, Rejuvenation, and Age-Related Disease. *Rejuvenation Res.* **15,** 483–494 (2012).
17. Tollervey, J. R. *et al.* Analysis of alternative splicing associated with aging and neurodegeneration in the human brain. *Genome Res.* **21,** 1572–1582 (2011).
18. Lord, J. & Cruchaga, C. The epigenetic landscape of Alzheimer's disease. *Nature Neuroscience* **17,** 1138–1140 (2014).
19. De Jager, P. L. *et al.* Alzheimer's disease: Early alterations in brain DNA methylation at ANK1, BIN1, RHBDF2 and other loci. *Nat. Neurosci.* **17,** 1156–1163 (2014).
20. Kovacs, G. G. Molecular pathological classification of neurodegenerative diseases: Turning towards precision medicine. *International Journal of Molecular Sciences* **17,** (2016).
21. Carrell, R. W. & Lomas, D. A. Conformational disease. *Lancet* **350,** 134–138 (1997).
22. Cornejo, V. H. & Hetz, C. The unfolded protein response in Alzheimer's disease. *Seminars in Immunopathology* **35,** 277–292 (2013).
23. Nijholt, D. a T., De Kimpe, L., Elfrink, H. L., Hoozemans, J. J. M. & Scheper, W. Removing protein aggregates: the role of proteolysis in neurodegeneration. *Curr. Med. Chem.* **18,** 2459–2476 (2011).
24. von Bernhardi, R. & Eugenín, J. Alzheimer's Disease: Redox Dysregulation As a Common Denominator for Diverse Pathogenic Mechanisms. *Antioxid. Redox Signal.* **16,** 974–1031 (2012).
25. Soto, C. Unfolding the role of protein misfolding in neurodegenerative diseases. *Nat. Rev. Neurosci.* **4,** 49–60 (2003).
26. Skovronsky, D. M., Lee, V. M.-Y. & Trojanowski, J. Q. Neurodegenerative diseases: new concepts of pathogenesis and their therapeutic implications. *Annu. Rev. Pathol.* **1,** 151–170 (2006).
27. Kovacs, G. G. CURRENT CONCEPTS OF NEURODEGENERATIVE DISEASES. *Cit. EMJ Neurol* **1,** 78–86 (2014).
28. Kovacs, G. G. *et al.* Non-Alzheimer neurodegenerative pathologies and their combinations are more frequent than commonly believed in the elderly brain: A community-based autopsy series. *Acta Neuropathol.* **126,** 365–384 (2013).
29. Polymenidou, M. & Cleveland, D. W. Prion-like spread of protein aggregates in neurodegeneration: Figure 1. *J. Exp. Med.* **209,** 889–893 (2012).
30. Lill, C. M. & Bertram, L. Towards unveiling the genetics of neurodegenerative

diseases. *Semin. Neurol.* **31,** 531–541 (2011).

31. Kovacs, G. G., Botond, G. & Budka, H. Protein coding of neurodegenerative dementias: The neuropathological basis of biomarker diagnostics. *Acta Neuropathologica* **119,** 389–408 (2010).
32. Ignatius, S. O., Harrich, D., F Garc A-mart Nez, L. N. & Gaynor, R. B. Cloning and Characterization of a Novel Cellular Protein, TDP-43, That Binds to Human Immunodeficiency Virus Type 1 TAR DNA Sequence Motifs. *J. Virol.* **69,** 3584–3596 (1995).
33. Neumann, M. *et al.* FET proteins TAF15 and EWS are selective markers that distinguish FTLD with FUS pathology from amyotrophic lateral sclerosis with FUS mutations. *Brain* **134,** 2595–2609 (2011).
34. Lagier-Tourenne, C. & Cleveland, D. W. Rethinking ALS: The FUS about TDP-43. *Cell* **136,** 1001–1004 (2009).
35. Bertram, L. & Tanzi, R. E. The genetic epidemiology of neurodegenerative disease. *Journal of Clinical Investigation* **115,** 1449–1457 (2005).
36. Cannon, J. R. & Greenamyre, J. T. The role of environmental exposures in neurodegeneration and neurodegenerative diseases. *Toxicol. Sci.* **124,** 225–250 (2011).
37. La Spada, A. R. & Taylor, J. P. Repeat expansion disease: Progress and puzzles in disease pathogenesis. *Nature Reviews Genetics* **11,** 247–258 (2010).
38. Renoux, A. J. & Todd, P. K. Neurodegeneration the RNA way. *Progress in Neurobiology* **97,** 173–189 (2012).
39. Anderson, P. & Ivanov, P. tRNA fragments in human health and disease. *FEBS Lett* (2014). doi:10.1016/j.febslet.2014.09.001
40. Belzil, V. V., Gendron, T. F. & Petrucelli, L. RNA-mediated toxicity in neurodegenerative disease. *Mol. Cell. Neurosci.* **56,** 406–419 (2013).
41. Bentmann, E., Haass, C. & Dormann, D. Stress Granules in Neurodegeneration - Lessons learnt from TDP-43 and FUS. *FEBS J.* 1–23 (2013). doi:10.1111/febs.12287
42. Halliday, G. *et al.* Mechanisms of disease in frontotemporal lobar degeneration: Gain of function versus loss of function effects. *Acta Neuropathologica* **124,** 373–382 (2012).
43. Liu, E. Y., Cali, C. P. & Lee, E. B. RNA metabolism in neurodegenerative disease. *Dis. Model. Mech.* **10,** 509–518 (2017).
44. Holly, A. C. *et al.* Changes in splicing factor expression are associated with

advancing age in man. *Mech. Ageing Dev.* **134,** 356–366 (2013).

45. Zhou, H., Mangelsdorf, M., Liu, J., Zhu, L. & Wu, J. Y. RNA-binding proteins in neurological diseases. *Sci. China Life Sci.* **57,** 432–444 (2014).
46. Glisovic, T., Bachorik, J. L., Yong, J. & Dreyfuss, G. RNA-binding proteins and post-transcriptional gene regulation. *FEBS Letters* **582,** 1977–1986 (2008).
47. Chen, Y. & Varani, G. Protein families and RNA recognition. *FEBS Journal* **272,** 2088–2097 (2005).
48. Dyson, H. J. & Wright, P. E. Intrinsically unstructured proteins and their functions. *Nature Reviews Molecular Cell Biology* **6,** 197–208 (2005).
49. Vassileva, M. T. & Matunis, M. J. SUMO modification of heterogeneous nuclear ribonucleoproteins. *Mol. Cell. Biol.* **24,** 3623–3632 (2004).
50. Keene, J. D. Ribonucleoprotein infrastructure regulating the flow of genetic information between the genome and the proteome. *Proc. Natl. Acad. Sci.* **98,** 7018–7024 (2001).
51. Lee, M.-H. & Schedl, T. RNA-binding proteins. *WormBook* 1–13 (2006). doi:10.1895/wormbook.1.79.1
52. Geuens, T., Bouhy, D. & Timmerman, V. The hnRNP family: insights into their role in health and disease. *Human Genetics* **135,** 851–867 (2016).
53. Krecic, A. M. & Swanson, M. S. hnRNP complexes: Composition, structure, and function. *Current Opinion in Cell Biology* **11,** 363–371 (1999).
54. Dreyfuss, G., Kim, V. N. & Kataoka, N. Messenger-RNA-binding proteins and the messages they carry. *Nature Reviews Molecular Cell Biology* **3,** 195–205 (2002).
55. Zhang, M., Han, N. & Li, W. The function of the RNA-binding protein hnRNP in cancer metastasis. *J. Cancer Res. Ther.* **9,** 129 (2013).
56. Mayeda, A. & Krainer, A. R. Regulation of alternative pre-mRNA splicing by hnRNP A1 and splicing factor SF2. *Cell* **68,** 365–375 (1992).
57. Expert-Bezançon, A. *et al.* hnRNP A1 and the SR proteins ASF/SF2 and SC35 have antagonistic functions in splicing of β-tropomyosin exon 6B. *J. Biol. Chem.* **279,** 38249–38259 (2004).
58. Gallouzi, I. E. & Steitz, J. A. Delineation of mRNA export pathways by the use of cell-permeable peptides. *Science (80-.).* **294,** 1895–1901 (2001).
59. Carson, J. H. *et al.* RNA Trafficking in Oligodendrocytes. *Results Probl Cell Differ* **34,** 69–81 (2001).
60. Habelhah, H. *et al.* ERK phosphorylation drives cytoplasmic accumulation of hnRNP-K and inhibition of mRNA translation. *Nat. Cell Biol.* **3,** 325–330 (2001).

61. Xu, K., Yen, T. & Geczy, C. L. IL-10 Up-Regulates Macrophage Expression of the S100 Protein S100A8. *J. Immunol.* **166,** 6358–6366 (2001).
62. Howard, J. M. & Sanford, J. R. The RNAissance family: SR proteins as multifaceted regulators of gene expression. *Wiley Interdisciplinary Reviews: RNA* **6,** 93–110 (2015).
63. Jeong, S. SR Proteins: Binders, Regulators, and Connectors of RNA. *Mol. Cells* **40,** 1–9 (2017).
64. Xiang, S. *et al.* Phosphorylation drives a dynamic switch in serine/arginine-rich proteins. *Structure* **21,** 2162–2174 (2013).
65. Matlin, A. J., Clark, F. & Smith, C. W. J. Understanding alternative splicing: Towards a cellular code. *Nature Reviews Molecular Cell Biology* **6,** 386–398 (2005).
66. Lin, S., Xiao, R., Sun, P., Xu, X. & Fu, X. D. Dephosphorylation-dependent sorting of SR splicing factors during mRNP maturation. *Mol. Cell* **20,** 413–425 (2005).
67. Lemaire, R. *et al.* Stability of a PKCI-1-related mRNA is controlled by the splicing factor ASF/SF2: A novel function for SR proteins. *Genes Dev.* **16,** 594–607 (2002).
68. Matera, A. G. & Wang, Z. A day in the life of the spliceosome. *Nat. Rev. Mol. Cell Biol.* **15,** 108–21 (2014).
69. Mills, J. D. & Janitz, M. Alternative splicing of mRNA in the molecular pathology of neurodegenerative diseases. *Neurobiology of Aging* **33,** (2012).
70. Bryant, C. D. & Yazdani, N. RNA-binding proteins, neural development and the addictions. *Genes, Brain and Behavior* **15,** 169–186 (2016).
71. Szabo, A. *et al.* HuD, a paraneoplastic encephalomyelitis antigen, contains RNA-binding domains and is homologous to Elav and Sex-lethal. *Cell* **67,** 325–333 (1991).
72. Albert, M. L. & Darnell, R. B. Paraneoplastic neurological degenerations: keys to tumour immunity. *Nat. Rev. Cancer* **4,** 36–44 (2004).
73. Buckanovich, R. J., Posner, J. B. & Darnell, R. B. Nova, the paraneoplastic Ri antigen, is homologous to an RNA-binding protein and is specifically expressed in the developing motor system. *Neuron* **11,** 657–672 (1993).
74. Jin, Y. *et al.* A vertebrate RNA-binding protein Fox-1 regulates tissue-specific splicing via the pentanucleotide GCAUG. *EMBO J.* **22,** 905–912 (2003).
75. Voineagu, I. *et al.* Transcriptomic analysis of autistic brain reveals convergent molecular pathology. *Nature* **474,** 380–386 (2011).
76. Gehman, L. T. *et al.* The splicing regulator Rbfox1 (A2BP1) controls neuronal

excitation in the mammalian brain. in *Nature Genetics* **43,** 706–711 (2011).

77. Larocque, D. & Richard, S. QUAKING KH Domain Proteins as Regulators of Glial Cell Fate and Myelination. *RNA Biol.* **2,** 37–40 (2005).
78. Chénard, C. A. & Richard, S. New implications for the QUAKING RNA binding protein in human disease. *Journal of Neuroscience Research* **86,** 233–242 (2008).
79. Bardoni, B., Davidovic, L., Bensaid, M. & Khandjian, E. W. The fragile X syndrome: Exploring its molecular basis and seeking a treatment. *Expert Reviews in Molecular Medicine* **8,** 1–16 (2006).
80. Jin, P. & Warren, S. T. Understanding the molecular basis of fragile X syndrome. *Hum. Mol. Genet.* **9,** 901–908 (2000).
81. De Conti, L., Baralle, M. & Buratti, E. Neurodegeneration and RNA-binding proteins. *Wiley Interdisciplinary Reviews: RNA* **8,** (2017).
82. Zukin, R. S. Signals, synapses, and synthesis: how new proteins control plasticity. *Front. Neural Circuits* **3,** (2009).
83. Alberti, S., Mateju, D., Mediani, L. & Carra, S. Granulostasis: Protein Quality Control of RNP Granules. *Front. Mol. Neurosci.* **10,** (2017).
84. Buchan, J. R. & Parker, R. Eukaryotic Stress Granules: The Ins and Outs of Translation. *Molecular Cell* **36,** 932–941 (2009).
85. Krichevsky, A. M. & Kosik, K. S. Neuronal RNA granules: A link between RNA localization and stimulation-dependent translation. *Neuron* **32,** 683–696 (2001).
86. Zeitelhofer, M. *et al.* Dynamic Interaction between P-Bodies and Transport Ribonucleoprotein Particles in Dendrites of Mature Hippocampal Neurons. *J. Neurosci.* **28,** 7555–7562 (2008).
87. Alami, N. H. *et al.* Axonal Transport of TDP-43 mRNA Granules Is Impaired by ALS-Causing Mutations. *Neuron* **81,** 536–543 (2014).
88. Vanderweyde, T., Youmans, K., Liu-Yesucevitz, L. & Wolozin, B. The Role Stress Granules and RNA Binding Proteins in Neurodegeneration. *Gerontology* **59,** 524–533 (2013).
89. Morimoto, R. I. The heat shock response: Systems biology of proteotoxic stress in aging and disease. *Cold Spring Harb. Symp. Quant. Biol.* **76,** 91–99 (2011).
90. Anderson, P. & Kedersha, N. Stressful initiations. *J. Cell Sci.* **115,** 3227–3234 (2002).
91. Kedersha, N. *et al.* Stress granules and processing bodies are dynamically linked sites of mRNP remodeling. *J. Cell Biol.* **169,** 871–884 (2005).
92. Taylor, J. P., Brown, R. H. & Cleveland, D. W. Decoding ALS: From genes to

mechanism. *Nature* **539,** 197–206 (2016).

93. Lagier-Tourenne, C., Polymenidou, M. & Cleveland, D. W. TDP-43 and FUS/TLS: Emerging roles in RNA processing and neurodegeneration. *Hum. Mol. Genet.* **19,** (2010).
94. Prudlo, J. *et al.* TDP-43 pathology and cognition in ALS. *Neurology* **87,** 1019–1023 (2016).
95. Hackman, P. *et al.* Welander distal myopathy is caused by a mutation in the RNA-binding protein TIA1. *Ann. Neurol.* **73,** 500–509 (2013).
96. Kim, H. J. *et al.* Mutations in prion-like domains in hnRNPA2B1 and hnRNPA1 cause multisystem proteinopathy and ALS. *Nature* **495,** 467–473 (2013).
97. Lee, K. H. *et al.* C9orf72 Dipeptide Repeats Impair the Assembly, Dynamics, and Function of Membrane-Less Organelles. *Cell* **167,** 774–788.e17 (2016).
98. Monahan, Z., Shewmaker, F. & Pandey, U. B. Stress granules at the intersection of autophagy and ALS. *Brain Research* **1649,** 189–200 (2016).
99. Gensler, H. L. & Bernstein, H. DNA Damage as the Primary Cause of Aging. *Q. Rev. Biol.* **56,** 279–303 (1981).
100. de Magalhães, J. P., Curado, J. & Church, G. M. Meta-analysis of age-related gene expression profiles identifies common signatures of aging. *Bioinformatics* **25,** 875–881 (2009).
101. Beyer, K. & Ariza, A. Alpha-Synuclein Posttranslational Modification and Alternative Splicing as a Trigger for Neurodegeneration. *Mol. Neurobiol.* **47,** 509–524 (2013).
102. Zhu, H. & Ding, Q. Lower expression level of two RAGE alternative splicing isoforms in Alzheimer's disease. *Neurosci. Lett.* **597,** 66–70 (2015).
103. Lee, V. M.-Y., Goedert, M. & Trojanowski, J. Q. Neurodegenerative Tauopathies. *Annu. Rev. Neurosci.* **24,** 1121–1159 (2001).
104. Sergeant, N., Delacourte, A. & Buée, L. Tau protein as a differential biomarker of tauopathies. *Biochimica et Biophysica Acta - Molecular Basis of Disease* **1739,** 179–197 (2005).
105. Fiesel, F. C., Weber, S. S., Supper, J., Zell, A. & Kahle, P. J. TDP-43 regulates global translational yield by splicing of exon junction complex component SKAR. *Nucleic Acids Res.* **40,** 2668–2682 (2012).
106. Prudencio, M. *et al.* Misregulation of human sortilin splicing leads to the generation of a nonfunctional progranulin receptor. *Proc. Natl. Acad. Sci.* (2012). doi:10.1073/pnas.1211577110

107. De Conti, L. *et al.* TDP-43 affects splicing profiles and isoform production of genes involved in the apoptotic and mitotic cellular pathways. *Nucleic Acids Res.* (2015). doi:10.1093/nar/gkv814
108. Zhang, Y.-J. *et al.* Aberrant cleavage of TDP-43 enhances aggregation and cellular toxicity. *Proc. Natl. Acad. Sci.* (2009). doi:10.1073/pnas.0900688106
109. Neumann, M. *et al.* Ubiquitinated TDP-43 in frontotemporal lobar degeneration and amyotrophic lateral sclerosis. *Science* **314,** 130–3 (2006).
110. Licatalosi, D. D. & Darnell, R. B. Splicing Regulation in Neurologic Disease. *Neuron* (2006). doi:10.1016/j.neuron.2006.09.017
111. Lardenoije, R. *et al.* The epigenetics of aging and neurodegeneration. *Progress in Neurobiology* **131,** 21–64 (2015).
112. Berger, S. L. The complex language of chromatin regulation during transcription. *Nature* **447,** 407–412 (2007).
113. Bernstein, B. E., Meissner, A. & Lander, E. S. The Mammalian Epigenome. *Cell* **128,** 669–681 (2007).
114. Luger, K., Mäder, A. W., Richmond, R. K., Sargent, D. F. & Richmond, T. J. Crystal structure of the nucleosome core particle at 2.8 Å resolution. *Nature* **389,** 251–260 (1997).
115. Jenuwein, T. & Allis, C. D. Translating the histone code. *Science* **293,** 1074–1080 (2001).
116. Gonzalo, S. Epigenetic alterations in aging. *J. Appl. Physiol.* **109,** 586–597 (2010).
117. Dhalluin, C. *et al.* Structure and ligand of a histone acetyltransferase bromodomain. *Nature* **399,** 491–496 (1999).
118. Grunstein, M. Histone acetylation in chromatin structure and transcription. *Nature* **389,** 349–352 (1997).
119. Kouzarides, T. Histone methylation in transcriptional control. *Curr. Opin. Genet. Dev.* **12,** 198–209 (2002).
120. Grillari, J. & Grillari-Voglauer, R. Novel modulators of senescence, aging, and longevity: Small non-coding RNAs enter the stage. *Experimental Gerontology* **45,** 302–311 (2010).
121. Cech, T. R. & Steitz, J. A. The noncoding RNA revolution - Trashing old rules to forge new ones. *Cell* **157,** 77–94 (2014).
122. Costa, F. F. Non-coding RNAs: Meet thy masters. *BioEssays* **32,** 599–608 (2010).
123. Casadesús, J. & Low, D. Epigenetic gene regulation in the bacterial world. *Microbiol. Mol. Biol. Rev.* **70,** 830–56 (2006).

124. Zemach, A., McDaniel, I. E., Silva, P. & Zilberman, D. Genome-wide evolutionary analysis of eukaryotic DNA methylation. *Science* **328,** 916–9 (2010).
125. Thomas, B. *et al.* A novel method for detecting 7-methyl guanine reveals aberrant methylation levels in Huntington disease. *Anal. Biochem.* **436,** 112–120 (2013).
126. Bird, A. P. & Wolffe, A. P. Methylation-Induced Repression— Belts, Braces, and Chromatin. *Cell* **99,** 451–454 (1999).
127. Jones, P. L. *et al.* Methylated DNA and MeCP2 recruit histone deacetylase to repress transcription. *Nat. Genet.* **19,** 187–191 (1998).
128. Fraga, M. F. *et al.* The affinity of different MBD proteins for a specific methylated locus depends on their intrinsic binding properties. *Nucleic Acids Research* **31,** 1765–1774 (2003).
129. Wu, S. C. & Zhang, Y. Active DNA demethylation: Many roads lead to Rome. *Nature Reviews Molecular Cell Biology* **11,** 607–620 (2010).
130. Ito, S. *et al.* Tet proteins can convert 5-methylcytosine to 5-formylcytosine and 5-carboxylcytosine. *Science (80-.).* **333,** 1300–1303 (2011).
131. Cortázar, D. *et al.* Embryonic lethal phenotype reveals a function of TDG in maintaining epigenetic stability. *Nature* **470,** 419–423 (2011).
132. He, Y. F. *et al.* Tet-mediated formation of 5-carboxylcytosine and its excision by TDG in mammalian DNA. *Science (80-.).* **333,** 1303–1307 (2011).
133. Xu, X. DNA methylation and cognitive aging. *Oncotarget* **6,** 13922–13932 (2015).
134. Lipman, T. & Tiedje, L. B. Epigenetic Differences Arise During the Lifetime of Monozygotic Twins. *MCN, The American Journal of Maternal/Child Nursing* **31,** 204 (2006).
135. Horvath, S. DNA methylation age of human tissues and cell types. *Genome Biol.* **14,** (2013).
136. Jintaridth, P. & Mutirangura, A. Distinctive patterns of age-dependent hypomethylation in interspersed repetitive sequences. *Physiol. Genomics* **41,** 194–200 (2010).
137. Zampieri, M. *et al.* Reconfiguration of DNA methylation in aging. *Mechanisms of Ageing and Development* **151,** 60–70 (2015).
138. Weidner, C. I. & Wagner, W. The epigenetic tracks of aging. *Biological Chemistry* **395,** 1307–1314 (2014).
139. Franzen, J. *et al.* Senescence-associated DNA methylation is stochastically acquired in subpopulations of mesenchymal stem cells. *Aging Cell* (2017). doi:10.1111/acel.12544

140. Christensen, B. C. *et al.* Aging and environmental exposures alter tissue-specific DNA methylation dependent upon CPG island context. *PLoS Genet.* **5,** (2009).
141. Bellizzi, D. *et al.* Global DNA methylation in old subjects is correlated with frailty. *Age (Omaha)*. **34,** 169–179 (2012).
142. Esteller, M. Epigenetic gene silencing in cancer: The DNA hypermethylome. *Human Molecular Genetics* (2007). doi:10.1093/hmg/ddm018
143. Kwabi-Addo, B. *et al.* Age-related DNA methylation changes in normal human prostate tissues. *Clin. Cancer Res.* **13,** 3796–3802 (2007).
144. Lin, M. J., Tang, L. Y., Reddy, M. N. & Shen, C. K. J. DNA methyltransferase gene dDnmt2 and longevity of Drosophila. *J. Biol. Chem.* **280,** 861–864 (2005).
145. Vanyushin, B. F., Nemirovsky, L. E., Klimenko, V. V., Vasiliev, V. K. & Belozersky, A. N. The 5-methylcytosine in DNA of rats: Tissue and age specificity and the changes induced by hydrocortisonc and other agents. *Gerontology* **19,** 138–152 (1973).
146. Singhal, R. P., Mays-Hoopes, L. L. & Eichhorn, G. L. DNA methylation in aging of mice. *Mech. Ageing Dev.* **41,** 199–210 (1987).
147. Tohgi, H. *et al.* The methylation status of cytosines in a τ gene promoter region alters with age to downregulate transcriptional activity in human cerebral cortex. *Neurosci. Lett.* **275,** 89–92 (1999).
148. Morrison, L. D., Smith, D. D. & Kish, S. J. Brain S-Adenosylmethionine Levels Are Severely Decreased in Alzheimer's Disease. *J. Neurochem.* **67,** 1328–1331 (2002).
149. Mastroeni, D., McKee, A., Grover, A., Rogers, J. & Coleman, P. D. Epigenetic differences in cortical neurons from a pair of monozygotic twins discordant for Alzheimer's disease. *PLoS One* **4,** (2009).
150. Mukaetova-Ladinska, E. B., Harrington, C. R., Roth, M. & Wischik, C. M. Alterations in tau protein metabolism during normal aging. *Dementia* **7,** 95–103 (1996).
151. Matsumoto, L. *et al.* CpG demethylation enhances alpha-synuclein expression and affects the pathogenesis of Parkinson's disease. *PLoS One* **5,** (2010).
152. International Parkinson's Disease Genomics Consortium, * *et al.* A two-stage meta-analysis identifies several new Loci for Parkinson's disease. *PLoS Genet.* **7,** e1002142 (2011).
153. Klein, C. J. *et al.* Mutations in DNMT1 cause hereditary sensory neuropathy with dementia and hearing loss. *Nat. Genet.* **43,** 595–600 (2011).
154. Egger, G., Liang, G., Aparicio, A. & Jones, P. A. Epigenetics in human disease and

prospects for epigenetic therapy. *Nature* **429,** 457–463 (2004).

155. Abdulhaq, H. & Rossetti, J. M. The role of azacitidine in the treatment of myelodysplastic syndromes. *Expert Opin. Investig. Drugs* (2007). doi:10.1517/13543784.16.12.1967

156. Keating, G. M. Azacitidine: A review of its use in higher-risk myelodysplastic syndromes acute myeloid leukaemia. *Drugs* (2009). doi:10.2165/11202840-000000000-00000

157. Park, L. K., Friso, S. & Choi, S. W. Nutritional influences on epigenetics and age-related disease. in *Proceedings of the Nutrition Society* **71,** 75–83 (2012).

158. Batra, V., Sridhar, S. & Devasagayam, T. P. A. Enhanced one-carbon flux towards DNA methylation: Effect of dietary methyl supplements against γ-radiation-induced epigenetic modifications. *Chem. Biol. Interact.* **183,** 425–433 (2010).

159. Leu, Y. W. *et al.* Double RNA interference of DNMT3b and DNMT1 enhances DNA demethylation and gene reactivation. *Cancer Res.* **63,** 6110–6115 (2003).

160. Arai, T. *et al.* TDP-43 is a component of ubiquitin-positive tau-negative inclusions in frontotemporal lobar degeneration and amyotrophic lateral sclerosis. *Biochem. Biophys. Res. Commun.* **351,** 602–611 (2006).

161. Deng, H. X. *et al.* FUS-immunoreactive inclusions are a common feature in sporadic and non-SOD1 familial amyotrophic lateral sclerosis. *Ann. Neurol.* (2010). doi:10.1002/ana.22051

162. Mackenzie, I. R., Rademakers, R. & Neumann, M. TDP-43 and FUS in amyotrophic lateral sclerosis and frontotemporal dementia. *Lancet Neurol* (2010). doi:10.1016/S1474-4422(10)70195-2

163. Ling, S. C., Polymenidou, M. & Cleveland, D. W. Converging mechanisms in als and FTD: Disrupted RNA and protein homeostasis. *Neuron* **79,** 416–438 (2013).

164. Al-Chalabi, A. & Hardiman, O. The epidemiology of ALS: A conspiracy of genes, environment and time. *Nature Reviews Neurology* **9,** 617–628 (2013).

165. Hardiman, O. *et al.* Amyotrophic lateral sclerosis. *Nature Reviews Disease Primers* **3,** (2017).

166. Talbot, K. Amyotrophic lateral sclerosis: Cell vulnerability or system vulnerability? *Journal of Anatomy* **224,** 45–51 (2014).

167. Zarei, S. *et al.* A comprehensive review of amyotrophic lateral sclerosis. *Surg. Neurol. Int.* (2015). doi:10.4103/2152-7806.169561

168. Chio, A., Calvo, A., Moglia, C., Mazzini, L. & Mora, G. Phenotypic heterogeneity of amyotrophic lateral sclerosis: a population based study. *J. Neurol. Neurosurg.*

Psychiatry **82,** 740–746 (2011).

169. Rosen, D. R. *et al.* Mutations in Cu/Zn superoxide dismutase gene are associated with familial amyotrophic lateral sclerosis. *Nature* **362,** 59–62 (1993).
170. Chen, S., Sayana, P., Zhang, X. & Le, W. Genetics of amyotrophic lateral sclerosis: An update. *Molecular Neurodegeneration* **8,** (2013).
171. Cooper-Knock, J. *et al.* Clinico-pathological features in amyotrophic lateral sclerosis with expansions in C9ORF72. *Brain* **135,** 751–764 (2012).
172. Elden, A. C. *et al.* Ataxin-2 intermediate-length polyglutamine expansions are associated with increased risk for ALS. *Nature* **466,** 1069–1075 (2010).
173. Van Hoecke, A. *et al.* EPHA4 is a disease modifier of amyotrophic lateral sclerosis in animal models and in humans. *Nat. Med.* **18,** 1418–1422 (2012).
174. Van Blitterswijk, M. *et al.* Evidence for an oligogenic basis of amyotrophic lateral sclerosis. *Hum. Mol. Genet.* **21,** 3776–3784 (2012).
175. Renton, A. E., Chiò, A. & Traynor, B. J. State of play in amyotrophic lateral sclerosis genetics. *Nature Neuroscience* **17,** 17–23 (2014).
176. Steele, J. C. & McGeer, P. L. The ALS/PDC syndrome of Guam and the cycad hypothesis. *Neurology* **70,** 1984–1990 (2008).
177. Bradley, W. G. *et al.* Is exposure to cyanobacteria an environmental risk factor for amyotrophic lateral sclerosis and other neurodegenerative diseases? *Amyotroph. Lateral Scler. Frontotemporal Degener.* **14,** 325–33 (2013).
178. Gallo, V. *et al.* Physical activity and risk of Amyotrophic Lateral Sclerosis in a prospective cohort study. *Eur. J. Epidemiol.* (2016). doi:10.1007/s10654-016-0119-9
179. Wang, M.-D., Little, J., Gomes, J., Cashman, N. R. & Krewski, D. Identification of risk factors associated with onset and progression of amyotrophic lateral sclerosis using systematic review and meta-analysis. *Neurotoxicology* (2016). doi:10.1016/j.neuro.2016.06.015
180. Van Damme, P., Robberecht, W. & Van Den Bosch, L. Modelling amyotrophic lateral sclerosis: progress and possibilities. *Dis. Model. Mech.* **10,** 537–549 (2017).
181. Webster, C. P., Smith, E. F., Shaw, P. J. & De Vos, K. J. Protein Homeostasis in Amyotrophic Lateral Sclerosis: Therapeutic Opportunities? *Front. Mol. Neurosci.* **10,** (2017).
182. Webster, C. P. *et al.* The C9orf72 protein interacts with Rab1a and the ULK1 complex to regulate initiation of autophagy. *EMBO J.* **35,** 1656–1676 (2016).
183. Goode, A. *et al.* Defective recognition of LC3B by mutant SQSTM1/p62 implicates

impairment of autophagy as a pathogenic mechanism in ALS-FTLD. *Autophagy* **12,** 1094–1104 (2016).

184. Urushitani, M., Kurisu, J., Tsukita, K. & Takahashi, R. Proteasomal inhibition by misfolded mutant superoxide dismutase 1 induces selective motor neuron death in familial amyotrophic lateral sclerosis. *J. Neurochem.* **83,** 1030–1042 (2002).
185. Chang, H. Y., Hou, S. C., Way, T. Der, Wong, C. H. & Wang, I. F. Heat-shock protein dysregulation is associated with functional and pathological TDP-43 aggregation. *Nat. Commun.* **4,** (2013).
186. Cooper-Knock, J. *et al.* Sequestration of multiple RNA recognition motif-containing proteins by C9orf72 repeat expansions. *Brain* **137,** 2040–2051 (2014).
187. Hautbergue, G. M. *et al.* SRSF1-dependent nuclear export inhibition of C9ORF72 repeat transcripts prevents neurodegeneration and associated motor deficits. *Nat. Commun.* **8,** (2017).
188. Zhang, K. *et al.* The C9orf72 repeat expansion disrupts nucleocytoplasmic transport. *Nature* **525,** 56–61 (2015).
189. Martin, K. C. & Ephrussi, A. mRNA Localization: Gene Expression in the Spatial Dimension. *Cell* (2009). doi:10.1016/j.cell.2009.01.044
190. Sutton, M. A. & Schuman, E. M. Dendritic Protein Synthesis, Synaptic Plasticity, and Memory. *Cell* **127,** 49–58 (2006).
191. Smith, B. N. *et al.* Exome-wide rare variant analysis identifies TUBA4A mutations associated with familial ALS. *Neuron* **84,** 324–331 (2014).
192. Puls, I. *et al.* Mutant dynactin in motor neuron disease. *Nat. Genet.* **33,** 455–456 (2003).
193. Wu, C.-H. *et al.* Mutations in the profilin 1 gene cause familial amyotrophic lateral sclerosis. *Nature* **488,** 499–503 (2012).
194. Garcia, M. L. *et al.* Mutations in neurofilament genes are not a significant primary cause of non-SOD1-mediated amyotrophic lateral sclerosis. *Neurobiol. Dis.* **21,** 102–109 (2006).
195. Corrado, L. *et al.* A novel peripherin gene (PRPH) mutation identified in one sporadic amyotrophic lateral sclerosis patient. *Neurobiol. Aging* **32,** (2011).
196. Geloso, M. C. *et al.* The dual role of microglia in ALS: Mechanisms and therapeutic approaches. *Frontiers in Aging Neuroscience* (2017). doi:10.3389/fnagi.2017.00242
197. Harraz, M. M. *et al.* SOD1 mutations disrupt redox-sensitive Rac regulation of NADPH oxidase in a familial ALS model. *J. Clin. Invest.* **118,** 659–670 (2008).
198. O'Rourke, J. G. *et al.* C9orf72 is required for proper macrophage and microglial

function in mice. *Science (80-.).* **351,** 1324–1329 (2016).

199. Lee, Y. *et al.* Oligodendroglia metabolically support axons and contribute to neurodegeneration. *Nature* **487,** 443–448 (2012).
200. Rothstein, J. D., Van Kammen, M., Levey, a I., Martin, L. J. & Kuncl, R. W. Selective loss of glial glutamate transporter GLT-1 in amyotrophic lateral sclerosis. *Ann. Neurol.* **38,** 73–84 (1995).
201. Sreedharan, J. *et al.* TDP-43 mutations in familial and sporadic amyotrophic lateral sclerosis. *Science* **319,** 1668–72 (2008).
202. Vance, C. *et al.* Mutations in FUS, an RNA processing protein, cause familial amyotrophic lateral sclerosis type 6. *Science* **323,** 1208–11 (2009).
203. Tollervey, J. R. *et al.* Characterising the RNA targets and position-dependent splicing regulation by TDP-43; implications for neurodegenerative diseases. *Nat. Neurosci.* **14,** 452–8 (2011).
204. Huelga, S. C. *et al.* Integrative Genome-wide Analysis Reveals Cooperative Regulation of Alternative Splicing by hnRNP Proteins. *Cell Rep.* **1,** 167–178 (2012).
205. Buratti, E. & Baralle, F. E. Chapter 1 The Molecular Links Between TDP-43 Dysfunction and Neurodegeneration. *Advances in Genetics* **66,** 1–34 (2009).
206. Ou, S. H., Wu, F., Harrich, D., García-Martínez, L. F. & Gaynor, R. B. Cloning and characterization of a novel cellular protein, TDP-43, that binds to human immunodeficiency virus type 1 TAR DNA sequence motifs. *J. Virol.* **69,** 3584–3596 (1995).
207. Nehls, J., Koppensteiner, H., Brack-Werner, R., Floss, T. & Schindler, M. HIV-1 replication in human immune cells is independent of TAR DNA binding protein 43 (TDP-43) expression. *PLoS One* **9,** (2014).
208. Buratti, E. *et al.* Nuclear factor TDP-43 and SR proteins promote in vitro and in vivo CFTR exon 9 skipping. *EMBO J.* **20,** 1774–1784 (2001).
209. Chen-Plotkin, A. S., Lee, V. M. Y. & Trojanowski, J. Q. TAR DNA-binding protein 43 in neurodegenerative disease. *Nature Reviews Neurology* **6,** 211–220 (2010).
210. Kabashi, E. *et al.* TARDBP mutations in individuals with sporadic and familial amyotrophic lateral sclerosis. *Nat. Genet.* **40,** 572–574 (2008).
211. Ayala, Y. M. *et al.* Human, Drosophila, and C. elegans TDP43: Nucleic acid binding properties and splicing regulatory function. *J. Mol. Biol.* **348,** 575–588 (2005).
212. Buratti, E. & Baralle, F. E. Characterization and Functional Implications of the RNA Binding Properties of Nuclear Factor TDP-43, a Novel Splicing Regulator of

CFTR Exon 9. *J. Biol. Chem.* **276,** 36337–36343 (2001).

213. Winton, M. J. *et al.* Disturbance of nuclear and cytoplasmic TAR DNA-binding protein (TDP-43) induces disease-like redistribution, sequestration, and aggregate formation. *J. Biol. Chem.* **283,** 13302–13309 (2008).
214. Ayala, Y. M., Misteli, T. & Baralle, F. E. TDP-43 regulates retinoblastoma protein phosphorylation through the repression of cyclin-dependent kinase 6 expression. *Proc. Natl. Acad. Sci.* **105,** 3785–3789 (2008).
215. Buratti, E. *et al.* TDP-43 binds heterogeneous nuclear ribonucleoprotein A/B through its C-terminal tail: An important region for the inhibition of cystic fibrosis transmembrane conductance regulator exon 9 splicing. *J. Biol. Chem.* **280,** 37572–37584 (2005).
216. Wang, H.-Y., Wang, I.-F., Bose, J. & Shen, C.-K. J. Structural diversity and functional implications of the eukaryotic TDP gene family. *Genomics* **83,** 130–139 (2004).
217. Ayala, Y. M. *et al.* Structural determinants of the cellular localization and shuttling of TDP-43. *J. Cell Sci.* **121,** 3778–3785 (2008).
218. Ayala, Y. M. *et al.* TDP-43 regulates its mRNA levels through a negative feedback loop. *EMBO J.* **30,** 277–288 (2011).
219. Bembich, S. *et al.* Predominance of spliceosomal complex formation over polyadenylation site selection in TDP-43 autoregulation. *Nucleic Acids Res.* **42,** 3362–3371 (2014).
220. Leigh, P. N. *et al.* Ubiquitin-immunoreactive intraneuronal inclusions in amyotrophic lateral sclerosis: Morphology, distribution, and specificity. *Brain* **114,** 775–788 (1991).
221. Okamoto, K., Hirai, S., Amari, M. & Sakurai, A. Electron micrograph of ubiquitin-positive intraneuronal inclusions in the extra-motor cortices in patients with amyotrophic lateral sclerosis. *Neuropathology* **16,** 112–116 (1996).
222. Cairns, N. J. *et al.* TDP-43 proteinopathy in familial motor neurone disease with TARDBP A315T mutation: A case report. *Neuropathology and Applied Neurobiology* **36,** 673–679 (2010).
223. Neumann, M. *et al.* A new subtype of frontotemporal lobar degeneration with FUS pathology. *Brain* **132,** 2922–2931 (2009).
224. Mackenzie, I. R. A. *et al.* Pathological TDP-43 distinguishes sporadic amyotrophic lateral sclerosis from amyotrophic lateral sclerosis with SOD1 mutations. *Ann. Neurol.* **61,** 427–434 (2007).

225. Hasegawa, M. *et al.* Phosphorylated TDP-43 in frontotemporal lobar degeneration and amyotrophic lateral sclerosis. *Ann. Neurol.* **64,** 60–70 (2008).
226. Inukai, Y. *et al.* Abnormal phosphorylation of Ser409/410 of TDP-43 in FTLD-U and ALS. *FEBS Lett.* **582,** 2899–2904 (2008).
227. Neumann, M., Kwong, L. K., Sampathu, D. M., Trojanowski, J. Q. & Lee, V. M. Y. TDP-43 proteinopathy in frontotemporal lobar degeneration and amyotrophic lateral sclerosis: Protein misfolding diseases without amyloidosis. *Archives of Neurology* **64,** 1388–1394 (2007).
228. Kwong, L. K., Uryu, K., Trojanowski, J. Q. & Lee, V. M. Y. TDP-43 proteinopathies: Neurodegenerative protein misfolding diseases without amyloidosis. *NeuroSignals* **16,** 41–51 (2007).
229. Westermark, G. T., Johnson, K. H. & Westermark, P. Staining methods for identification of amyloid in tissue. *Methods Enzymol.* **309,** 3–25 (1999).
230. Bigio, E. H. *et al.* Inclusions in frontotemporal lobar degeneration with TDP-43 proteinopathy (FTLD-TDP) and amyotrophic lateral sclerosis (ALS), but not FTLD with FUS proteinopathy (FTLD-FUS), have properties of amyloid. *Acta Neuropathologica* **125,** 463–465 (2013).
231. Robinson, J. L. *et al.* TDP-43 skeins show properties of amyloid in a subset of ALS cases. *Acta Neuropathol.* **125,** 121–131 (2013).
232. Geser, F., Martinez-Lage, M., Kwong, L. K., Lee, V. M. Y. & Trojanowski, J. Q. Amyotrophic lateral sclerosis, frontotemporal dementia and beyond: The TDP-43 diseases. *Journal of Neurology* **256,** 1205–1214 (2009).
233. Baloh, R. H. TDP-43: the relationship between protein aggregation and neurodegeneration in amyotrophic lateral sclerosis and frontotemporal lobar degeneration. *FEBS J.* **278,** 3539–49 (2011).
234. Geser, F. *et al.* Pathological 43-kDa transactivation response DNA-binding protein in older adults with and without severe mental illness. *Arch. Neurol.* **67,** 1238–1250 (2010).
235. Uchino, A. *et al.* Incidence and extent of TDP-43 accumulation in aging human brain. *Acta Neuropathol. Commun.* **3,** 35 (2015).
236. Smethurst, P., Sidle, K. C. L. & Hardy, J. Review: Prion-like mechanisms of transactive response DNA binding protein of 43 kDa (TDP-43) in amyotrophic lateral sclerosis (ALS). *Neuropathol. Appl. Neurobiol.* **41,** 578–597 (2015).
237. Nonaka, T. *et al.* Prion-like Properties of Pathological TDP-43 Aggregates from Diseased Brains. *Cell Rep.* **4,** 124–134 (2013).

238. Furukawa, Y., Kaneko, K., Watanabe, S., Yamanaka, K. & Nukina, N. A seeding reaction recapitulates intracellular formation of sarkosyl-insoluble transactivation response element (TAR) DNA-binding protein-43 inclusions. *J. Biol. Chem.* **286,** 18664–18672 (2011).

239. Kasai, T. *et al.* Increased TDP-43 protein in cerebrospinal fluid of patients with amyotrophic lateral sclerosis. *Acta Neuropathol.* **117,** 55–62 (2009).

240. Braak, H. *et al.* Amyotrophic lateral sclerosis - A model of corticofugal axonal spread. *Nature Reviews Neurology* **9,** 708–714 (2013).

241. Che, M. X., Jiang, L. L., Li, H. Y., Jiang, Y. J. & Hu, H. Y. TDP-35 sequesters TDP-43 into cytoplasmic inclusions through binding with RNA. *FEBS Lett.* (2015). doi:10.1016/j.febslet.2015.06.009

242. Igaz, L. M. *et al.* Expression of TDP-43 C-terminal fragments in vitro recapitulates pathological features of TDP-43 proteinopathies. *J. Biol. Chem.* **284,** 8516–8524 (2009).

243. Nonaka, T., Kametani, F., Arai, T., Akiyama, H. & Hasegawa, M. Truncation and pathogenic mutations facilitate the formation of intracellular aggregates of TDP-43. *Hum. Mol. Genet.* **18,** 3353–3364 (2009).

244. Zhang, Y. J. *et al.* Phosphorylation regulates proteasomal-mediated degradation and solubility of TAR DNA binding protein-43 C-terminal fragments. *Mol. Neurodegener.* **5,** (2010).

245. Li, H. Y., Yeh, P. A., Chiu, H. C., Tang, C. Y. & Tu, B. P. hsien. Hyperphosphorylation as a defense mechanism to reduce TDP-43 aggregation. *PLoS One* **6,** (2011).

246. Cragnaz, L. *et al.* Aggregate formation prevents dTDP-43 neurotoxicity in the Drosophila melanogaster eye. *Neurobiol. Dis.* **71,** 74–80 (2014).

247. Budini, M., Romano, V., Quadri, Z., Buratti, E. & Baralle, F. E. TDP-43 loss of cellular function through aggregation requires additional structural determinants beyond its C-terminal Q/N prion-like domain. *Hum. Mol. Genet.* (2015). doi:10.1093/hmg/ddu415

248. Geser, F. *et al.* Clinical and pathological continuum of multisystem TDP-43 proteinopathies. *Arch. Neurol.* **66,** 180–189 (2009).

249. Rutherford, N. J. *et al.* Novel Mutations in TARDBP (TDP-43) in Patients with Familial Amyotrophic Lateral Sclerosis. *PLoS Genet.* **4,** e1000193 (2008).

250. Budini, M. *et al.* Cellular model of TAR DNA-binding Protein 43 (TDP-43) aggregation based on its C-terminal Gln/Asn-rich region. *J. Biol. Chem.* **287,** 7512–

7525 (2012).

251. Fuentealba, R. A. *et al.* Interaction with polyglutamine aggregates reveals a Q/N-rich domain in TDP-43. *J. Biol. Chem.* **285,** 26304–26314 (2010).

252. King, O. D., Gitler, A. D. & Shorter, J. The tip of the iceberg: RNA-binding proteins with prion-like domains in neurodegenerative disease. *Brain Research* **1462,** 61–80 (2012).

253. Cushman, M., Johnson, B. S., King, O. D., Gitler, A. D. & Shorter, J. Prion-like disorders: blurring the divide between transmissibility and infectivity. *J. Cell Sci.* **123,** 1191–1201 (2010).

254. Furukawa, Y., Kaneko, K. & Nukina, N. Molecular properties of TAR DNA binding protein-43 fragments are dependent upon its cleavage site. *Biochim. Biophys. Acta - Mol. Basis Dis.* **1812,** 1577–1583 (2011).

255. Sasaguri, H. *et al.* The extreme N-terminus of TDP-43 mediates the cytoplasmic aggregation of TDP-43 and associated toxicity in vivo. *Brain Research* **1647,** 57–64 (2016).

256. Budini, M. & Buratti, E. TDP-43 autoregulation: Implications for disease. in *Journal of Molecular Neuroscience* **45,** 473–479 (2011).

257. D'Ambrogio, A. *et al.* Functional mapping of the interaction between TDP-43 and hnRNP A2 in vivo. *Nucleic Acids Res.* **37,** 4116–4126 (2009).

258. Zhang, Y.-J. *et al.* Progranulin Mediates Caspase-Dependent Cleavage of TAR DNA Binding Protein-43. *J. Neurosci.* **27,** 10530–10534 (2007).

259. Cragnaz, L. *et al.* An age-related reduction of brain TBPH/TDP-43 levels precedes the onset of locomotion defects in a Drosophila ALS model. *Neuroscience* **311,** 415–421 (2015).

260. Ceballos-Diaz, C. *et al.* Viral expression of ALS-linked ubiquilin-2 mutants causes inclusion pathology and behavioral deficits in mice. *Mol. Neurodegener.* (2015). doi:10.1186/s13024-015-0026-7

261. Majumder, V., Gregory, J. M., Barria, M. A., Green, A. & Pal, S. TDP-43 as a potential biomarker for amyotrophic lateral sclerosis: A systematic review and meta-analysis. *BMC Neurol.* (2018). doi:10.1186/s12883-018-1091-7

262. Xu, Z. & Yang, C. TDP-43—The key to understanding amyotrophic lateral sclerosis. *Rare Dis.* (2014). doi:10.4161/21675511.2014.944443

263. Blokhuis, A. M., Groen, E. J. N., Koppers, M., Van Den Berg, L. H. & Pasterkamp, R. J. Protein aggregation in amyotrophic lateral sclerosis. *Acta Neuropathologica* (2013). doi:10.1007/s00401-013-1125-6

264. Feiguin, F. *et al.* Depletion of TDP-43 affects Drosophila motoneurons terminal synapsis and locomotive behavior. *FEBS Lett.* (2009). doi:10.1016/j.febslet.2009.04.019

265. Hua, Y. *et al.* Peripheral SMN restoration is essential for long-term rescue of a severe spinal muscular atrophy mouse model. *Nature* (2011). doi:10.1038/nature10485

266. Donnelly, C. J. *et al.* RNA Toxicity from the ALS/FTD C9ORF72 Expansion Is Mitigated by Antisense Intervention. *Neuron* (2013). doi:10.1016/j.neuron.2013.10.015

267. Kordasiewicz, H. B. *et al.* Sustained Therapeutic Reversal of Huntington's Disease by Transient Repression of Huntingtin Synthesis. *Neuron* (2012). doi:10.1016/j.neuron.2012.05.009

268. Faghihi, M. A. *et al.* Expression of a noncoding RNA is elevated in Alzheimer's disease and drives rapid feed-forward regulation of β-secretase. *Nat. Med.* (2008). doi:10.1038/nm1784

269. Martin, L. J. & Wong, M. Aberrant Regulation of DNA Methylation in Amyotrophic Lateral Sclerosis: A New Target of Disease Mechanisms. *Neurotherapeutics* (2013). doi:10.1007/s13311-013-0205-6

270. Chestnut, B. A. *et al.* Epigenetic Regulation of Motor Neuron Cell Death through DNA Methylation. *J. Neurosci.* (2011). doi:10.1523/JNEUROSCI.1639-11.2011

271. Hamzeiy, H. *et al.* Elevated Global DNA Methylation Is Not Exclusive to Amyotrophic Lateral Sclerosis and Is Also Observed in Spinocerebellar Ataxia Types 1 and 2. *Neurodegener. Dis.* (2018). doi:10.1159/000486201

272. Coppedè, F. *et al.* Increase in DNA methylation in patients with amyotrophic lateral sclerosis carriers of not fully penetrant SOD1 mutations. *Amyotroph. Lateral Scler. Front. Degener.* **19,** 93–101 (2018).

273. Tremolizzo, L. *et al.* Whole-blood global DNA methylation is increased in amyotrophic lateral sclerosis independently of age of onset. *Amyotroph. Lateral Scler. Front. Degener.* (2014). doi:10.3109/21678421.2013.851247

274. Figueroa-Romero, C. *et al.* Identification of Epigenetically Altered Genes in Sporadic Amyotrophic Lateral Sclerosis. *PLoS One* (2012). doi:10.1371/journal.pone.0052672

275. Masala, A. *et al.* Epigenetic Changes Associated with the Expression of Amyotrophic Lateral Sclerosis (ALS) Causing Genes. *Neuroscience* (2018). doi:10.1016/j.neuroscience.2018.08.009

276. Xi, Z. *et al.* Hypermethylation of the CpG-island near the C9orf72 G4C2-repeat expansion in FTLD patients. *Hum. Mol. Genet.* (2014). doi:10.1093/hmg/ddu279

277. Xi, Z. *et al.* Hypermethylation of the CpG island near the G4C2repeat in ALS with a C9orf72 expansion. *Am. J. Hum. Genet.* (2013). doi:10.1016/j.ajhg.2013.04.017

278. Russ, J. *et al.* Hypermethylation of repeat expanded C9orf72 is a clinical and molecular disease modifier. *Acta Neuropathol.* (2015). doi:10.1007/s00401-014-1365-0

279. Wang, L. L. & Zhang, C. L. Engineering new neurons: in vivo reprogramming in mammalian brain and spinal cord. *Cell and Tissue Research* (2018). doi:10.1007/s00441-017-2729-2

280. Suchy, J., Lee, S., Ahmed, A. & Shea, T. B. Dietary supplementation with S-adenosyl methionine delays the onset of motor neuron pathology in a murine model of amyotrophic lateral sclerosis. *NeuroMolecular Med.* (2010). doi:10.1007/s12017-009-8089-7

281. Edlin, R. *et al.* Azacitidine for the treatment of myelodysplastic syndrome, chronic myelomonocytic leukaemia and acute myeloid leukaemia. *Health technology assessment (Winchester, England)* (2010). doi:10.1016/S1470-2045(11)70066-3

282. Raj, K. & Mufti, G. J. Azacytidine (Vidaza®) in the treatment of myelodysplastic syndromes. *Therapeutics and Clinical Risk Management* (2006). doi:10.2147/tcrm.2006.2.4.377

283. Chabo, G. G., Rivard, G. E., Momparler, R. L., Chabo, G. G. & Momparler, R. L. Plasma and Cerebrospinal Fluid Pharmacokinetics of 5-Aza-2‘-Deoxycytidine in Rabbits and Dogs. *Cancer Res.* (1983).

284. Capuano, F., Mülleder, M., Kok, R., Blom, H. J. & Ralser, M. Cytosine DNA methylation is found in drosophila melanogaster but absent in saccharomyces cerevisiae, schizosaccharomyces pombe, and other yeast species. *Anal. Chem.* (2014). doi:10.1021/ac500447w

285. Gowher, H., Leismann, O. & Jeltsch, A. DNA of Drosophila melanogaster contains 5-methylcytosine. *EMBO J.* (2000). doi:10.1093/emboj/19.24.6918

Università degli Studi di Ferrara

Sezioni

Dottorati di ricerca

Il tuo indirizzo e-mail

miriam.pacetti@student.unife.it

Oggetto:

Dichiarazione di conformità della tesi di Dottorato

Io sottoscritto Dott. (Cognome e Nome)

Pacetti Miriam

Nato a:

Vallo della Lucania

Provincia:

Salerno

Il giorno:

31/08/1991

Avendo frequentato il Dottorato di Ricerca in:

Scienze biomediche e biotecnologiche

Ciclo di Dottorato

31

Titolo della tesi:

Mouse TDP-43 expression during development is epigenetically modulated

Titolo della tesi (traduzione):

L'espressione della proteina TDP-43 murina durante lo sviluppo è modulata mediante regolazione epigenetica

Tutore: Prof. (Cognome e Nome)

Pagani Franco

Settore Scientifico Disciplinare (S.S.D.)

BIO/10

Parole chiave della tesi (max 10):

TDP-43, TARDBP, SLA, metilazione, ALS, methylation

Consapevole, dichiara

CONSAPEVOLE: (1) del fatto che in caso di dichiarazioni mendaci, oltre alle sanzioni previste dal codice penale e dalle Leggi speciali per l'ipotesi di falsità in atti ed uso di atti falsi, decade fin dall'inizio e senza necessità di alcuna formalità dai benefici conseguenti al provvedimento emanato sulla base di tali dichiarazioni; (2) dell'obbligo per l'Università di provvedere al deposito di legge delle tesi di dottorato al fine di assicurarne la conservazione e la consultabilità da parte di terzi; (3) della procedura adottata dall'Università di Ferrara ove si richiede che la tesi sia consegnata dal dottorando in 2 copie, di cui una in formato cartaceo e una in formato pdf non modificabile su idonei supporti (CD-ROM, DVD) secondo le istruzioni pubblicate sul sito : http://www.unife.it/studenti/dottorato alla voce ESAME FINALE – disposizioni e modulistica; (4) del fatto che l'Università, sulla base dei dati forniti, archivierà e renderà consultabile in rete il testo completo della tesi di dottorato di cui alla presente dichiarazione attraverso l'Archivio istituzionale ad accesso aperto "EPRINTS.unife.it" oltre che attraverso i Cataloghi delle

Biblioteche Nazionali Centrali di Roma e Firenze. DICHIARO SOTTO LA MIA RESPONSABILITA': (1) che la copia della tesi depositata presso l'Università di Ferrara in formato cartaceo è del tutto identica a quella presentata in formato elettronico (CD-ROM, DVD), a quelle da inviare ai Commissari di esame finale e alla copia che produrrà in seduta d'esame finale. Di conseguenza va esclusa qualsiasi responsabilità dell'Ateneo stesso per quanto riguarda eventuali errori, imprecisioni o omissioni nei contenuti della tesi; (2) di prendere atto che la tesi in formato cartaceo è l'unica alla quale farà riferimento l'Università per rilasciare, a mia richiesta, la dichiarazione di conformità di eventuali copie. PER ACCETTAZIONE DI QUANTO SOPRA RIPORTATO

Dichiarazione per embargo

12 mesi

Richiesta motivata embargo

1. Tesi in corso di pubblicazione

Liberatoria consultazione dati Eprints

Consapevole del fatto che attraverso l'Archivio istituzionale ad accesso aperto "EPRINTS.unife.it" saranno comunque accessibili i metadati relativi alla tesi (titolo, autore, abstract, ecc.)

Firma del dottorando

Ferrara, li 24/01/2019 Firma del Dottorando

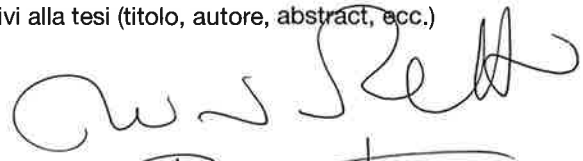

Firma del Tutore

Visto: Pagani Franco Si approva Firma del Tutore